Formation of Silica Microstructures between Inundated Stressed Silica Grains: Effect on Intergranular Tensile Strength

by

Rui Guo

Department of Civil and Environmental Engineering
Duke University

Date:_____

Approved:

_____
Tomasz A Hueckel, Supervisor

_____
Piotr E Marszalek

_____
Fred K Boadu

_____
Joseph C Nadeau

_____
Xuanhe Zhao

Dissertation submitted in partial fulfillment of
the requirements for the degree of Doctor
of Philosophy in the Department of
Civil and Environmental Engineering in the Graduate School
of Duke University

2014

ABSTRACT

Formation of Silica Microstructures between Inundated Stressed Silica Grains: Effect on Intergranular Tensile Strength

by

Rui Guo

Department of Civil and Environmental Engineering
Duke University

Date:_____

Approved:

_____
Tomasz A Hueckel, Supervisor

_____
Piotr E Marszalek

_____
Fred K Boadu

_____
Joseph C Nadeau

_____
Xuanhe Zhao

An abstract of a dissertation submitted in partial
fulfillment of the requirements for the degree
of Doctor of Philosophy in the Department of
Civil and Environmental Engineering in the Graduate School of
Duke University

2014

Abstract

Laboratory tests on microscale are reported in which amorphous silica grains were compressed in a liquid environment, namely in solutions with different silica ion concentrations for up to four weeks. Such an arrangement represents an idealized representation of two sand grains. The grain surfaces and asperities were examined in Scanning Electron Microscopy (SEM) and Atomic Force Microscopy (AFM) for fractures, silica polymer growth, and polymer strength. Single chains of silica polymers are found to have a failure pulling force of 330 – 450 nN.

A chain of observations are reported for the first time, using Pneumatic Grain Indenter and Grain Indenter-Puller apparatuses, confirming a long-existing hypothesis that a stressed contact with microcracks generates dissolved silica in the contact (asperity) vicinity, which eventually polymerizes, forming a structure between the grains on a timescale in the order of weeks. Such structure exhibits intergranular tensile force of 1 – 1.5 mN when aged in solutions containing silica ion concentrations of 200- to 500 ppm. Stress appears to accelerate the generation of silica polymers around stressed contact regions, so does mica-silica contacts. The magnitude of intergranular tensile force is 2 to 3 times greater than that of water capillary effect between grains.

Dedication

To my family, for always being there for me through thick and thin.

Contents

List of Tables

List of Figures

Acknowledgements

I would like to gratefully and sincerely thank Professor Tomasz Hueckel for his guidance, understanding, and patience during my graduate studies at Duke University. For everything you've done for me, Prof. Hueckel, I thank you.

I would like to thank the Department of Civil and Environmental Engineering at Duke University, especially those members of my doctoral committee, Professor Piotr Marszalek, Professor Fred Boadu, Professor Joseph Nadeau, and Professor Xuanhe Zhao, for their input, valuable discussions and accessibility.

I am also thankful to the following former or current staff at Duke University, for their various forms of support during my graduate studies – Ruby Nell Carpenter, Eli Nichols, Dwina Martin and Rebecca Dupre.

Many friends have helped me stay sane through these difficult years. Their support and care helped me overcome setbacks and stay focused on my graduate study. I greatly value their friendship and I deeply appreciate their belief in me.

Most importantly, none of this would have been possible without the love and patience of my family. My parents and my wife have been a constant source of love, concern, support and strength all these years.

Finally, I appreciate the financial support from the National Science Foundation that funded the research discussed in this dissertation.

1. Introduction

Granular soil exhibits significant stiffening and strengthening when subjected to a prolonged compression at a constant load in saturated conditions over engineering timescales. This effect is known under the name of soil aging and has been subject of interest for decades (Mitchell and Solymar 1984, Schmertmann 1991, Hueckel et al. 2001, Hueckel et al. 2005). Anderson and Stokoe (1978) found that coarse sand exhibits a low-amplitude shear modulus that increases linearly per log cycle time. In saturated sands, normalized tip resistance after blasting increases with time by up to 18% whereas local friction decreases by 39% in the same time period (Charlie et al. 1992). Under high pressure at room temperature, clean sand was found to have developed significant intergranular adhesion bonds (Lee 1977). Field observations at Jebba Dam project in Nigeria showed a substantial increase in penetration resistance in sand, weeks after blasting or vibrocompaction, even though density changes in soil were complete (Mitchell and Solymar 1984). Similar results were observed in laboratory setting where cone penetration resistance of loose sand increased with time after blasting (Dowding and Hryciw 1986).

While soil stiffening has been extensively measured in the field and in the laboratory experiments, the mechanisms behind it and variables controlling it remain a subject of intense research (Baxter and Mitchell 2004). It has been well established that in dry granular soil, creep is an important contribution to soil aging over engineering

timescale. From field and laboratory results, it was hypothesized that granular soil underwent macrolocking, where grains were more efficiently packed under load, and microlocking, where surface roughness caused an increase in sliding resistance (Mesri et al. 1990, Schmertmann 1991, Joshi et al. 1995, Bowman and Soga 2003). Joshi *et al*., however, acknowledged that in submerged conditions, a portion of the increase in penetration resistance of sand cannot be attributed to rearrangement of particles and speculated that dissolution and precipitation of salt and possibly silica may be involved. The presence of fines in dry sand was found to increase creep strain and aging rate and a discrete element model developed for aging in dry sand supports this hypothesis (Wang et al. 2008, Wang and Tsui 2009). Mechanical properties of granular assemblies at macroscopic level are known to be affected by contact networks, on one hand, and the local response of grain contact neighborhoods on the other (Parry 2004). In the latter case, the response is determined not only by the material itself, but also by how grains of the material interact with each other under stress. Such interactions are not purely mechanical, but are coupled with chemical processes such as dissolution, precipitation, polymerization and gelation of materials around contact region (Hu and Hueckel 2007a, Hu and Hueckel 2007b, Soulie et al. 2007). Therefore, we claim that from strain and stress alone one cannot accurately predict the long-term mechanical properties of even perfectly granular materials.

Grain material within a stressed and submerged contact area undergoes evolution following two distinct mechanisms beyond the range of the grain elastic deformation. The first mechanism, past the elastic limit, the grain in the zone of contact exhibits micro-cracking resulting in an inelastic deformation. The second mechanism, mineral mass dissolution rate increases above the background level as a result of an additional inter-phase interface surface area being generated through micro-cracking. At constant stress, the softening of the grain due to mass dissolution is counterbalanced by irreversible strain hardening. In nature, processes of dissolution and redistribution of mass in granular media may occur on a geological timescale, such as the formation of sandstone by amorphous mass that binds the sand grains together (Worden and Morad 2000). However, experiments and various engineering geotechnologies have shown that such processes can also occur on a time scale of weeks or months (Denisov and Reltov 1961, Meyer et al. 2006, Hu and Hueckel 2007b).

Silica is the most abundant element in the Earth's crust. Common soils are made mostly of sand, which in turn is mostly quartz or SiO_2. Although quartz is almost insoluble in water (Iler 1955), experiments indicate that water presence and flow can significantly reduce the strength of quartz, though the mechanisms behind such phenomenon are still not well understood (Gratier et al. 2009). However, it was also shown that in some cases the dissolution and re-deposition of silica at intergranular

contact in sand can improve the strength of quartz by as much as hundreds of kPa (Mitchell 1993). This water-silica paradox was partly what motivated this research.

One of the early hypotheses explaining the changes in strength of sand was put forward by Denisov and Reltov (1961), who conducted experiments indicating that strength of compacted submerged granular medium increased gradually due to formation of silicic acid gel on top of undisturbed silica layer and acted as cementing bonds that provided adhesive force between sand grains. On the other hand, in studies of pressure solution it was noticed that the presence of clay in the vicinity of contact enhances substantially dissolution of quartz and the ensuing compaction of sediments (Becker 1995, Bjorkum 1996, Kristiansen et al. 2011). Much more recently Atomic Force Microscopy (AFM) and Scanning Electron Microscopy (SEM) studies of stressed silica-muscovite contact have shown indeed almost an order of magnitude higher silica dissolution rate (Houseknecht et al. 1987, Meyer et al. 2006).

This research is based on the hypothesis that the mechanism through which a submerged granular material stiffens in stressed conditions consists in generation of micro-cracking near the intergranular contact and micro-cracking constitutes a source of an increasing surface area of the inter-phase interface from which dissolution of quartz occurs. The dissolution removes the material from the solid phase, making the material in that zone weaker, and further enhancing the process of micro-cracking (Hueckel et al. 2001). The dissolved mineral may either migrate away in the presence of advective

gradients (open system) or, in their absence, when local concentrations grow sufficiently, precipitate, polymerize, or gelate (close system).

Recent work by Israelachvili and co-workers at University of California, Santa Barbara (Meyer et al. 2006, Greene et al. 2009, Kristiansen et al. 2011) has shown that a difference in electrochemical surface potentials between muscovite mica sheet and silica surfaces is the driving force behind the accelerated dissolution of silica. Muscovite clay particles are present in different quantities in most soils. It is possible that under stressed conditions, silica grains dissolve locally in the presence of muscovite and re-precipitate to other muscovite-free surfaces as silica gel structures, connecting between silica grains and therefore enhancing the macroscopic mechanical properties of sand soil. Verifying this hypothesis of soil aging is another motivation for this research. To investigate the role of muscovite mica in soil aging, both mica powder and mica sheet were incorporated in grain-to-grain crushing experiment as well as macroscopic soil experiment such as consolidation and penetrometer tests.

2. Objectives and Tasks

The main objectives of this research are:

- To examine the chemo-mechanical mechanisms behind the time-dependent behavior of silica grain aging in the presence of silica solution.
- Specifically to verify, through experiments, the hypothesis that silica surface structures such as silica polymers generated through the local dissolution and re-precipitation of silica is a noble mechanism to increase soil stiffness and strength over time.
- To quantify the evolution of mechanical properties, such as tensile strength, elasticity, and adhesive strength, of individual silica polymer links growing naturally between silica grains in stressed contact region.
- To develop a theoretical model incorporating relevant parameters to estimate and predict in-situ soil properties based on laboratory testing.
- To verify the postulation that different electrochemical potential between surfaces stimulates and accelerates silica dissolution.

This work focuses on the soil aging processes in several laboratory-simulated micro-, meso-, and nano-scale experiments. The main tasks include:

- To identify microscopic physical, chemical, and mechanical processes and corresponding variables during soil aging. The level of pH in water, surface area of grains, as well as grain arrangement may all have effects on how silica is dissolved and

precipitated. Silica grain space is to be saturated in different solutions and compressed under various pressure and orientations to identify any change in silica precipitation behavior.

- To develop an understanding of mechanisms governing the microscopic processes and growth of silica gel structures near the stressed contact. Different imaging techniques and aging experiments will be adopted and results examined.
- To quantify the strength of silica polymer bonds on silica grains, the use of AFM pulling for individual polymer branch strength and of Grain Indenter-Puller for intergranular tensile strength should help with determining the above values. Comparison of such data provides insight into how different variables in experiments contribute to growth of silica surface structures.
- To verify the effect of mica on soil aging, including silica dissolution and precipitation rate. In recent developments muscovite mica particles were discovered to stimulate silica dissolution by electrochemical potential difference across different contact surfaces. Mica powder and mica sheet are to be introduced in grain crushing experiments for SEM imaging and grain pulling tests.
- To establish force vs displacement relationships for silica polymers between silica surfaces in semi-contact. Polymer network length at failure and its strength are to be analyzing the force vs displacement curves. These results are expected

to provide the most direct evidence that the presence of silica polymers and gel create an adhesive force between silica grain surfaces.

3. Outline of the Experimentation Strategy

Since soil aging is a multi-scale problem, the mesoscopic properties of silica gel structures and their effects on microscopic mechanical properties of silica grains are to be investigated separately. Using Atomic Force Microscopy (AFM), pulling experiments are conducted on individual silica polymer fibers to test their tensile strength. Various AFM cantilever tips are used to map small stressed contact regions between silica grains and to reach in to crack trenches to hook up nano-structures that cannot be studied otherwise. This technique allows surface mapping to be conducted in early stages of silica gel growth with a nanometer scale resolution to detect extremely small silica polymers. Operating in a custom-made fluid chamber, the disturbance to structures on grain surfaces by AFM would be minimal.

To study mechanism of precipitation and polymerization of soil aging in solution, Scanning Electron Microscopy (SEM) is used to capture silica structure images in the micrometer scale, revealing a microscopic picture of how silica polymers connected different surfaces. A Pneumatic Grain Indenter is used for this purpose, pressing together two silica grains in a fluid chamber with controlled silica concentration in solution. A series of grain crushing experiments are conducted to investigate the effects of silica gel structures on couples of silica grains. Small silica grains are pressed together over weeks by a constant pressure in a fluid chamber

containing solution with various concentrations of silica ions to obtain SEM images of silica structure growth.

On a microscopic scale, intergranular tensile strength of silica gel structures growing between silica grain contacts is measured via a self-designed Grain Indenter-Puller (GIP) as well as a Micro-Strain Analyzer (MSA). To use the Grain Indenter-Puller, silica grains are oriented such that a sharp corner of one grain is in contact with a flat surface of another grain to simulate real-life scenarios where micro-cracks and debris are generated on sand grains by uneven loading. After an aging period is completed, the device is connected to a load frame and an analytic scale to measure tensile force between the grains during separation. The force required to separate two silica grains after weeks of stressed contact in silica solution is an indication of the microscopic tensile strength of structures growing between silica grains.

MSA, on the other hand, is used to investigate aging of contact between two silica grains when flat surfaces of grains are in contact with each other. Two silica grains are pressed together by a mounting stage for a few weeks in silica solution to simulate aging at low stress. At the end of aging, the stage was mounted to MSA and slowly separated. The force required to separate the grains can be measured and plotted against separation distance between the two grain surfaces.

In both Grain Indenter-Puller and the MSA methods, different amounts of muscovite mica powder are added to the silica solution. This creates a presence of mica

in the vicinity of the silica contact region in order to investigate the role that clay particles play in soil aging. Other than mica powder, mica strips were also inserted between grain contacts to generate silica-mica-silica contacts and to compare with results from silica-silica contact scenarios. It was observed in early experiments that silica polymers grew primarily between mica sheet and silica surfaces near stressed contact region, likely due to electrochemical potential differences between mica and silica surfaces (Kristiansen et al. 2011).

4. Literature Review

4.1 Chemistry of silica

Silica has a very low dissolution rate in water. According to Krauskopf, who provided a state of the art on silica dissolution and precipitation, the dissolution of amorphous silica at room temperature is between 100 – 140 parts per million (ppm) whereas at 90 °C its dissolution rises to 300 – 380 ppm. It is understood that the solubility of silica remains largely constant between pH 0-9 but increases significantly at pH > 9 (Krauskopf 1956).

However, some slightly different data on solubility of amorphous silica was offered later by Iler in a comprehensive review of laboratory data on silica solubility (Iler 1979). At room temperature, the solubility of amorphous silica ranges from 70 to more than 150 ppm. Such wide range of solubility is due to many factors such as silica particle size, state of internal hydration, and the presence of other minerals. The solubility possibly reaches a minimum at pH 7-8, but the reasons behind the slightly higher solubility at lower pH values are unknown.

According to Iler, silica dissolution occurs in an excess of water in the following chemical reaction:

$$SiO_2(s) + 2H_2O(l) = Si(OH)_4(aq)$$

Because the soluble form of silica on the right hand side of the equation contains only one silicon atom, it is often named monosilicic acid. The most common form of

monosilicic acid, as found during both amorphous silica and crystalline silica dissolution, involves one silicon atom coordinated with four oxygen atoms. OH^- ions acted as catalyst in the hydration and dehydration of silica:

$$(SiO_2)_x + 2H_2O = Si(OH)_4 + (SiO_2)_{x-1}$$

Silica sand is a common example of crystalline silica, or quartz. According to Iler (1979), the solubility of SiO_2 in crystalline silica is 6 ppm. More recent work has shown that at 25 °C, quartz has a solubility of around 10 ppm (Rimstidt 1997).

On the other hand, it is widely accepted (see e.g. Iler 1979) that amorphous silica has a much higher solubility compared to crystalline silica, because amorphous silica has a more open surface structure, allowing more hydroxyl ions to replace silicon atoms. Silica surface bears an ionic charge which attracts hydroxyl ions in water and a silicon atom is exchanged into solution as a form a soluble silica. The solubility of anhydrous nonporous amorphous silica oxide is 70 ppm at 25 °C. Fused glass (amorphous silica) has a dissolution rate of 39 ppm/day whereas quartz has a dissolution rate of only 2.8 ppm/day. However, most common amorphous silica exists in very small particles that form porous aggregates with hydrated SiOH groups on the surface. Thus solubility of SiO_2 in powders and gels made with amorphous silica ranges between 70 to 150 ppm and remains largely unchanged between pH 2 to 8. However, solubility of amorphous silica in water increases drastically at higher pH. This is because at higher pH, soluble

silica includes both the monomer mentioned above and silicate ions which form in higher pH as shown in the equation below:

$$Si(OH)_4 + OH^- = Si(OH)_5^-$$

At pH values higher than 10.7, $Si(OH)_4$ is converted to ions and all solid phase amorphous silica dissolve to form soluble silicate (Alexander et al. 1954, Iler 1979).

In the presence of low concentration NaCl ions in water at neutral pH, the surface reactivity of dissolved amorphous silica is enhanced and thus the dissolution rate of amorphous silica is found to be about twenty times higher (Icenhower and Dove 2000). Due to the fact that silica dissolution rate is very slow, super-saturation or under-saturation of silica in water can exist for long periods of time before reaching equilibrium by precipitation or dissolution. In super-saturated solutions, silica changes to a sol in a process that could take weeks or months and such sols at a few hundreds ppm can remain stable (Krauskopf 1956).

Iler schematized the polymerization and gelation of silica into three steps. First, monomers ($Si(OH)_4$) polymerize to form particles by condensing silanol groups into siloxane (Si-O-Si) bonds as shown below:

$$-SiOH + HOSi- = -SiOSi - + H_2O$$

Second, the particles are subsequently allowed to grow by extending the siloxane bonds. Third, at low pH (<7), silica particles are able to aggregate into branches and ultimately gel structures because they possess little ionic charge. As shown in previous work, silica

aggregates in the order of 10 nm form after a week in a super-saturated solution, and significant gel network is observed a week later (Guo and Hueckel 2013).

4.2 Soil aging in dry conditions

Some form and extent of aging is seen in soils that does not involve water. Hence, predominantly mechanical particle rearrangement are postulated as causing mechanisms of aging. Specific physical (or chemical) driving processes behind particle system rearrangement under constant load and their rates are not well known, and are hypothesized to be mostly local, interparticle processes: time-dependent interparticle friction, plastic yielding of grain asperities following a low rate chemical reaction (Eyring 1936, Kuhn and Mitchell 1993), capillary condensation of atmospheric moisture (Paterson and Kekulawala 1979, Israelachvili 2011), plastic or viscoplastic microcracking due to indentation in the contact area (Scholz and Engelder 1976, Tada et al. 1987, Hickman and Evans 1995, Hu and Hueckel 2007a). However, the links between such microscopic and localized processes and possibly ensuing reconfiguration of particle chains, and then the strengthening of soil at a macroscale, while very likely, are far from being proven, as stressed by Kuhn and Mitchell, 1993. Still efforts using numerical tools to show that such hypothetical microscale mechanisms are consistent with the upscaled macroscopic behavior of soils (see *e.g.* Kuhn and Mitchell, 1993; Hu and Hueckel, 2007a).

A numerical model of contact creep in dry, clean sand was developed by Wang *et al.* (2008), which simulated sand particles undergoing a homogenization process under load. These authors focused on purely mechanical aspects of aging and found that contact creep resulted in a redistribution of contact forces, allowing more stable force

chains to be established with limited decrease in porosity. Such behaviors caused increases in small-strain stiffness over time. The model was further developed to include loose and dense sands under various pressures, effect of unloading-reloading cycles, and how fines could increase aging rate due to higher creep in Wang and Tsui (2009).

4.3 Soil aging in saturated conditions

The hypothesis that dissolution and precipitation of silica led to the formation of silica films between sand grains and created a cementing effect was first brought up by Denisov and Reltov in 1961. They measured the amount of force required to displace a sand grain on quartz or glass plate in water over time. From the experiments it was concluded that "the gradual strengthening of sands in hydraulically placed embankments is due to the formation of silicic acid gel films on the surface quartz grains".

Mitchell and Solymar (1984) have reviewed an evidence showing a time-dependent stiffening and strengthening of soil in laboratory setting and field observations prior to 1984. They conducted several tests on soils in the foundation of the Jebba Dam in Nigeria, and found that the penetration resistance of saturated clean sand on site increased significantly eleven weeks after blasting. They stated that such time-dependent behaviors cannot be attributed to excess pore pressures or explosive gases and suggested that cement bonding had developed at particle contacts.

Schmertmann (1991) suggested that secondary compression was an important part of soil aging. He demonstrated that the strain of soil, ϕ'', a basic soil frictional strength, increased over time for up to five weeks using an IDS test designed by himself. The paper suggested that aging phenomenon in sands was frictional and was due to sand particles interlocking more effectively in compression, resulting in increases in the

frictional component of sand's shear resistance. However, the author did not attempt to study sand grains contact surfaces and pore fluid to rule out possible cementation or bonding of silica materials.

Similar hypotheses were stated by Mesri *et al.* (1990) and Bowman and Soga (2003). Mesri and co-workers suggested that particles continued rearranging themselves during secondary compression and developed higher frictional resistance to deformation through increase in interlocking of particle surface roughness topography and more efficient packing of particles. They proposed an empirical equation they claimed satisfactorily predicted an increase in shear modulus and penetration resistance after primary consolidation. However, there was no direct evidence to reject or accept the hypothesis that silica precipitated and bonded sand grains together.

Bowman and Soga (2003) conducted a series of triaxial tests on dense granular soils to examine their creep response and found that particles rotated and aligned to form tighter clusters and different local void ratios. A model was developed suggesting that frictional slippage of particles contributes to soil aging.

In saturated conditions, sand exhibits a 200% (with sea water) to 220% (with distilled water) larger penetration resistance after one year of aging compared to 30% larger penetration resistance in dry conditions (Joshi et al. 1995). Joshi and co-workers stated that, while the increase in penetration resistance of dry sand is due to secondary compression and rearrangement of grains, precipitation of salts and silica and

cementation cause large increases in penetration resistance in saturated state. Scanning electron microscopy images show large amount of precipitates bonding between sand grains when soil is aged in a submerged state. It is worth mentioning that the solution used in some of those experiments had a pH value of 8.4. While the solubility of amorphous silica above pH 8 is significantly higher, precipitation, however, becomes more difficult. Hence, the mechanisms of aging in saturated condition are not purely mechanical, but are coupled with much more significant chemical processes such as dissolution, precipitation, and possibly polymerization and gelation of materials around contact region (Hu and Hueckel 2007a, Hu and Hueckel 2007b). We are confident that aging phenomenon due to precipitation such as observed by Joshi and co-workers would be even more pronounced in solutions with lower pH values.

In a series of sand aging experiments conducted by Baxter and Mitchell (2004), small strain shear modulus was found to have increased over time. Electrical conductivity measurements and mineralogical studies of pore fluid in sand indicated that there was dissolution of carbonate and silica. But corresponding small strain shear modulus data did not mirror a higher value, prompting the authors to suggest that dissolution and precipitation of carbonate and silica were not responsible for aging phenomenon. But in this series of experiments, the silica used and tested was in the form of quartz SiO_2, which had significantly lower solubility comparing with amorphous

silica. Therefore the amount of silica precipitation in this setting was expected to be lower than if amorphous silica was used.

Hu and Hueckel (2007b) argued that in saturated conditions, creep of material under stress was also linked to damages to grains and subsequent mineral dissolution. Mass removal due to dissolution and precipitation at stressed contacts caused chemical softening of material at damage sites and strain hardening at precipitation sites. Creep, in this case, was interpreted in terms of dissolution and precipitation mechanisms.

Quartz cementation in natural sandstones was well documented but its origin and the controls on its distribution were still uncertain. In nature, the processes of dissolution and redistribution of mass in tight rocks takes time on the geological scale, such as during formation of sandstone by amorphous silica mass that binds the sand grains together (Worden and Morad 2000). Worden and Morad identified temperature, pressure, and presence of clay as factors strongly related to quartz cementation. It was interesting that the authors believed clays would inhibit quartz cementation by coating over clean substrates that were needed for cementation to grow.

Interestingly, in terms of compressibility decline monitored during three months, up to 85% of the change occurs in the first two weeks of the process (Hueckel et al. 2001). Similar conclusion in terms of mass transfer was reached by Oelkers *et al.* (Oelkers et al. 2008).

Soulie et al. (2007) used unloaded sand in a water solution saturated with sodium chloride to demonstrate that bonds formed from crystallization of salt at grain contacts enhanced mechanical strength of the soil. Samples of unloaded clean sand were mixed with water saturated with sodium chloride and allowed to evaporate, creating cemented bonds between local grains. In the test times ranging from 15 minutes to 20 hours, the macroscopic strength of soil was considerably higher, reflected from the magnitude of force required to rupture the sample.

A model of aging sediment with evolving secondary structure was developed by Hueckel *et al.* (2001) where the development of secondary structures had four phases. In the first phase, irreversible aging strain was developed during dissolution of soil grains under stress. High concentration gradient formed around grains and precipitation occurred in unstressed solution, which was the second phase. In the third phase, further compression caused failure to primary structure and, possibly, secondary structure that was just formed. In the last phase, during sample retrieval, tension formed between grains and led to failure of the precipitate.

A three-scale numerical model was built by Hu and Hueckel (2007a) to study mineral dissolution in stressed grain contact regions with asperities developed from irreversible damages. At the micro-scale, rigid chemo-plasticity was applied to grain contacts under stress. Mesoscopically, intergranular forces due to precipitation of minerals acted on granular systems. The effect on soil porosity and stiffness was studied

at the macro-scale. Cross-scale transfer functions of mass dissolution and precipitation were proposed.

Research showed that a thin film of silanol and silicic acid chains would develop on amorphous silica surfaces in the presence of water (Vigil et al. 1994). Oedometer tests conducted on dense Ottawa sand in the presence of biofilms showed no difference on the ultimate shear strength of the sand (Perkins et al. 2000). However, this result was contradicted by another research which stated that the addition of biofilms for a few days had caused a statistically significant increase in the shear strength of Ottawa sand (Banagan et al. 2010).

4.4 Effect of clay

Another factor that affected silica dissolution in stressed granular contacts was the presence of clay (muscovite) particles, as noted by Becker (1995) and Bjorkum (1996). Both papers exhibited images of muscovite mica grains penetrating deep into adjacent quartz silica grains in sandstones. In addition, Bjorkum claimed that pressure in the silica-mica contact that lead to silica dissolution is small, and that silica precipitation is the rate-limiting factor in quartz cementation process. Similar observations are made in sandstones in the presence of mica (Heald 1955, Renard et al. 1997). Heald noted that muscovite penetrates quartz grains in large quantities whereas quartz hardly penetrates into muscovite and postulated that the silica dissolved in sandstone may have created cementation effect.

Calcite ($CaCO_3$) crystals are found growing between two closely apposed mica surfaces under pressure in calcium solutions when the bulk solution is under-saturated with calcite (Alcantar et al. 2003). More recently, Israelachvili and co-workers at University of California, Santa Barbara discovered that the presence of muscovite mica creates a difference in electrochemical potentials between silica contacts and thus induces dissolution of silica. A surface forces apparatus was used to study the thickness of silica layers in contact with mica or other silica contacts, and discovered that dissolution of silica is accelerated significantly when there is a difference in electrochemical potential, even between silica-silica contacts (Meyer et al. 2006).

However, no attempt was made to study where the dissolved silica went. But they postulated that fragile silica gel could have grown between contacts. This postulation was later built into an electrochemical corrosion model where they proposed that silica gel grew in micro-pits developed on quartz grains between stressed mica and quartz contact (Greene et al. 2009).

In another paper published by the same group, Kristiansen *et al.* (2011), it was stated that pressure, apart from bringing surfaces into contact, did not have any significant effects on silica dissolution, similar to a statement made by Bjorkum (1996). They also revealed that using solutions with low pH values (<3) would reduce the latency period of silica dissolution without altering the end result, thus increasing the time efficiency of experiments involving silica dissolution.

5. Experimental Methods

Five different experimental methods studying effects of silica gel growth in the vicinity of stressed silica grains contacts on intergranular tensile strength were used in this research. Since soil aging is a multi-scale problem, experimental methods used in this research aimed to study silica structures and granular soils and both mesoscopic, and microscopic scales, with future implications into macroscopic scale. Super-saturated silica solutions were studied for early-stage silica gel growth rate as well as silica polymer tensile strength using Atomic Force Microscopy (AFM). Pneumatic grain crushing experiments were conducted to study the growth of silica structures around stressed grain contacts by Scanning Electron Microscopy (SEM). Aging and subsequent pulling experiments were conducted using self-designed Grain Indenter-Puller (GIP) to measure granular bonding force silica structures exerted on neighboring silica grains. Micro-strain testing was performed using Micro-Strain Analyzer (MSA) to measure the same bonding force between silica grains, as an alternative method to GCP. Finally, muscovite mica was added to silica solution and aging experiments were then conducted to investigate effect of mica on silica dissolution and precipitation.

Quartz grains in stressed contact were simulated using amorphous silica grains. In granular soil, sand grains are randomly packed and experience stressed contacts at various angles with neighboring grains, as represented by Figure 1.

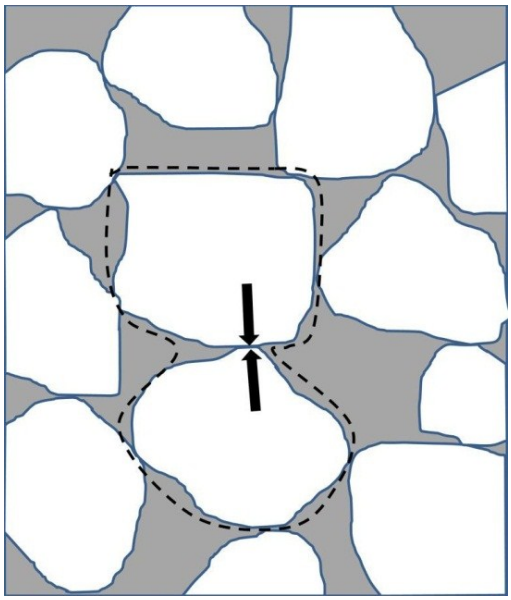

Figure 1: Granular assembly of sand grains. Arrows indicate one stressed contact developed by the two grains in dotted line.

Silica is found in both crystalline and amorphous forms in nature. Crystalline silica has long-ranged orders, involving a tetrahedral coordination of four oxygen atoms around a silica atom. Quartz is by far the most common crystalline form of silica found in natural sand (Iler 1955). Amorphous silica, on the other hand, does not have any long-range order, but a tetrahedral arrangement between oxygen and silica atoms still exists locally. The choice of using amorphous silica for experiments in this research was motivated by two substantial considerations. First, the rate of dissolution of amorphous silica is about one order of magnitude greater than that of its crystalline counterpart (Iler 1955). It appears that higher silica dissolution rate would not only reduce the time of the experiments, but also lower the risk of biological contamination, since grains were to be kept in stressed state for three to four weeks in saturated condition at room temperature.

Second, most quartz grains in nature, which are predominantly crystalline, are enveloped by a layer of amorphous quartz (Oelkers et al. 1992). It is believed that such an envelope is generated by silica dissolved from rocks in the presence of mica (muscovite). Hence, for two grains in contact, the indentation of an asperity would penetrate first through the amorphous coating, creating surface contacts between amorphous silica.

The silica grains used in this research were made of unpolished amorphous quartz (Prism Research Glass Inc, NC) and came in two sizes: 1.5 mm by 1.5 mm by 1.5 mm (Figure 2), and 3 mm by 3 mm by 3 mm (Figure 3).

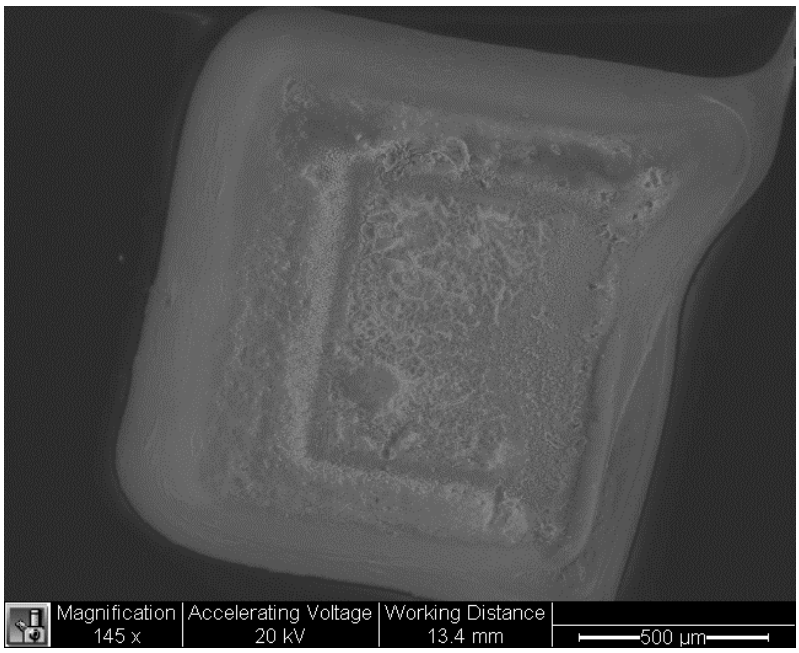

Figure 2: a clean 1.5 mm by 1.5 mm by 1.5 mm amorphous silica grain under SEM with 55x magnification.

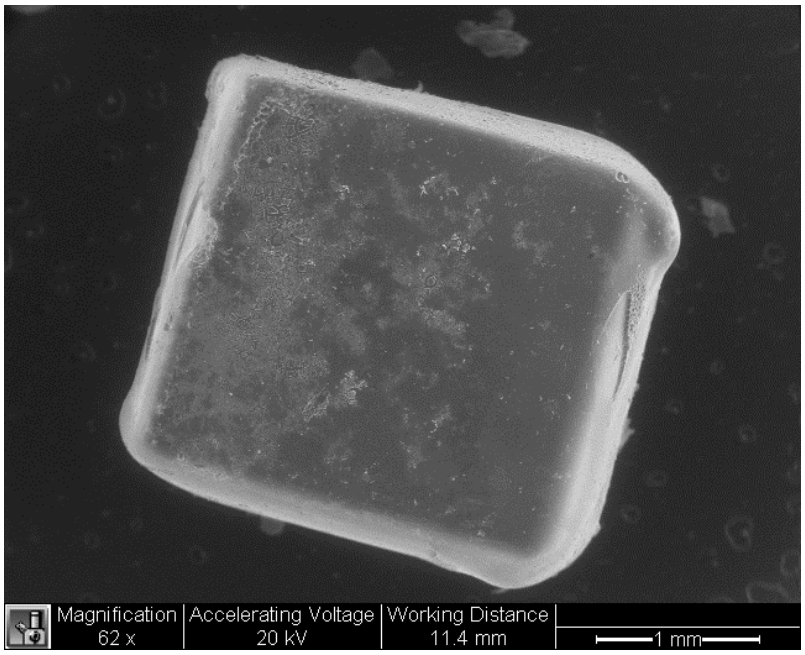

Figure 3: SEM image of a clean 3 mm by 3 mm by 3 mm amorphous silica grain, 62x magnified.

As can be observed from the above two figures, silica grains used in this research did not have perfectly sharp edges with smooth surfaces, most likely due to laser cutting during manufacturing that created high local temperatures and melted some silica to produce relatively round edges, irregular length, and inclination. Although effectiveness of such edges as indenters were reduced by the round edges, most natural sand grains do not have perfectly sharp edges anyway.

5.1 Silica gel studies

It is postulated that in stressed contact regions between silica grains, local concentration of silica in solution might exceed the saturation level even though overall concentration of silica in solution is still below saturation level. To recreate this scenario under laboratory conditions, since the dissolution rate of silica is extremely low, it would be far more efficient time-wise to have silica grains submerged in a solution that already contains an elevated level of silica ions near the saturation level. Thus when silica grains are under stress, a much smaller amount of silica dissolution is needed to bring local concentration of silica between grains higher than the saturation level to trigger precipitation of silica.

In the initial stage of this research, conducting experiments with solutions containing silica ions concentration that is higher than the saturation rate also serves as an initial validation of our hypothesis. If initial experiments showed evidence of silica gel growth in solution with higher concentration of silica ions, it is more likely that silica will dissolve in stressed contact regions and precipitate to form gel structures between grains.

The solubility of silica is not significantly affected by pH values in the range of 2-9, but is considerably greater and proceeds much more rapidly at pH > 9 (Krauskopf 1956). Therefore for this research, a super-concentrated solution of silica ions was produced and maintained at a very high pH (>10.0) as a mother solution so that silica in

the solution would stay in ionized state. From this mother solution, solutions containing different silica ion concentrations can be made at any time with lower pH values.

Solutions containing silica ions were prepared to simulate soil pore fluid following the process described by Rimstidt and Barnes (Rimstidt and Barnes 1980). A 500 ml solution of 500 ppm silica ion concentration was made by ionizing 0.696 g of amorphous silicic acid powder (H_2SiO_3, Fisher Scientific) in 2 ml of 5 M NaOH solution mixed with 8 ml Nano-Pure Water under constant stirring at room temperature for 24 hours. After silicic acid powder had been completely ionized, the solution was then diluted with 490 ml of water to make a 500 ml mother solution with 500 ppm silica ion concentration. The pH value of this solution was 10.5. Subsequently, solutions with different silica ion concentrations were made from the mother solution by diluting it with water. 1 M nitric acid (HNO_3) or 1 M sodium hydroxide (NaOH) were used to control pH values of the test solutions.

As an initial validation of our hypothesis, an exploratory experiment was conducted to check if silica gel structures could grow from solutions containing high concentration of silica ions. 40 ml of solution containing 500 ppm silica ion concentration was taken from the mother solution with its pH value brought down to 5.0. It was stored in a petri dish at room temperature, sealed off by Parafilm to minimize water evaporation. After two weeks, a transparent gel formed at the bottom of the petri dish, confirming that gel structures would grow in supersaturated solution.

This gel was initially put directly in SEM (FEI XL30 ESEM) high vacuum mode for analysis but the near-vacuum chamber accelerated water evaporation process in the gel. Since water has high surface tension, the gel structure completely collapsed as water evaporated in vacuum. The hydrogel was crystallized to powder before meaningful images can be taken. Thus subsequent silica hydrogel was treated in Critical Point Dryer (Bal-Tec CPD 030) where water in gel was replaced by acetone, and acetone was subsequently replaced by liquid CO_2 and evaporated at its supercritical point to change the hydrogel into aerogel while retaining its structure (Schott et al. 2009). The aerogel was then sputter coated with gold for 120 seconds in a Dielectric Sputter System (Kurt Lesker PVD 75) to enhance the resolution of images taken in SEM by increasing surface electrical conductivity.

5.1.1 Atomic force microscopy

To study early growth rate of silica gel in solutions containing elevated levels of silica ions, an Atomic Force Microscopy (Digital Instruments Dimension 3100) with a Veeco TESP k cantilever was used to scan undisturbed solution containing silica ions, aiming to detect and measure silica nuclei formation. In AFM fluid imaging mode, a cantilever is submerged in water and sweeps across a designated area on a substrate, mapping its contour. The substrate is made from mica and a few layers are torn off using sticky tapes to ensure smoothness on a molecular level. A drop of solution containing silica polymers is diluted with water and dropped onto the substrate for

imaging. As the cantilever sweeps across the substrate, any objects on the surface will cause the cantilever to deflect and thus show up on the resulting image.

The same cantilever was also used in AFM pulling experiments to study the tensile strength of individual silica polymers growing on silica surfaces in solution. In pulling mode, the cantilever was repeatedly pushed onto substrate surface and lifted up, picking up silica polymers in the solution on its tip by effect of surface attraction forces. As the cantilever was lifted up, the silica polymer that it picked up was stretched and broken, exerting a tensile force on the cantilever that made it deflect to different angles. The deflections were measured and converted to force using the cantilever's elastic modulus. Hence the length and tensile strength of individual silica polymers can be estimated.

5.1.2 Scanning electron microscopy

It was discovered later that silica hydrogels could be kept intact in SEM under Variable Pressure Mode for 10 to 20 minutes before gel structure was destroying by drying. Traces of water vapor was introduced to the SEM chamber which reduces both water evaporation rate and electron charging on surfaces by enhanceing surface conductivity for better image resolution. Imaging of silica polymers and gel structures growing between silica grains after aging using SEM became possible. SEM imaging provide a much larger viewing area (up to 1,000 times) than AFM scanning and is extremely useful in visual observation of in-situ silica gel growth.

5.2 Pneumatic grain indenter

To test the hypothesis that silica gel structures grow in the vicinity of stressed contact regions between silica grains, silica surfaces need to be pressed together under pressure in solution containing different levels of silica ions to simulate soil pore water. Since sand is a granular material, each grain is in contact with its neighboring grains at different contact angles. A simplified contact model was developed in laboratory, shown in Figure 4, where the grain on top was pushed down at a constant force with one of its flat sides facing the edge of the other grain at the bottom.

An apparatus used to simulate sand grains in stressed contact in fluid needs to have the following characteristics: it needs to be able to apply a constant pressure on the grains for up to four weeks; it needs to have a fluid chamber sealed off from the environment to minimize water evaporation over long periods of time; the chamber has to be small enough to fit in the chamber of SEM and AFM.

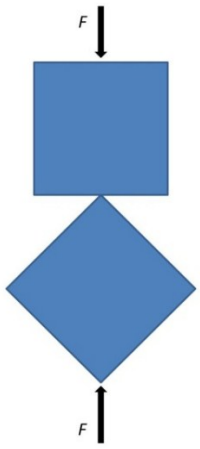

Figure 4: Simplified contact model of two isolated silica grains in contact in granular material.

Following the above mentioned design principles, a pneumatic grain crushing device was designed by Casey Rubin at Duke University and improved by the author in which two silica grains can be pushed together under pressure in a fluid chamber with the same orientation as described in the laboratory model (Rubin 2009). The configuration of the apparatus and the fluid chamber unit are shown in Figure 5 and Figure 6.

The fluid chamber is made with stainless steel to prevent rusting. The chamber is a separate unit and can be secured to a sturdy steel platform by seven screws around the edges. In the chamber, one silica grain is secured on a raised platform to the one side with one edge pointing to the other side. The other grain is clamped by a pincer and has a flat side in contact with the other grain's edge.

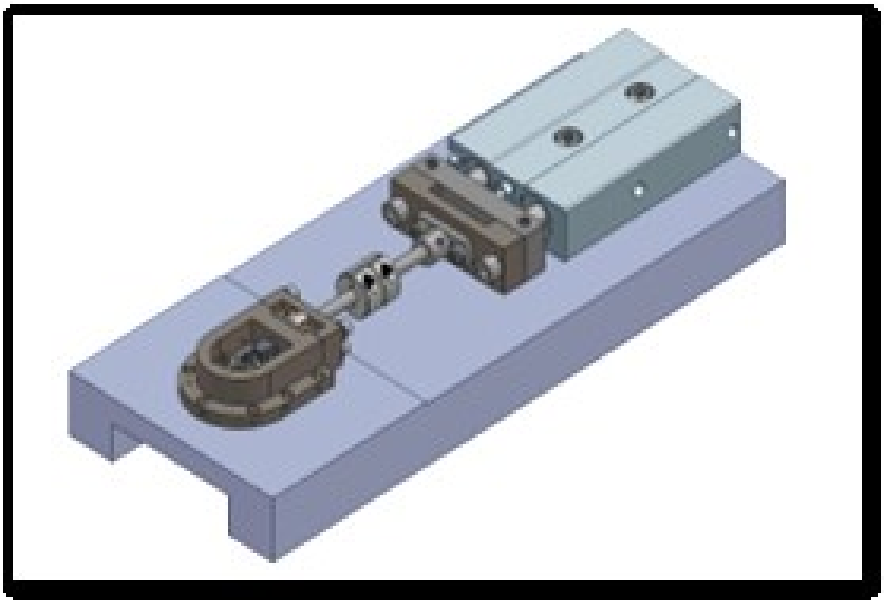

Figure 5: CAD rendering of pneumatic grain indenter (Rubin 2009).

A stainless steel shaft (Misumi, USA) goes through an O-ring to prevent water leakage and connects the pincer to a pneumatic actuator (Bimba TB-1625). Around the shaft there is a locking mechanism that secures the shaft in place by screwing tight a collar to the fluid chamber so the whole device can be detached from the pneumatic actuator and brought under an AFM or SEM for imaging. The top of the fluid chamber is sealed with Parafilm and aluminum foil during experiments to minimize water evaporation so that silica ion concentration of the solution in fluid chamber would not change over time from the decrease of water volume. Pressure is controlled by a pneumatic regulator (Norgren Excelon Pro B92G). The area of interest would be the contact region between two grains in the fluid chamber. The chamber was compatible for SEM imaging and AFM imaging.

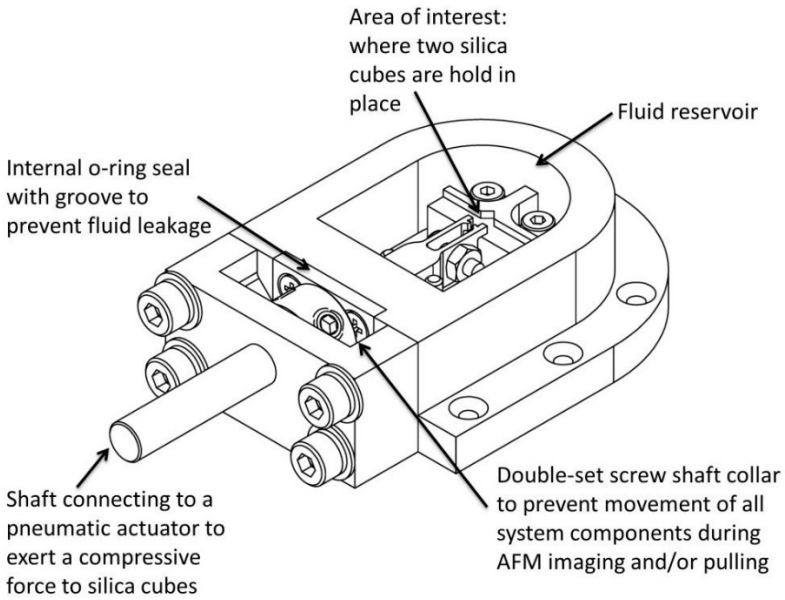

Figure 6: Detailed configuration of the fluid chamber in pneumatic grain indenter (Rubin 2009).

To perform a pneumatic grain indenting test, two amorphous silica grains with 1.5 mm x 1.5 mm x 1.0 mm dimensions were secured in the pincer and the platform (Figure 7). The shaft was then connected to the pneumatic actuator and pressure slowly increased to up to 170 kPa to prevent grains being crushed by the sudden movement of the rod. The fluid chamber was then filled with solution containing a certain level of silica ions and sealed by Parafilm and aluminum foil. At the end of the testing period which typically lasted two to four weeks, pressure from the actuator was gradually turned off. Solution was drained from the chamber and the chamber unit was taken out from the platform and transported to SEM or AFM for imaging.

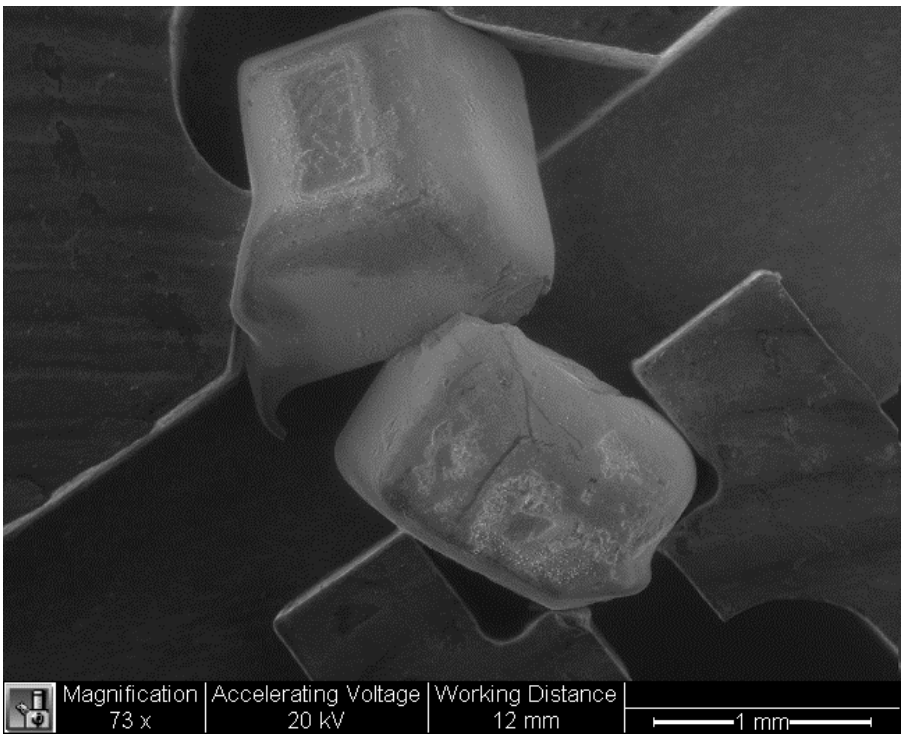

Figure 7: Amorphous silica grains in position in pneumatic grain indenter's fluid chamber unit, 73x magnification in AFM.

5.3 Grain indenter-puller

After studying the tensile strength of silica polymers, and silica gel growth in the vicinity of stressed silica contacts, the next step in the research was to study how the growth of silica gel affected bonding between silica grains. Based on our hypothesis, the growth of silica gel between stressed silica grain contacts must contribute a significant portion of bonding forces between silica grains to exhibit aging phenomena in soil such as increased compressibility over time.

An apparatus needs to be built where silica grains can be pressed together for up to four weeks under constant pressure in solution and then pulled apart at very slow speed while the pulling force was recorded. As the two grains are slowly separated, any gel structures attached to both grains would exert a tensile force to counter the pulling force applied to the grains until the structures breaks. Such sudden changes in forces would be reflected on the weight reading from the analytic scale. This way the bonding force due to the growth of silica gel between silica grain contacts can be recorded.

A Grain Indenter-Puller (GIP) was thus designed, as shown in Figure 8. Two silica grains are secured between the bottom and the middle metal plates. One grain sits on the bottom plate with an edge pointing upward. The other grain is fastened by screws onto the middle plate with a flat face facing downward. Four springs are placed between the middle and the top metal plates. Four long screws go through all three plates, securing them together with wing nuts on top. As the wing nuts are tightened,

the springs are compressed, exerting a constant downward force on the middle plate which holds the two silica grains together under constant pressure. The springs (McMaster-Carr) have a spring constant of 2960 N/m. The amount of force exerted by the springs can be calculated by multiplying the distance of compression (converted from the number of turns applied to the wing nuts) and the spring constant. The metal plates are made of aluminum to minimize weight and prevent rusting. All screws are made of stainless steel.

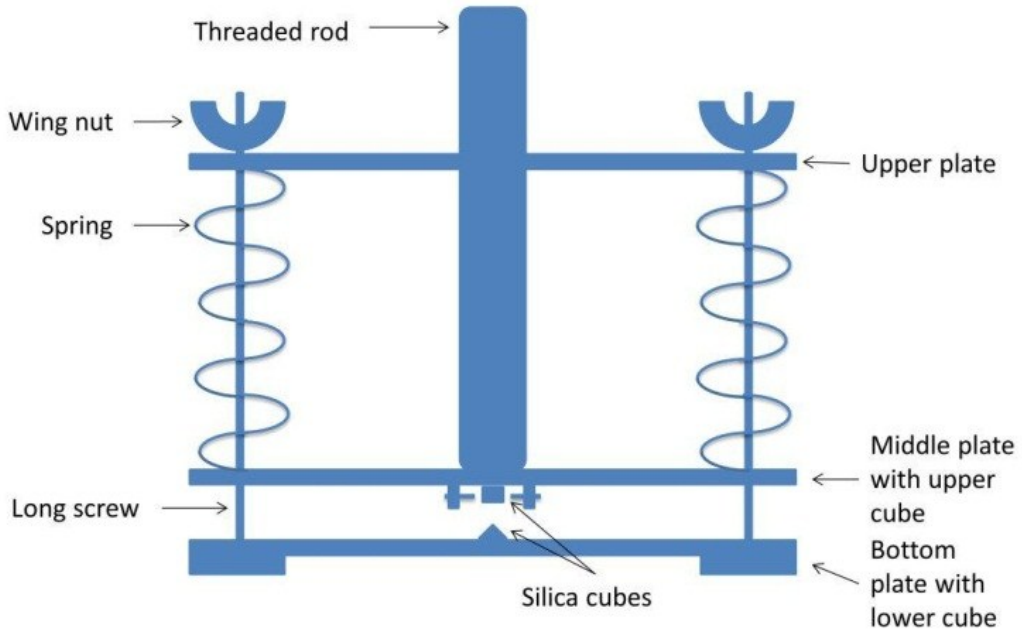

Figure 8: Schematics of Grain Indenter-Puller apparatus (not to scale).

To start an aging experiment, assemble the apparatus and tighten the wing nuts to compress the springs until up to 180 N of force is applied to the grains. The GIP with grains is then placed in an air- and water-tight polypropylene container (McMaster-

Carr), submerged in solution containing various concentrations of silica ions. The grains under stress are left to age for three to four weeks under a constant force from the springs. After the aging phase is completed, the apparatus is taken out of the container and attached to a load frame (benchtop universal testing machine, Tinius Olsen H50K-S) by a long threaded rod, as shown on Figure 9. Once the load frame brings the apparatus firmly in contact with an analytic scale (Mettler Toledo AL204), wing nuts, long screws, springs and the top plate are removed so that the two silica grains are now pressed together by the load frame through the long threaded rod.

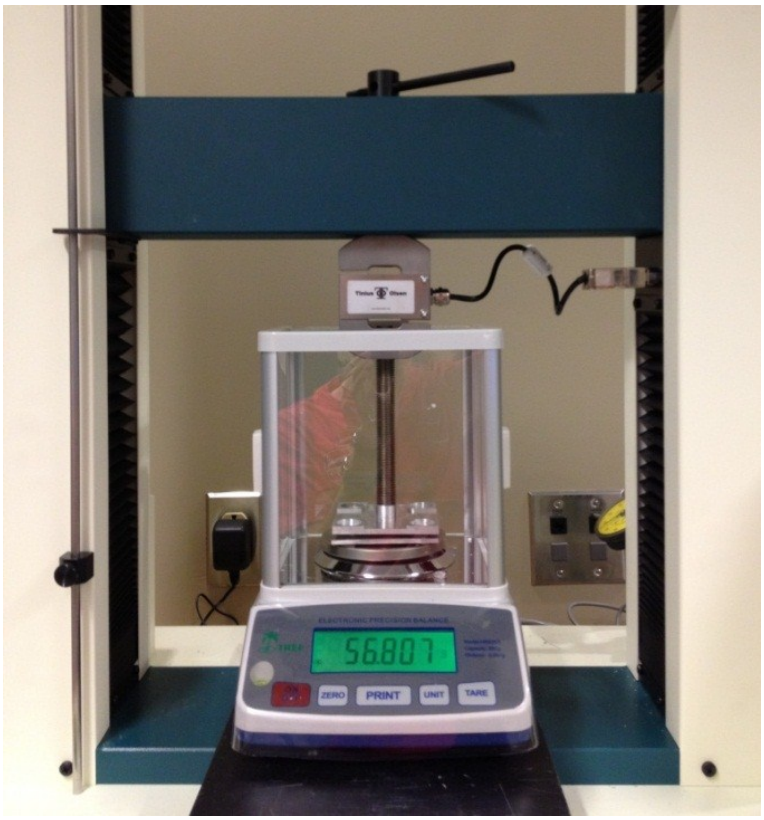

Figure 9: Grain Indenter-Puller attached to load frame and analytic scale.

Pulling is kinematically controlled. It is initiated with a speed of 0.020 mm/min (0.333 μm/s) for the first 15 minutes, or until the apparent weight reading on the scale steadily increases, after which the speed is increased to 0.100 mm/min to 0.200 mm/min (1.667 μm/s to 3.333 μm/s) for the remainder of the pulling process, until the grains are visibly separated with no water capillary bridge between grains. Apparent weight measurements on the analytic scale are recorded every second for the duration of the pulling experiment using a video camera.

As the top grain is pulled away from the bottom grain, any adhesive forces applied to the grains by silica gels growing between the two grains would be reflected on the analytic scale reading. When a silica polymer attached to both grains is being stretched, it exerts an uplifting force on the bottom grain, resulting in a gradual reduction in reading on the scale. As the grains are pulled further apart, such polymers would eventually break and the reading on the scale would increase slightly to reflect such action. Throughout the pulling experiment, water capillary bridge between the two grains get gradually thinner as the grains are separated further apart, thus results in a diminishing capillary effect that would cause the analytic scale reading to continuously increase. A force-extension curve can be plotted from the apparent weight, knowing the time and speed of separation between grains. Such data can provide an estimate to the size and strength of silica gels growing between two silica grains at the end of an aging period.

After the pulling experiment, images of grain surfaces were taken using SEM Variable Pressure Mode to observe silica gel growth in contact regions and to visually estimate polymer length and gel size.

5.4 Micro-strain testing

An alternative to Grain Indenter-Puller was developed in parallel to measure intergranular tensile strength of silica gel between silica grains after aging in unstressed conditions, utilizing a Micro-Strain Analyzer (TA Instruments RSA III), shown in Figure 10.

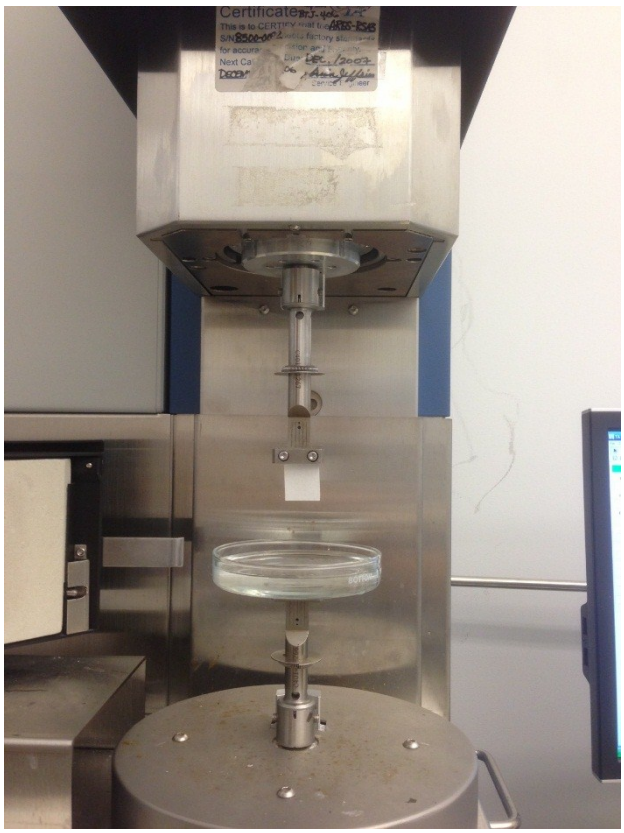

Figure 10: Micro-Strain Analyzer

A pair of aluminum brackets compatible with the Micro-Strain Analyzer (MSA) was designed, providing just enough pressure to hold two silica grains in contact during aging (Figure 11). The top grain has an edge pointing downward, whereas the bottom

grain as a flat surface pointing upward, creating identical contact configuration as used in Grain Indenter-Puller and Pneumatic Grain Indenter.

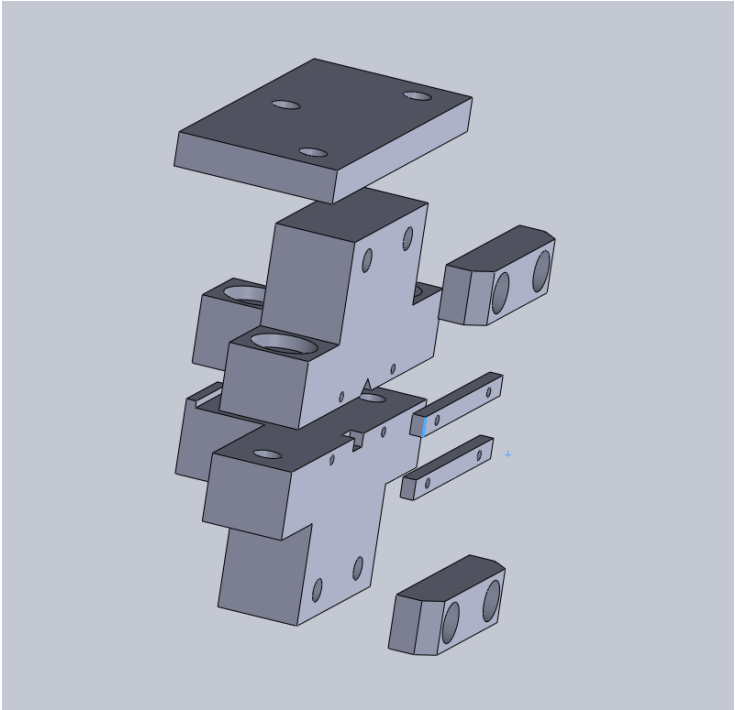

Figure 11: Assembly of top and bottom brackets holding silica grains and compatible with MSA.

Alternatively, a flat surface to flat surface contact between silica grains can be achieved using two aluminum beams with threaded holes at both ends and mounted to the brackets. After the grains are submerged in solution for a period of time with minimal pressure in contact, they are mounted to the MSA and gradually pulled apart. The amount of pulling force required is measured by the MSA and a force-extension curve can be plotted to estimate the magnitude of intergranular tensile force from potential silica polymers growing between the two grains unstressed contact region.

5.5 Aging in the presence of mica

To investigate how the presence of clay affects silica dissolution, precipitation and subsequent polymerization between stressed silica contacts, muscovite mica (S&J Trading, New York) in the form of a 10-micron-thin highest grade muscovite mica sheet was inserted between the grains prior to the start of aging. The grains were subsequently submerged and aged for three weeks under 140 kPa pressure and in solution with silica ion concentration of 300 ppm. The same method used in grain indenter-puller was used subsequently to measure and analyze intergranular tensile force between silica-mica-silica contacts.

6. Experimental Results

6.1 Growth of silica gel in solution

Samples of 150, 180, 210, and 300 ppm silica ion concentration solutions with pH value of 5.0 were taken from a sealed plastic test tube one week and two weeks after undisturbed silica gel growth experiment started, and imaged in AFM fluid imaging mode. To maintain the concentration of silica ions in the solution, the test tube was fully filled to minimize the air space between the liquid surface and lid in order to minimize evaporation. Figure 12 to Figure 15 show the growth of silica structures after one week in 150, 180, 210, and 300 ppm respectively on a 2 μm x 2 μm substrate area.

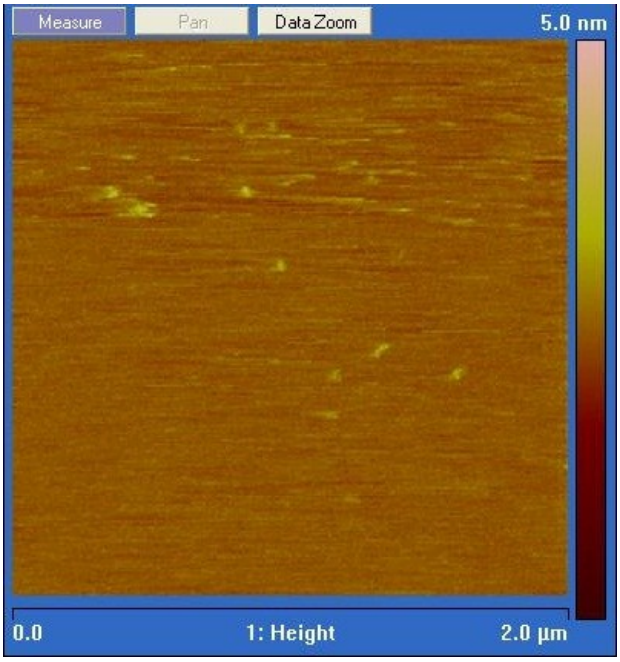

Figure 12: AFM image of 150 ppm pH 5 solution after one week.

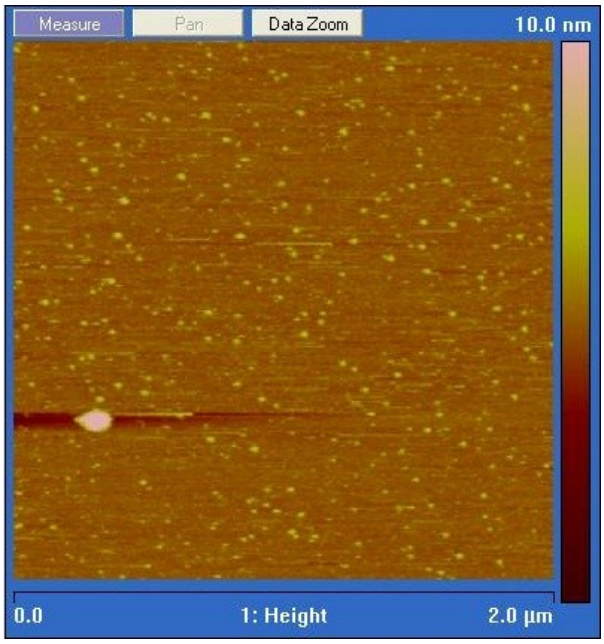

Figure 13: AFM image of 180 ppm pH 5 solution after one week.

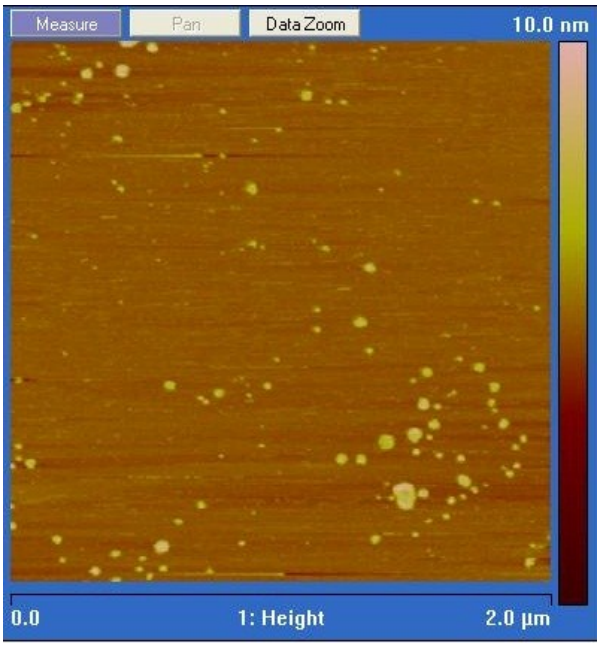

Figure 14: AFM image of 210 ppm pH 5 solution after one week.

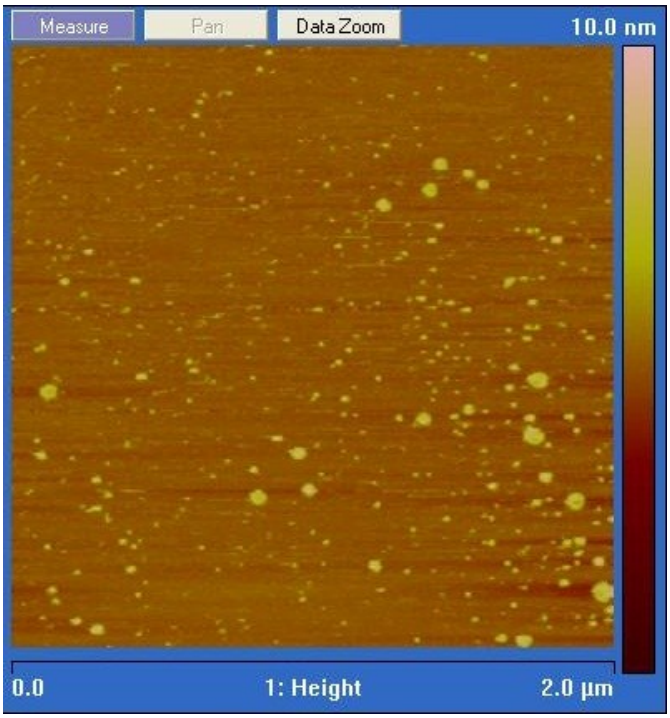

Figure 15: AFM image of 300 ppm pH 5 solution after one week.

After one week, there was no significant silica growth in 150 ppm solution as Figure 12 shows a rather smooth substrate. In 180 ppm and 210 ppm solutions, many nuclei with diameters of the order of 10 nanometers appeared in the solutions, represented as bright spots on the mica substrate. In 180 ppm solution, nuclei were smaller in size but larger in number comparing with that in 210 ppm solution. The big spot in the lower left corner of Figure 13 was probably a dust particle sticking on the mica substrate. In 300 ppm solution, as shown in Figure 15, nuclei exhibited a wide range of diameters and a large quantity.

After two weeks, no obvious changes were found in images of 150, 180, and 210 ppm solutions, but a significant structure was seen growing in 300 ppm solution

showing signs of a developing interconnecting gel network, as shown in Figure 16. The height of the structure was about 30 nm, and each polymer width was at least one magnitude less than 1 μm. Nevertheless, the density of such structures and their interconnectivity is quite impressive. With a scanning area of only 2 μm x 2 μm, the AFM was not able to give an estimate to the size of the complete gel structure at this stage.

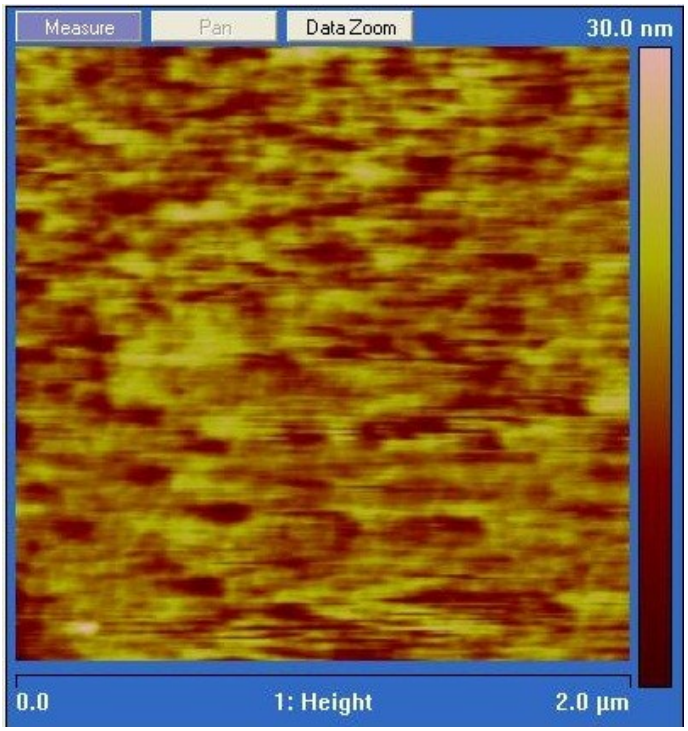

Figure 16: AFM image of 300 ppm pH 5 solution after two weeks.

As gel grows larger in higher concentration solutions, AFM fluid imaging capability is soon exceeded since the size of an AFM cantilever is only a few microns. When a visible layer of silica gel covered the bottom of a petri dish containing 500 ppm silica ion concentration solution, the gel was scooped up and converted into aerogel

form in Critical Point Dryer and then sputter coated with a thin layer of gold. Figure 17 shows a piece of silica aerogel prepared this way, in SEM high vacuum mode.

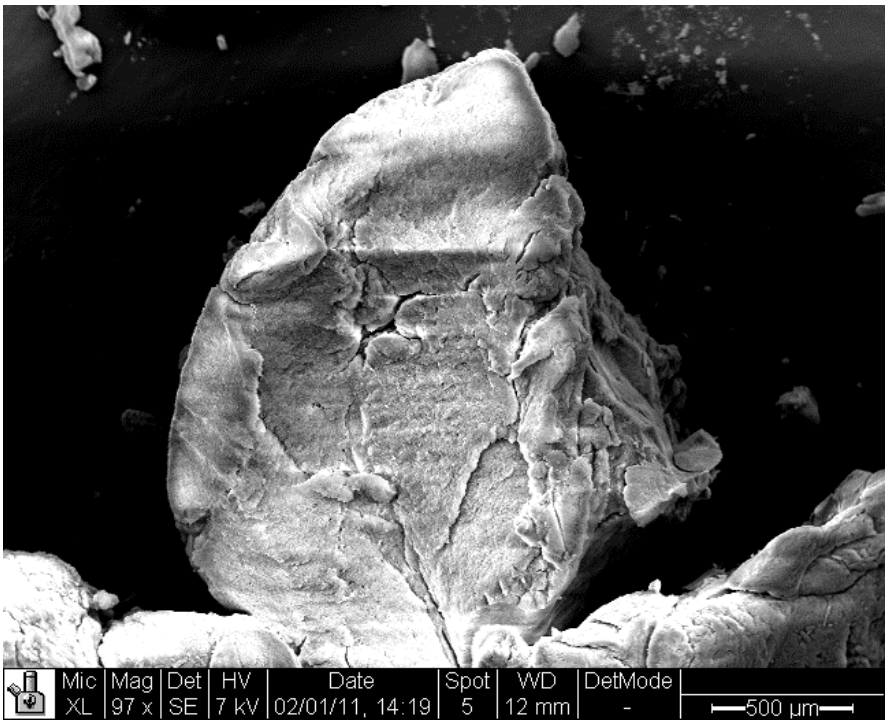

Figure 17: SEM image of silica aero gel, gold coated, magnification 97x.

Figure 18 shows the same piece of aero gel, under 50000x magnification in SEM high vacuum mode. The internal structure of silica aerogel was revealed to consist of a network of thin polymers and interconnected chambers much like the AFM image of 300 ppm solution after 2 weeks shown in Figure 16. The width of silica polymers in the image was in the order of 10 nm.

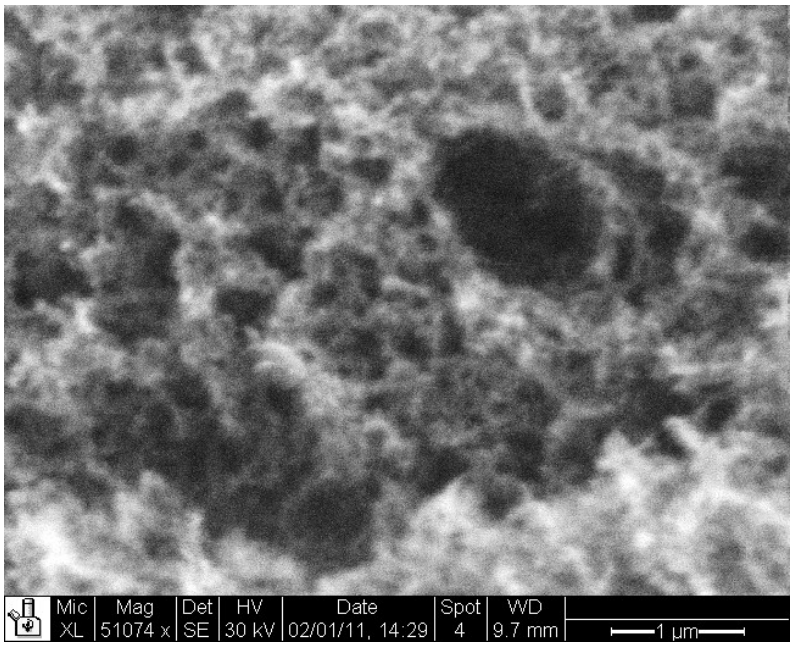

Figure 18: Internal structures of silica aerogel, SEM magnification 51074x

6.2 Growth of silica gel near stressed contacts

A series of tests to assess the growth rate of silica polymers were conducted at different elevated concentrations of silica ions in the environmental solution. The rationale for using an initial elevated concentration (Rubin 2009), after finding a concentration high enough to induce polymerization or gelation, is to bring the concentration somewhat below that level, then allow some time for sufficient dissolution from the damaged material to bring the solution to the concentration level at which silica will polymerize. The concentration of silica in the pore solution may be much higher locally and instantaneously near the asperities, and stressed and dissolving contacts than the average pore water concentration.

In 500 ppm silica ion concentration solution with pH 5.0, two silica grains were pressed against each other for three weeks in Pneumatic Grain Indenter. SEM images of before, and after aging are shown in Figure 19 and 20. Polymers were observed on the surfaces of both cubes after aging. Some of the polymers connected to both grains near the contact region were up to several hundred microns long (Figure 21 and 22).

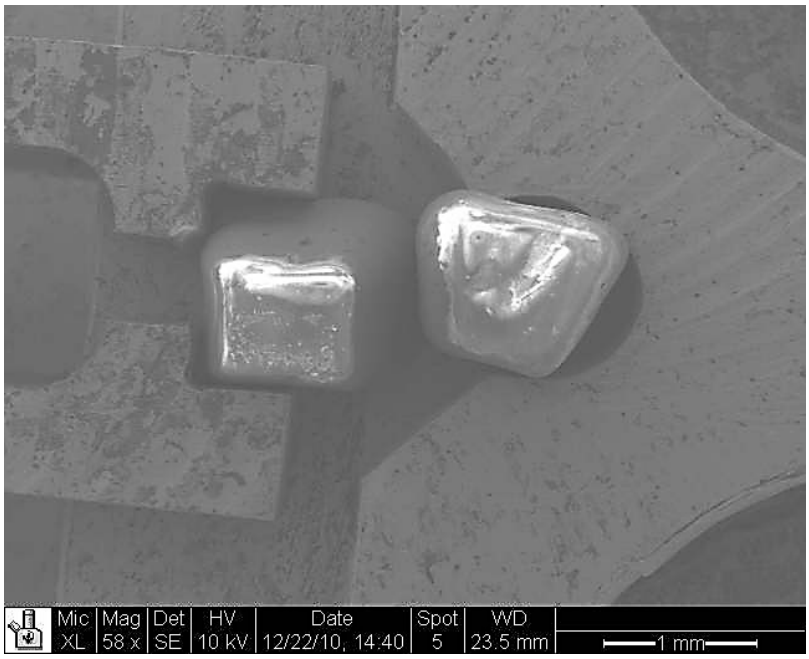

Figure 19: Overview of silica grains in stressed contact before 3 weeks of aging in 500 ppm pH 5 solution, 58x magnification in SEM.

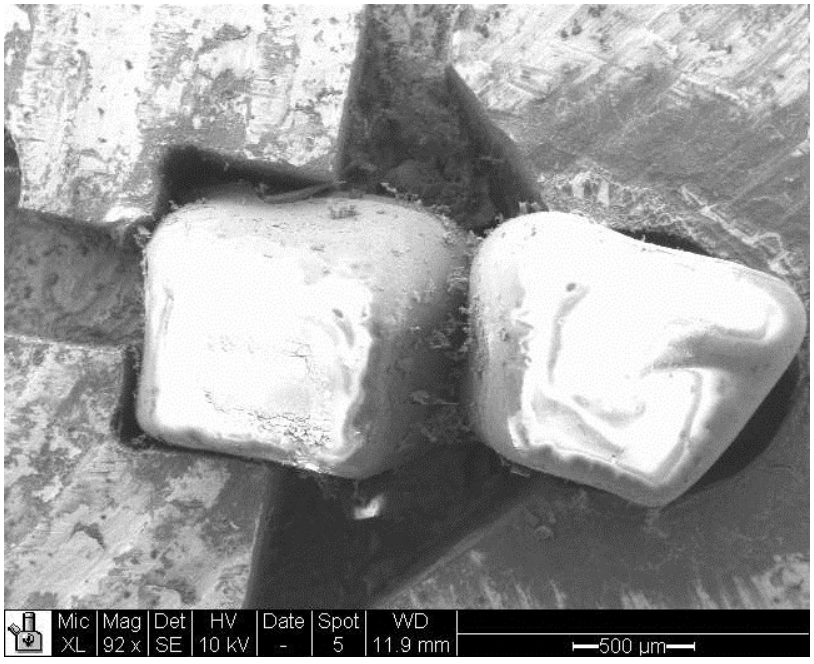

Figure 20: Overview of silica grains in stressed contact after 3 weeks in 500 ppm pH 5 solution, 92x magnification.

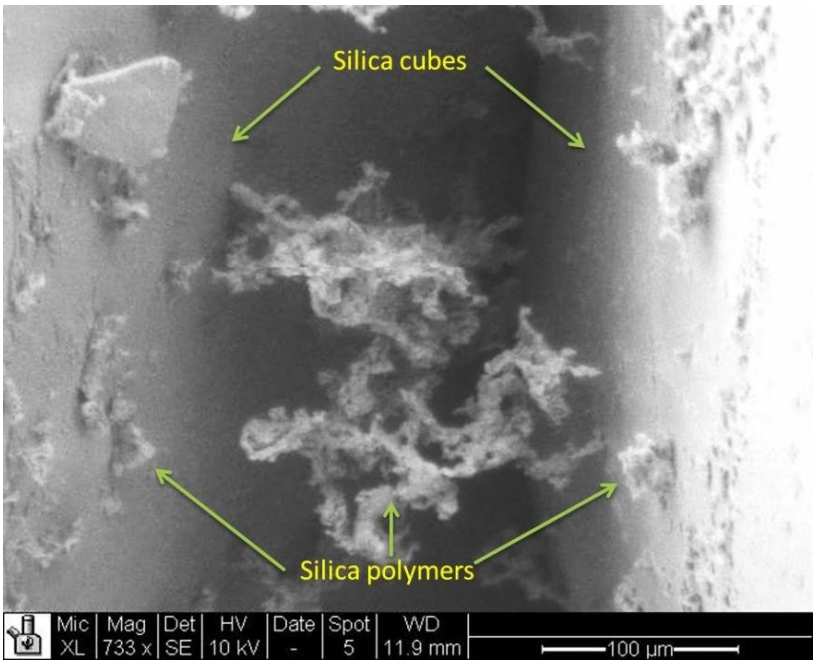

Figure 21: Silica polymers near stressed contact between two silica grains in 500 ppm pH 5 solution after 3 weeks, 733x magnification.

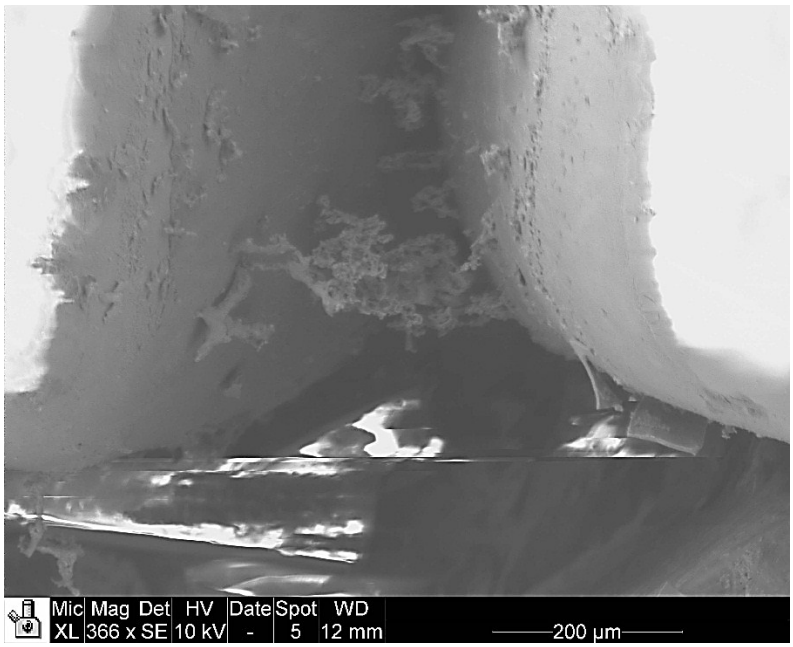

Figure 22: Silica polymers between two silica grains in 500 ppm pH 5 solution after 3 weeks, 368x magnificatio.

A composition analysis of such polymers using energy dispersive X-ray spectrometer (EDS) detector in the SEM chamber showed that the structures in the images were mostly silicon, with minor traces of chlorine, chromium, iron, sodium, and carbon elements (Figure 23). These minor elements were likely originated from the stainless steel fluid chamber and solution residues. The minimal amount of carbon in the sample may come from dust in the environment. It proved that the polymers in question was not of biological origin, otherwise carbon would be a dominant element in the polymer structure.

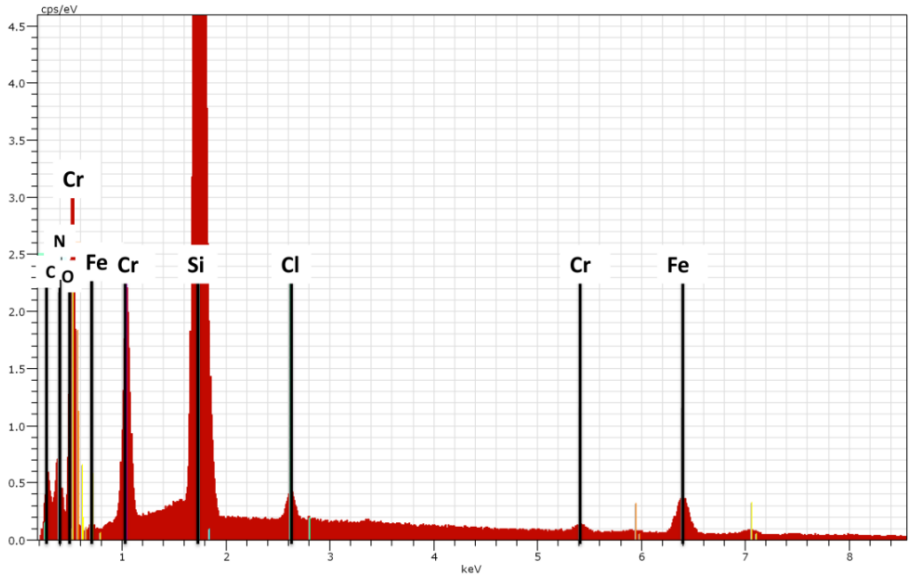

Figure 23: Energy Dispersive X-ray Spectrometer composition analysis of materials shown in Figure 21 and 22.

Another experiment was conducted in the same conditions except the grains were allowed to age for 4 weeks. SEM images showed, in addition to gel growing

between silica grains near contact region, a network of silica gel growing around a silica grain (Figure 24).

An individual silica polymer was imaged in Figure 25 and showed that it had a length in the order of 100 microns. During subsequent imaging this polymer had visibly shrunk from drying due to prolonged exposure in the low vapor pressure in the microscope chamber.

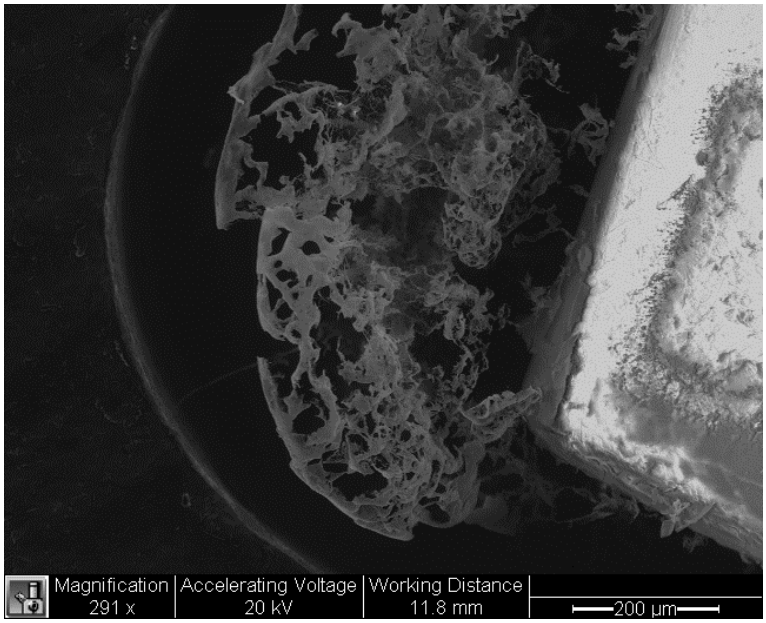

Figure 24: Silica gel growth on silica grain after 4 weeks in 500 ppm pH 5 solution, 291x magnification.

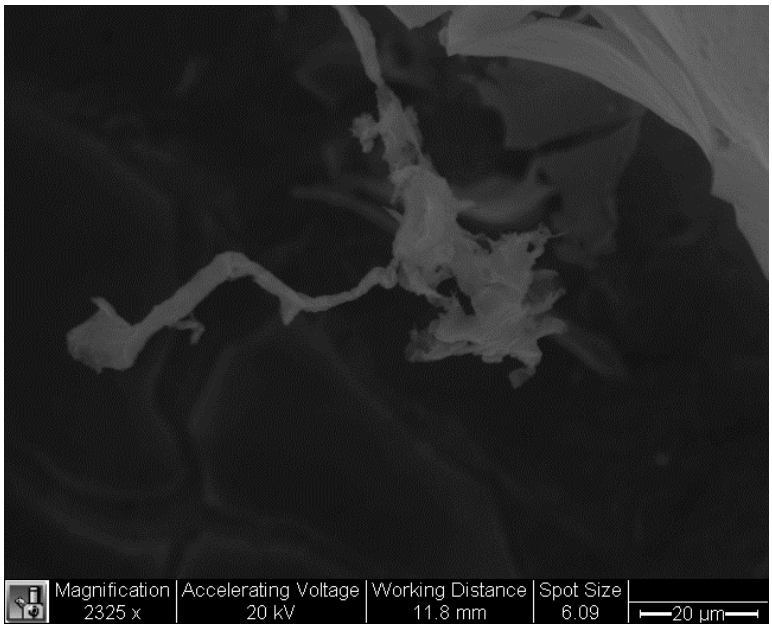

Figure 25: Silica polymer attached to a silica grain, after 4 weeks in 500 ppm pH 5 solution, 2325x magnification.

In 300 ppm Si ion concentration pH 5.0 solution, a similar experiment with the same set-up was conducted and aged for two weeks. A few cracks had developed across both grains as a result of sustained pressure over the two-week period (Figure 26). The results showed extensive silica deposits with size of the order of 10 µm developed near the asperities from compression (Figure 27 and 28).

The experiment was repeated in the same conditions except applying a lower pressure (120 kPa) to the grains through the pneumatic actuator. It was found that no microcracks had developed on either grain, and no silica polymer deposits were found anywhere in the fluid chamber (Figure 29).

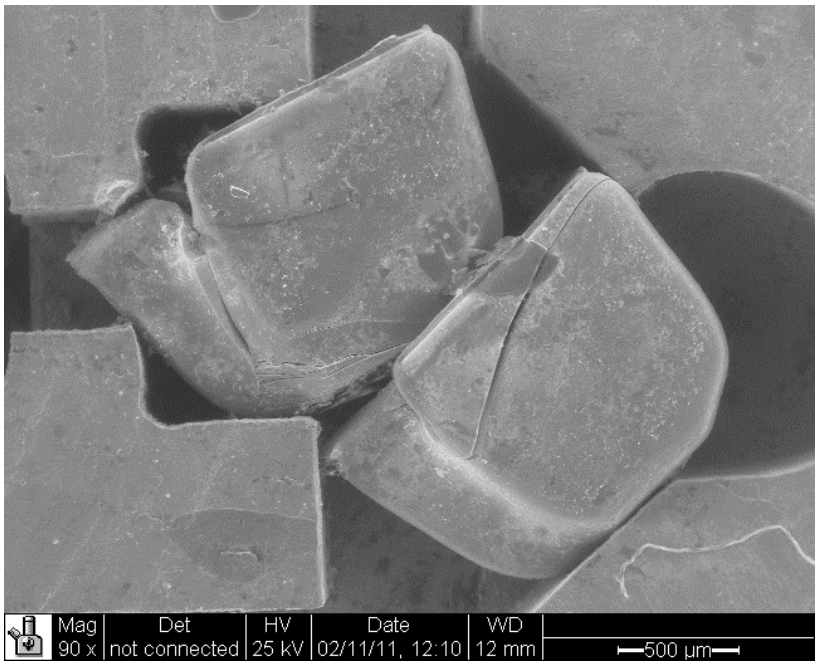

Figure 26: Overview of silica grains in Pneumatic Grain Indenter after being under compression for two weeks in 300 ppm pH 5 solution, 90x magnification.

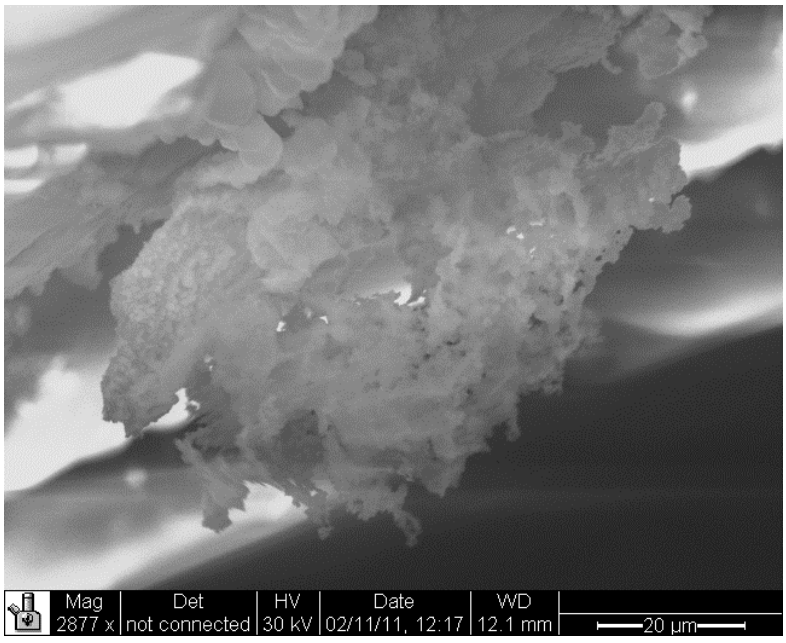

Figure 27: Silica deposits on silica grain surface near stressed contact region after 2 weeks aging in 300 ppm pH 5 solution, 2877x magnification.

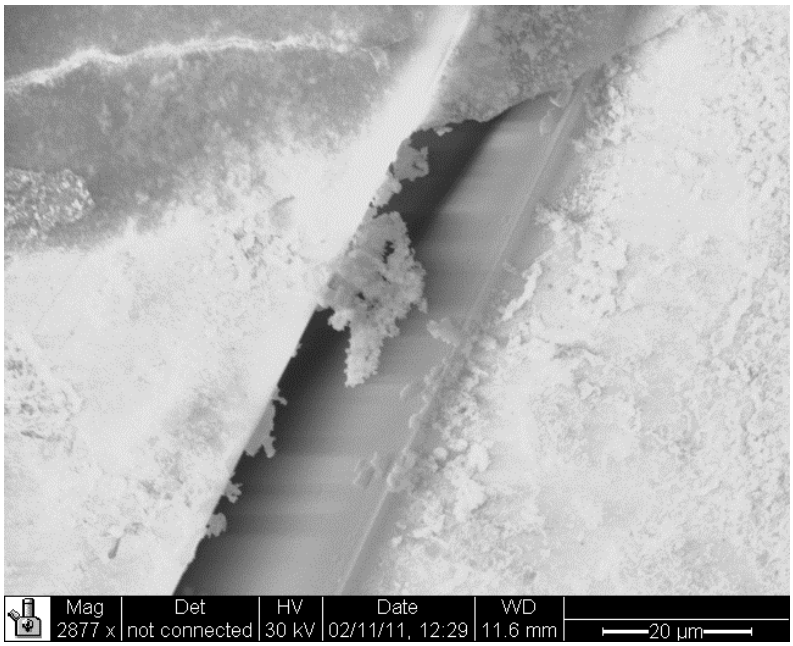

Figure 28: Silica deposits found inside cracks developed after 2 weeks aging in 300 ppm pH 5 solution, 2877x magnification.

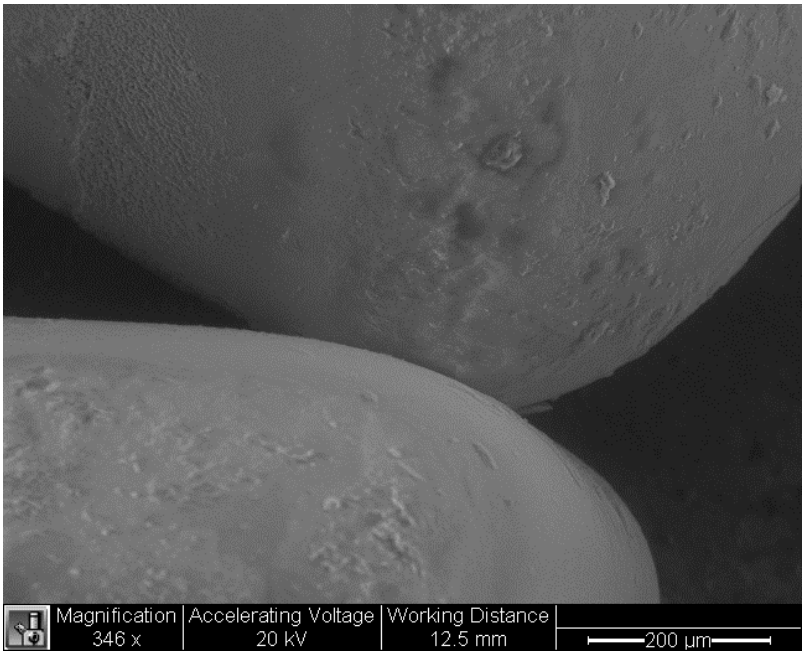

Figure 29: Clean cube surfaces around low stress contact region after 2 weeks aging in 300 ppm pH 5 solution, 346x magnification.

In 200 ppm Si ion concentration solution, at pH 2.5, two silica grains were compressed together and aged for 3 weeks. SEM images showed an extensive silica gel structure growing near the contact region between the two grains (Figure 30). Interestingly, some large polymers were seen connected to grain surfaces by very thin fibers, shown in Figure 31.

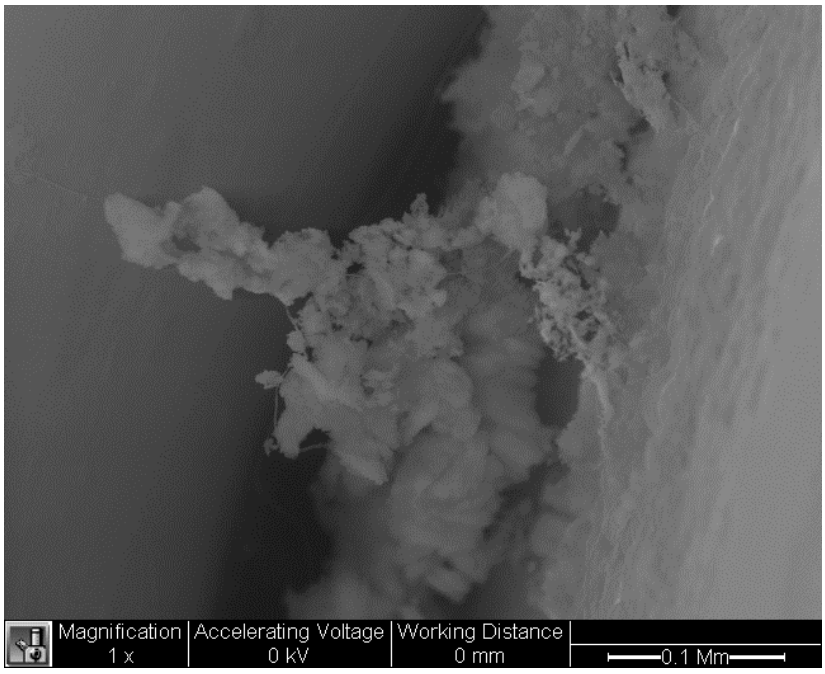

Figure 30: Silica polymers growing on grain surfaces near stressed contact after 3 weeks aging in 200 ppm pH 2.5 solution.

Figure 31: Thin fibers connecting larger polymers to grain surfaces, in 200 ppm pH 2.5 solution after 3 weeks aging.

In 90 ppm Si ion concentration solution with pH 5.0, polymers a few microns in length were found between a silica grain's main body and a piece of silica debris that was chipped off from 3 weeks of compression (Figure 32). No extensive silica deposits or silica polymers were found otherwise in the fluid chamber.

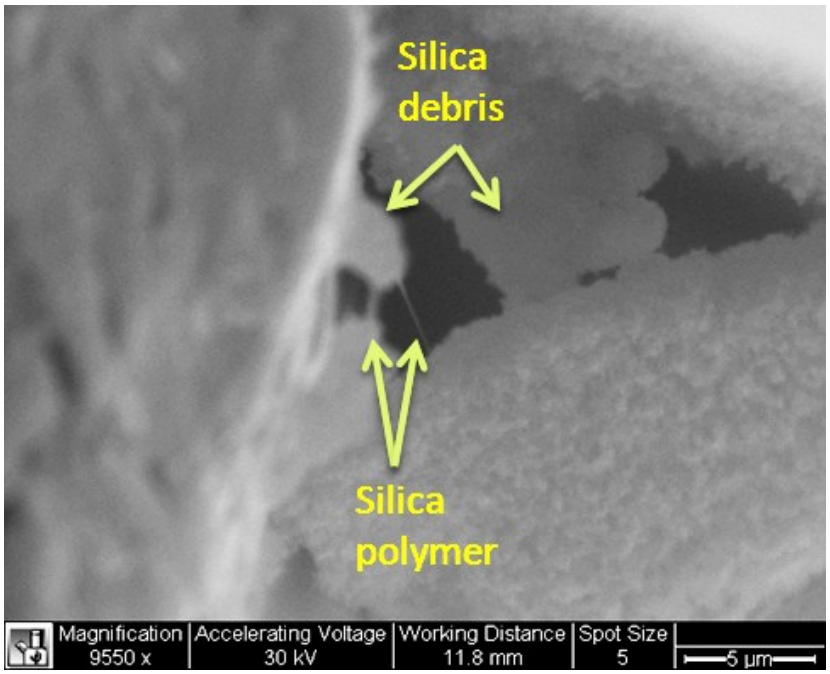

Figure 32: Silica polymers growing between silica surfaces in 90 ppm pH 5 solution after 3 weeks aging in Pneumatic Grain Indenter, 9550x magnification.

6.3 Tensile strength of individual silica polymers

AFM pulling experiments were conducted on silica grain surfaces to measure the tensile strength of individual silica polymers growing there. An AFM cantilever tip was slowly lowered in solution until it touched the grain surface, at which point it was gradually raised up from the surface. If the tip was in contact with any silica polymers on the surface, surface tension would result in the polymer attaching to the cantilever tip. As the cantilever was pulled away from the surface, the polymer was stretched between grain surface and cantilever until it broke. The deflection on the cantilever was recorded and, knowing the spring constant of the cantilever, the tensile strength of the polymer could be estimated.

Undisturbed (not loaded) silica grains in solutions with Si ion concentration ranging between 130 ppm and 210 ppm and pH 5.0 for two weeks were put in AFM, and pulling experiments in water were conducted on those grain surfaces. On grain surfaces in 210 ppm solution, distinctive step-like kinks were consistently captured on the force curves (Figure 33 and 34). X-axis indicated displacement of cantilever, in nanometer; y-axis indicated deflection rate in millivolts which can be converted to force.

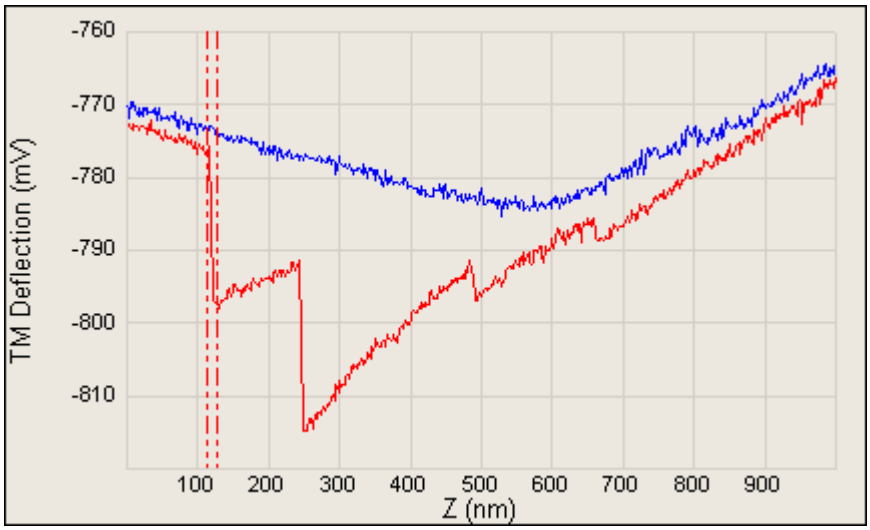

Figure 33: AFM force curve on grain surface after it was submerged in 210 ppm pH 5 solution for two weeks (a).

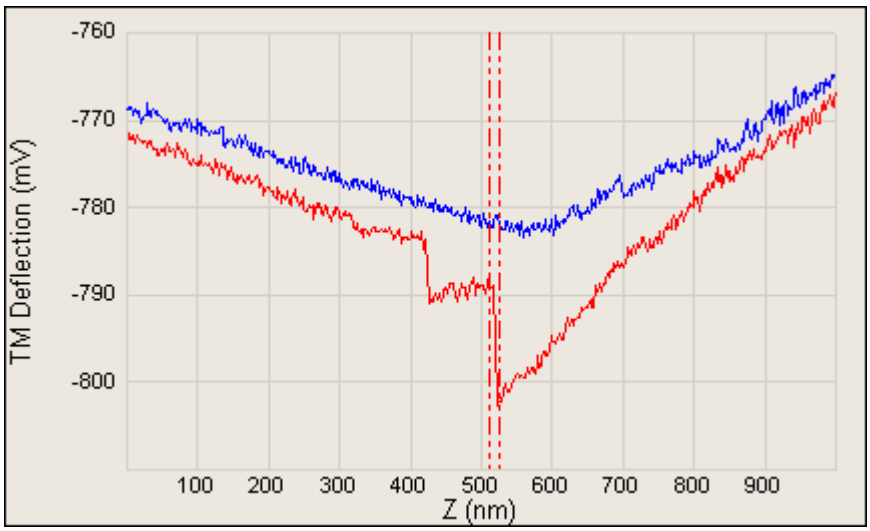

Figure 34: AFM force curve on grain surface after it was submerged in 210 ppm pH 5 solution for two weeks (b).

The top curve in each graph (blue color) represented the force curve of the cantilever as it approached the surface. The bottom curve (red color) represented the force curve as the cantilever pulled away from the surface. The vertical distance between

the two curves represented the additional force required for the cantilever to overcome surface tension, short-range forces, and any potential polymers connecting the tip to the surface. This force was calculated by multiplying the distance with cantilever deflection sensitivity (30 nm/mV) and spring constant (0.74 nN/nm). The peaks shown on the bottom curves in Figure 33 and 34 possibly indicated instances where polymer segments were broken as the cantilever was pulling away. Therefore the vertical distance between a peak in the retracting force curve to the approaching force curve can be converted to force for an estimation of polymer strength. In Figure 33, the distances between the two peaks to the approaching force curve, after converting from voltage to distance, was 604 nm and 677 nm respectively, which converted to 440 nN and 490 nN. In Figure 34, the distances between peaks in the retracting force curve and the approaching force curve after voltage-distance conversion were 255 nm and 407 nm respectively, which converted to 190 nN and 300 nN.

A few more pulling curves from the same experiment were exhibited in Figure 35.

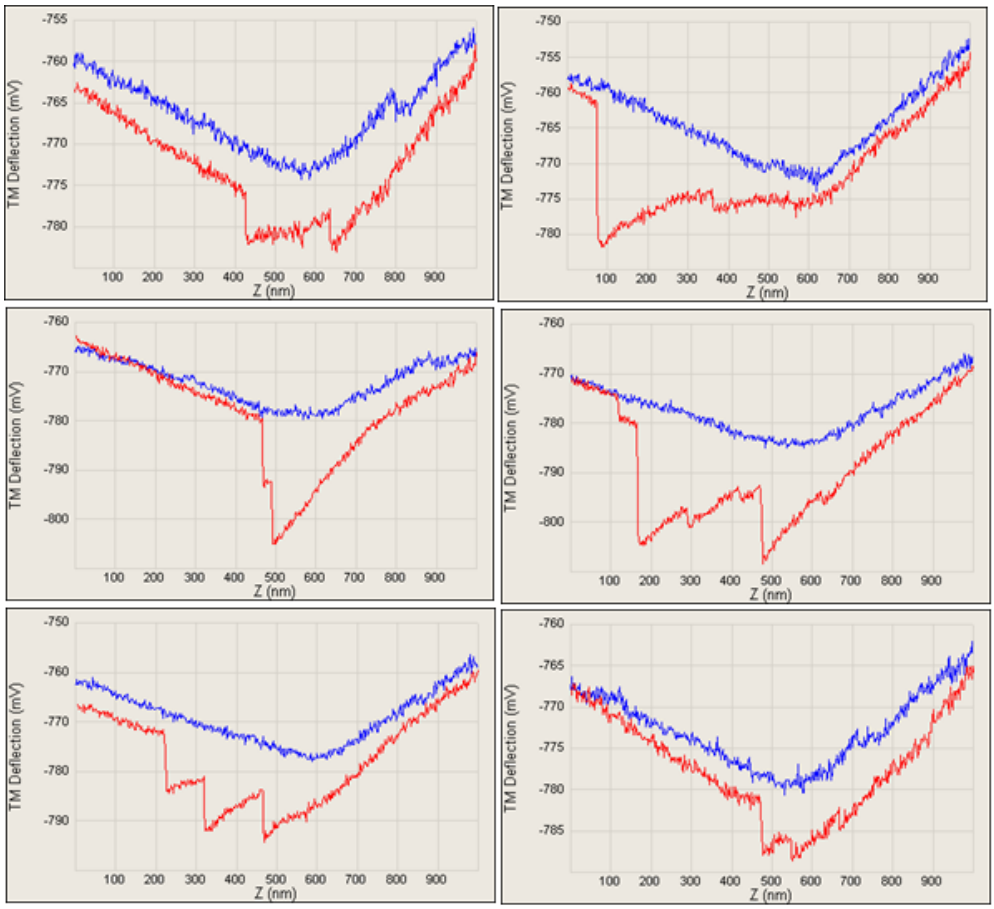

Figure 35: Additional AFM force curves on silica grain surface after submerged in 210 ppm pH 5 solution for 2 weeks.

In comparison to the above experiment, another pulling experiment was conducted on silica grain surface that was submerged in nano-pure water for 19 days. A typical result was shown in Figure 36. Only one peak was observed as the cantilever was about to break contact with grain surface. The distance between the peak of the retracting curve and the approaching curve was, after voltage to distance conversion, 180 nm, which converted to 130 nN.

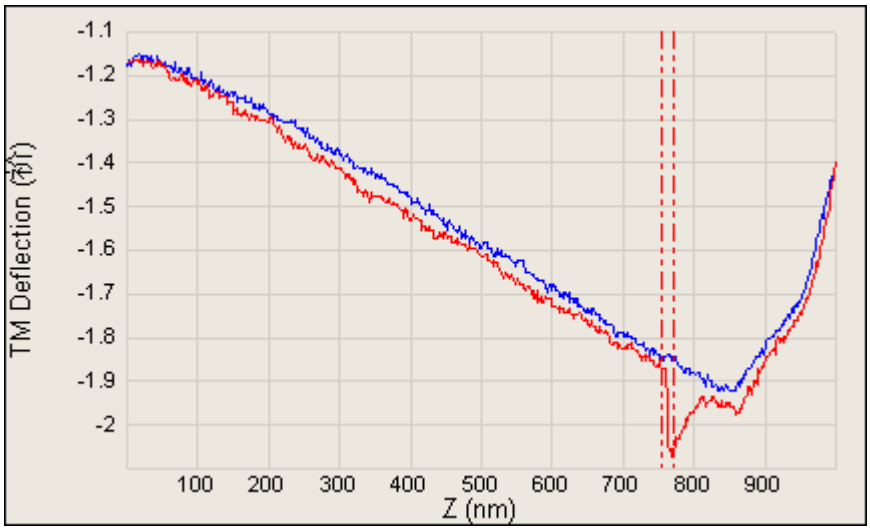

Figure 36: AFM force curve on silica grain surface after submerged in nano-pure water for 19 days.

A few more typical pulling curves on grain surface, after submerged in nano-pure water for 19 days, are shown in Figure 37. No step-like kinks were observed. Most peaks occurred when the retracting cantilever was about to break contact with the grain surface.

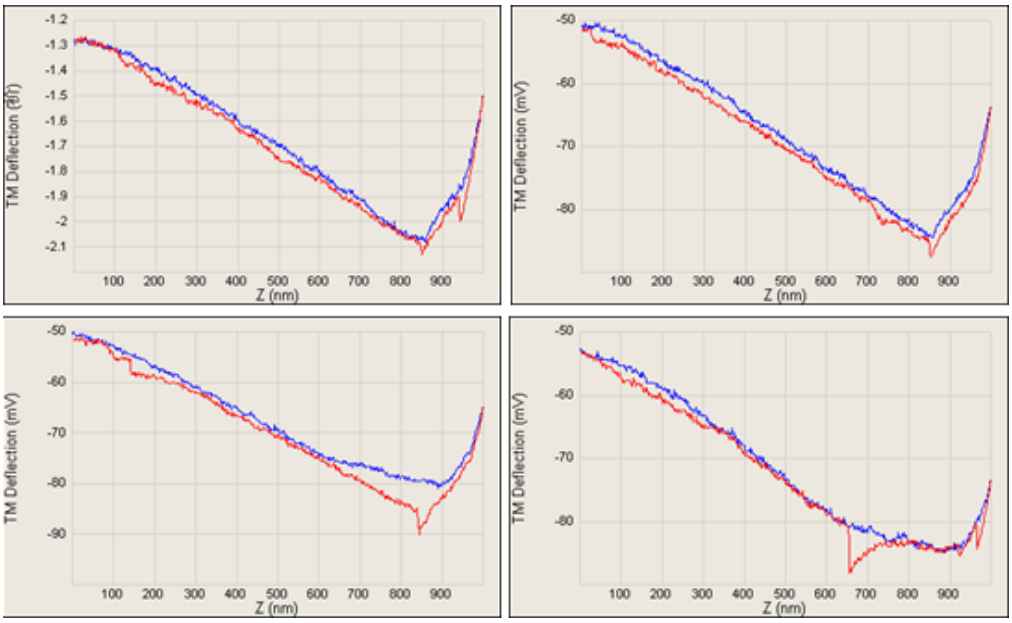

Figure 37: Additional AFM force curves on silica grain surface after submerged in nano-pure water for 19 days.

6.4 Intergranular tensile strength between silica grains

After measuring the tensile strength of individual silica polymers growing on silica surfaces in solutions containing Si ions, the next step was to measure the amount of intergranular bonding force that silica gels can exert between two silica grains. Grain Indenter-Puller (GIP) was used for this purpose.

After a GIP experiment was conducted, apparent weight (AW) readings recorded by an electronic scale were plotted against the change in separation between the grains. Initial points with extremely high AW reading are ignored because such AW values were a result of the load-frame pre-loading the grains against the scale to keep the grains pressed together while the top half of the GIP was disassembled. During pulling phase, the AW reading would stabilize to a certain degree where the load-frame is raised sufficiently to not to exert any downward force on the scale and the apparent weight separation curve starts to exhibit a relatively continuous pattern. Force data are hence measured and processed (i.e. force differences were calculated) from then onward in what will be referred to as the partial-contact phase. Ultimately the force readings will reach a plateau and stay constant, at which point the two grains are completely separated and the pulling experiment ends.

In the partial-contact phase, the upward displacement of the upper grain is very limited. However, four, practically consecutive, types of events are hypothesized to take place. First, direct interlocked contacts between asperities and cracks of the two grains

are unlocked at the smallest displacement. Subsequently, as the upper grain is pulled further away from the bottom grain, polymers attached to both grains are unraveled and stretched. Thirdly, when the individual links of the polymer being stretched reach their tensile strength and break, or become detached from the grain substrate and hence a corresponding drop in total force is registered. This process continues until no unbroken polymer links remain attached. At such a circumstance there is no bonding remains between the grains except for that of capillary water bridge stretched between the grains.

Apparent weight vs displacement curve was closely examined for any sudden drops in weight recorded as such drops would possibly indicate the existence of a silica polymer or gel cluster attached near a contact point between both grains. Silica gel tensile strength and size can be estimated from the curve. the force differences between neighboring points were also calculated and plotted against separation displacement as they can be used to estimate the maximum intergranular pulling force a silica polymer or gel structure can exert between two silica grains.

The results of pulling experiments conducted on silica grains aged under compression for 3 weeks in solutions with different silica ion concentrations are shown below.

6.4.1 In 500 ppm solution

Silica grains 3 mm x 3 mm x 3 mm were compressed in solution with silica ion concentration of 500 ppm and pH value 5.0 for 3 weeks. After aging was complete, pulling was performed at 0.020 mm/min speed and the Apparent Weight vs displacement curve was shown in Figure 38.

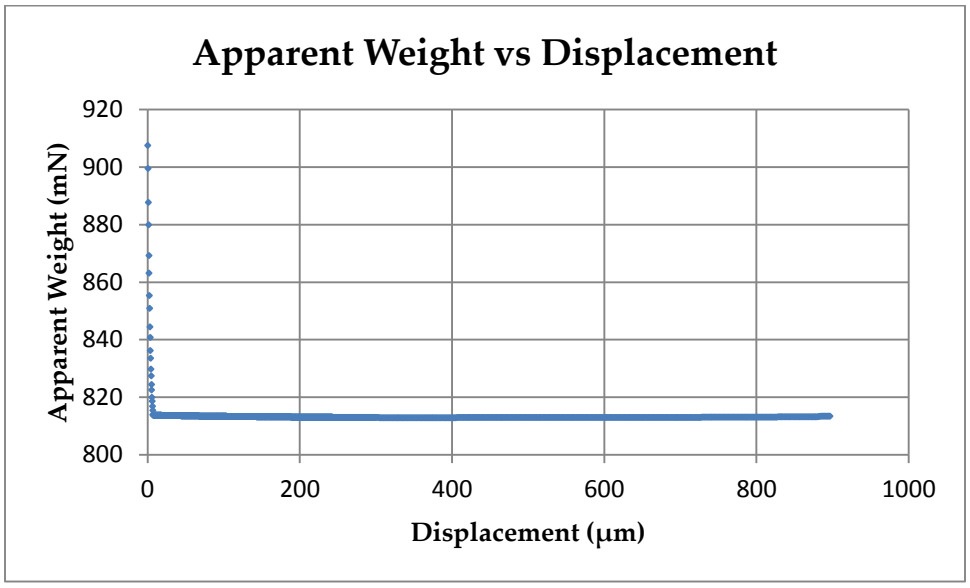

Figure 38: Plot of Apparent Weight vs Displacement for experiment in 500 ppm pH 5 solution after 3 weeks aging.

After removing the initial points with extremely high AW values during pre-loading stage, the partial-contact phase in pulling was shown in Figure 39, where it can be observed that most sudden changes in AW occurred in the early stage of pulling. All positive AW changes between neighboring data points were shown against displacement in Figure 40 and recorded in Table 1, where x denotes the difference in AW calculated between neighboring data points.

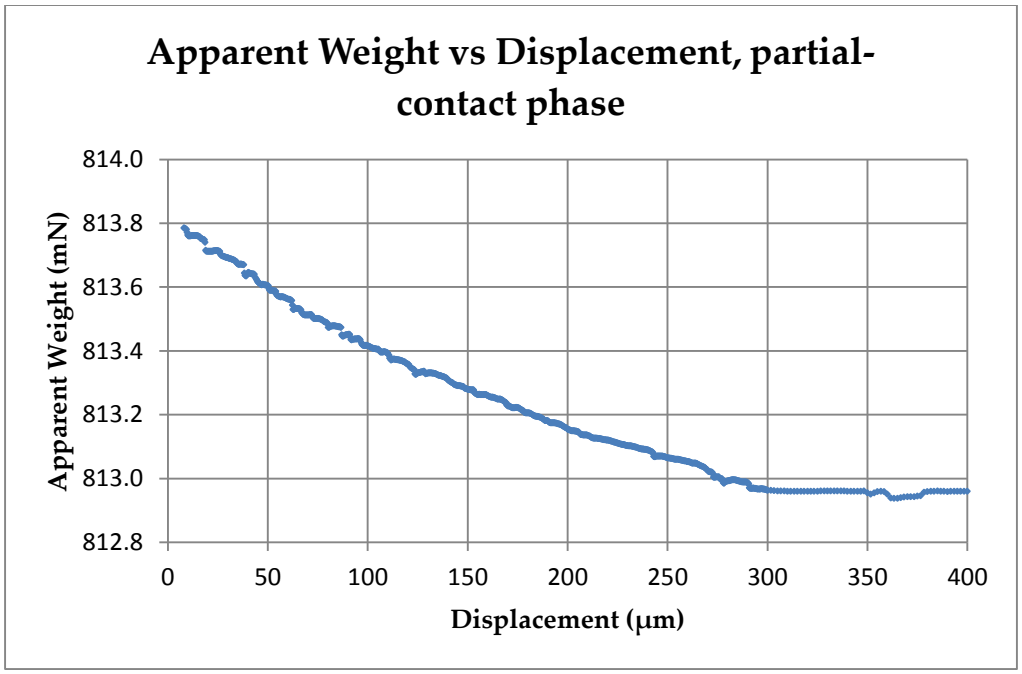

Figure 39: Partial-contact phase of apparent weight vs displacement curve, 500 ppm pH 5 solution 3 weeks.

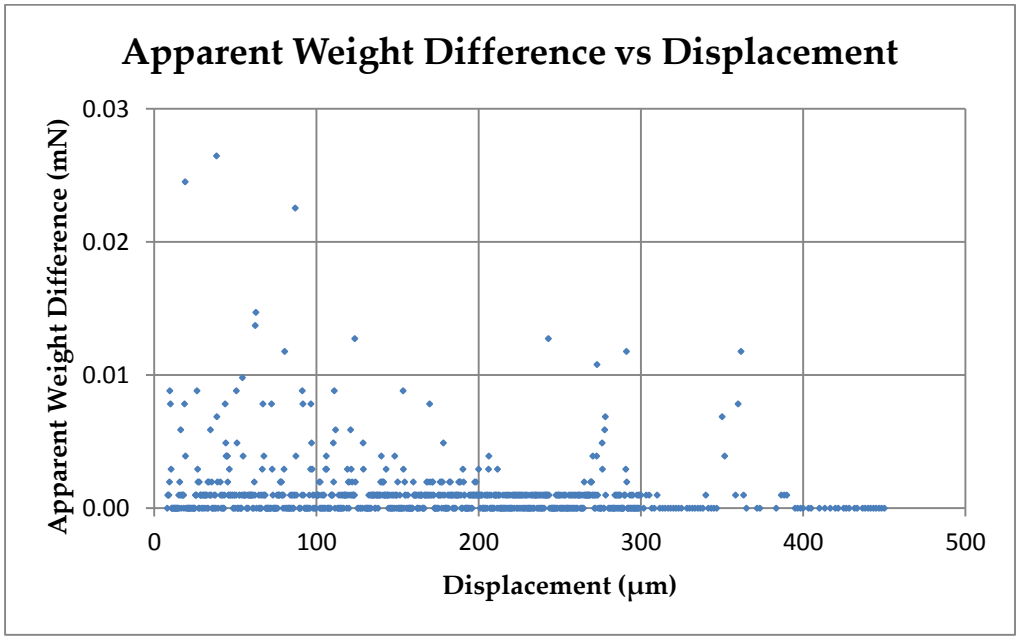

Figure 40: Difference in Apparent Weight between neighboring data points in partial-contact phase, 500 ppm pH 5 solution 3 weeks.

Table 1: Distribution of AW differences for experiment in 500 ppm pH 5 solution for 3 weeks.

Range of AW difference (mN)	Number of Events
$0 < x \leq 0.0100$	457
$0.0100 < x \leq 0.0200$	8
$0.0200 < x \leq 0.0300$	3
$0.0300 < x \leq 0.0400$	0
$0.0400 < x \leq 0.0500$	0

The total sum of all positive events recorded in distribution of AW difference will be termed net tensile force. For this experiment, the net tensile force was 0.9395 mN. The highest force difference between neighboring apparent weight measurements was 0.0265 mN at 38.333 μm.

Figure 41 and 42 are SEM images showing one of the silica grains after the aging experiment in 500 ppm solution for 3 weeks. Cracks were observed across the whole grain. Grain surfaces were covered by silica gel, especially on the contact surface. Such gel structures were seen growing over cracks generated from aging under compression.

Figure 41: Silica grain after aging in 500 ppm pH 5 solution for 3 weeks, 50x magnification in SEM.

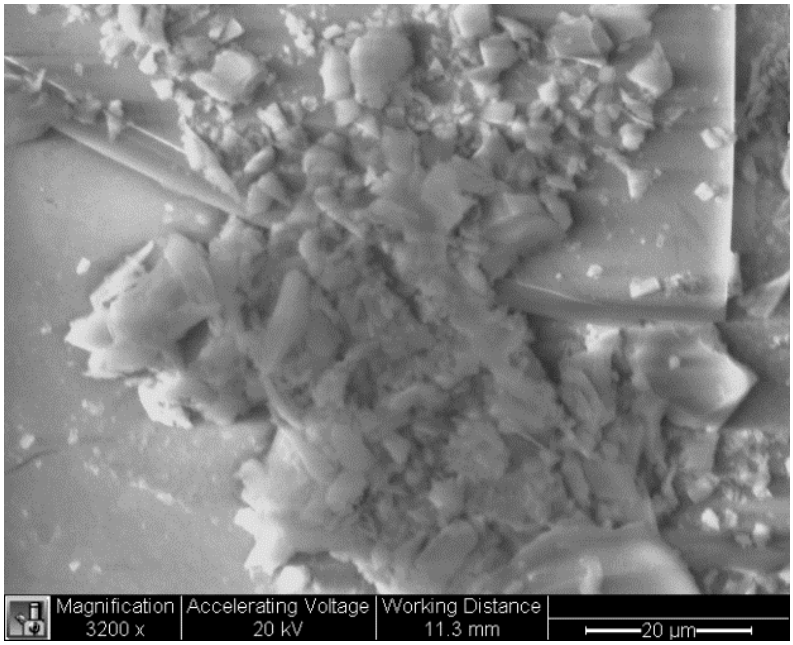

Figure 42: Grain surface with cracks after aging in compression in 500 ppm pH 5 solution for 3 weeks, 3200x magnification.

Two additional experiments were conducted in 500 ppm pH 5.0 solution; in one experiment the grains were aged for 3 weeks and pulled apart at 0.010 mm/min (half the original speed of 0.020 mm/min), and in the other experiment the grains were aged for 4 weeks and pulled at the original speed of 0.020 mm/min. Their AW difference distributions are shown in Table 2. Net tensile forces for 3-week half-speed and 4-week full-speed experiments were 0.8669 mN and 1.3318 mN respectively.

Table 2: Distribution of AW differences for two variations of aging experiments in 500 ppm pH 5 solution.

Range of AW difference (mN)	Number of Events	
	3-week half-speed	**4-week full-speed**
$0 < x \leq 0.0100$	57	1092
$0.0100 < x \leq 0.0200$	8	15
$0.0200 < x \leq 0.0300$	4	2
$0.0300 < x \leq 0.0400$	7	0
$0.0400 < x \leq 0.0500$	6	0

6.4.2 In 400 ppm solution

A GIP experiment was conducted after two silica grains were aged in solution with 400 ppm Si ion concentration at pH 5.0 for 3 weeks. The overall AW vs displacement, AW vs displacement at partial-contact phase, and AW difference vs displacement curves were shown in Figure 43 to 45 respectively.

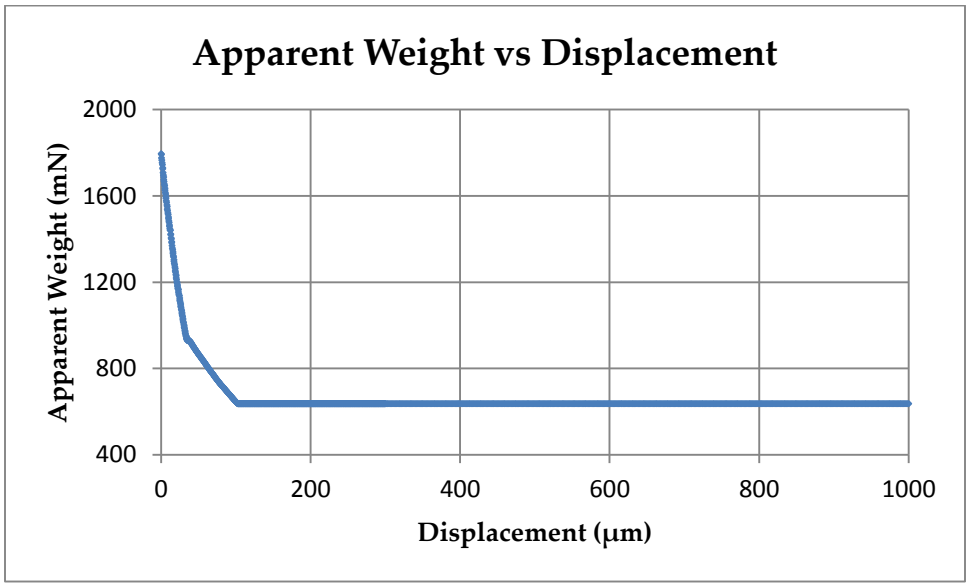

Figure 43: Plot of Apparent Weight vs Displacement for experiment in 400 ppm pH 5 solution after 3 weeks aging.

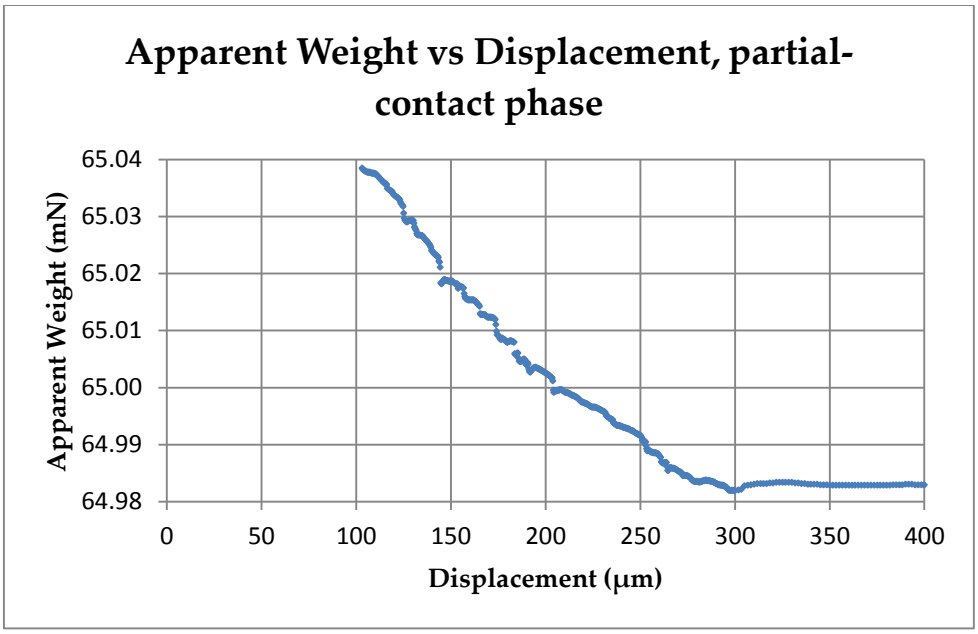

Figure 44: Partial-contact phase of apparent weight vs displacement curve, 400 ppm pH 5 solution 3 weeks.

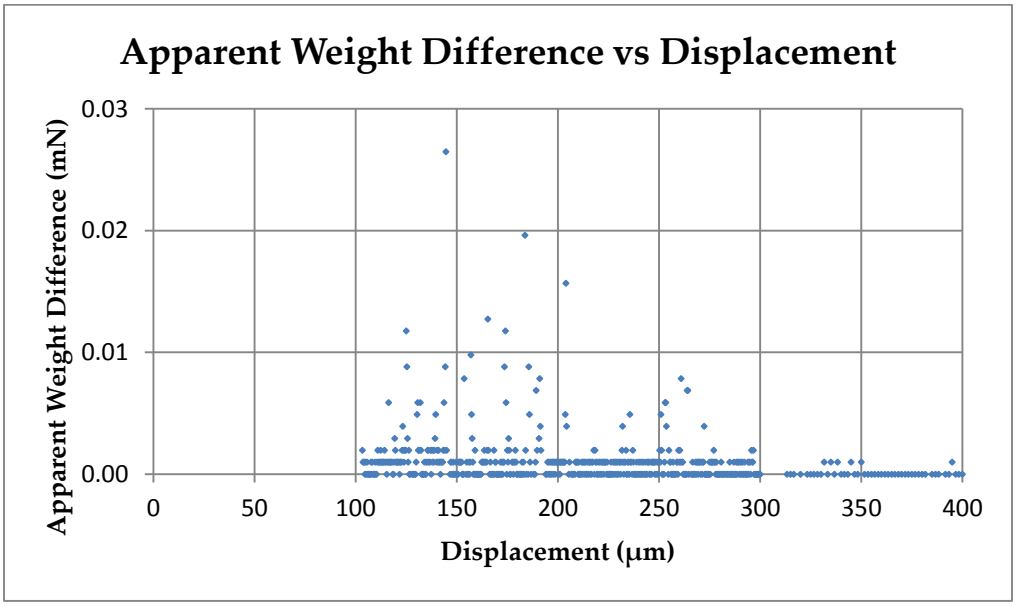

Figure 45: Difference in Apparent Weight between neighboring data points in partial-contact phase, 400 ppm pH 5 solution 3 weeks.

Table 3 shows the distribution of AW differences between neighboring data points for this experiment. Net tensile force was 0.6679 mN. The highest force difference between neighboring apparent weight measurements was 0.0265 mN at 144.67 μm.

Table 3: Distribution of AW differences for experiment in 400 ppm pH 5 solution for 3 weeks.

Range of AW difference (mN)	Number of Events
$0 < x \leq 0.0100$	307
$0.0100 < x \leq 0.0200$	5
$0.0200 < x \leq 0.0300$	1
$0.0300 < x \leq 0.0400$	0
$0.0400 < x \leq 0.0500$	0

SEM images of silica grain surfaces after the experiment ended are shown in Figure 46 and 47. Extensive silica gel can be seen growing on grain surfaces near contact region and over new cracks and asperities, joining small silica debris from aging to the main body.

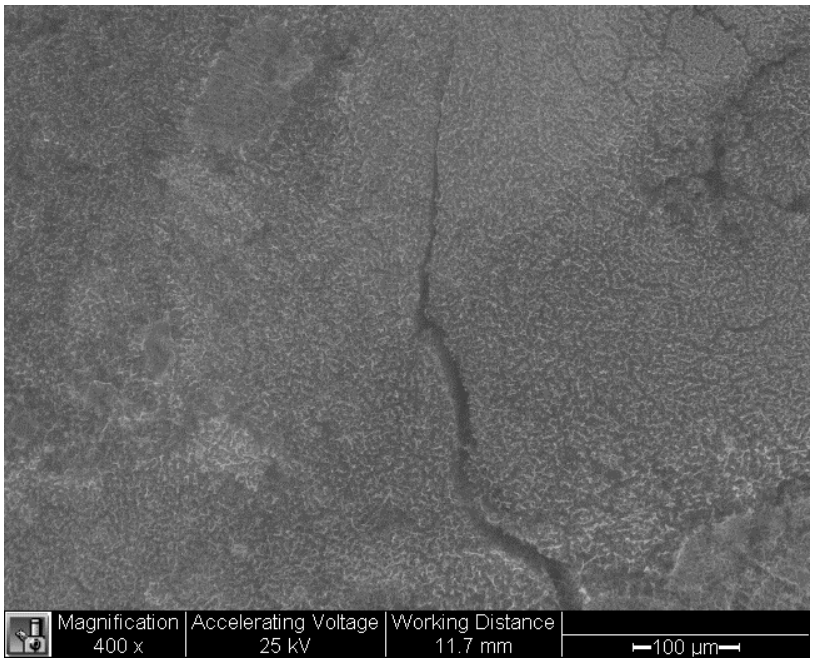

Figure 46: Silica grain surface, covered with silica gel after aging in 400 ppm pH 5 solution for 3 weeks, 400x magnification.

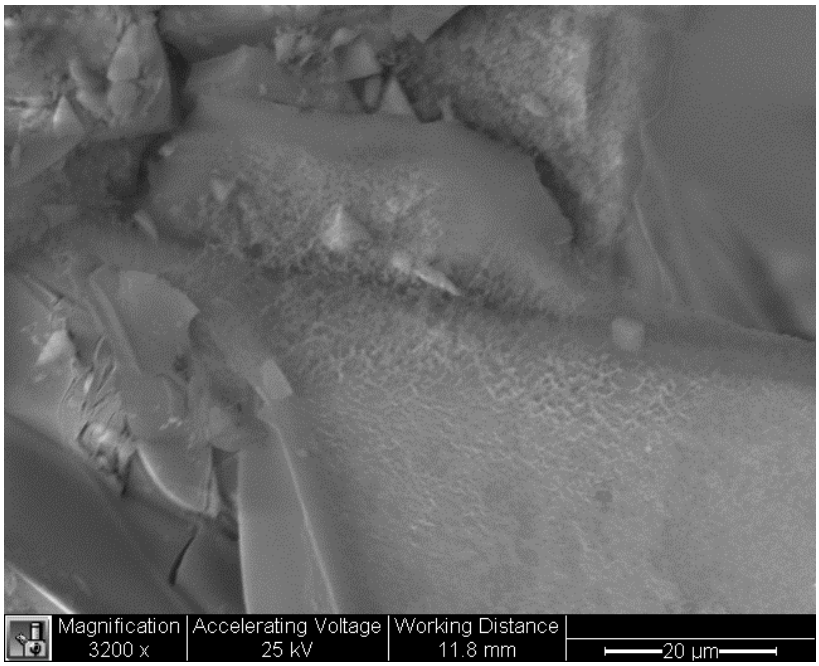

Figure 47: Silica gel growing over cracks and asperities near stressed contact, after aging in 400 ppm pH 5 solution for 3 weeks, 3200x magnification.

6.4.3 In 300 ppm solution

A GIP experiment was conducted with two silica grains aged in 300 ppm solution with pH value 5.0. The overall AW vs displacement, AW vs displacement at partial-contact phase, and AW difference vs displacement curves were shown in Figure 48 to 50 respectively.

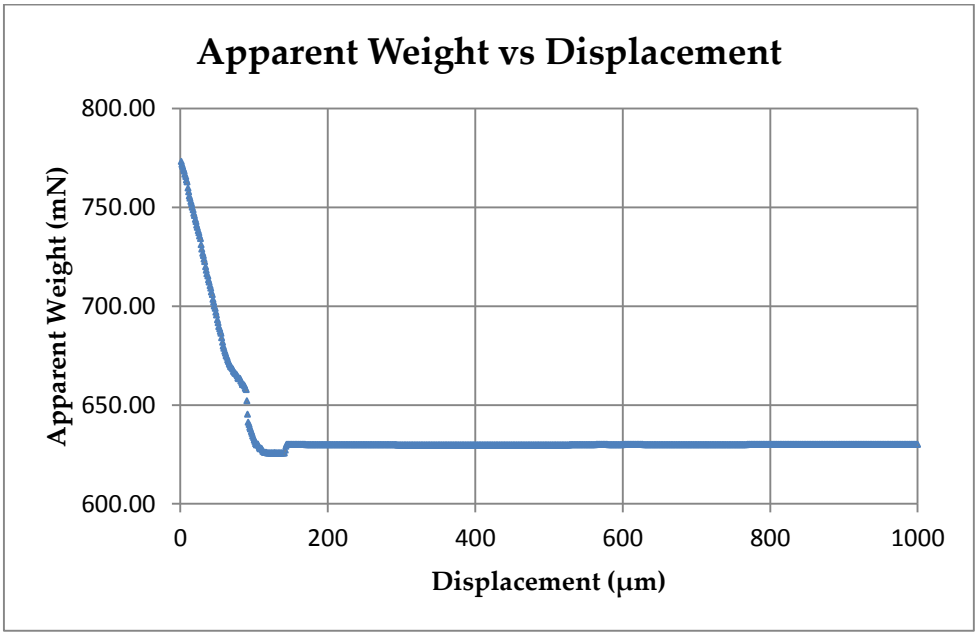

Figure 48: Plot of Apparent Weight vs Displacement for experiment in 300 ppm pH 5 solution after 3 weeks aging.

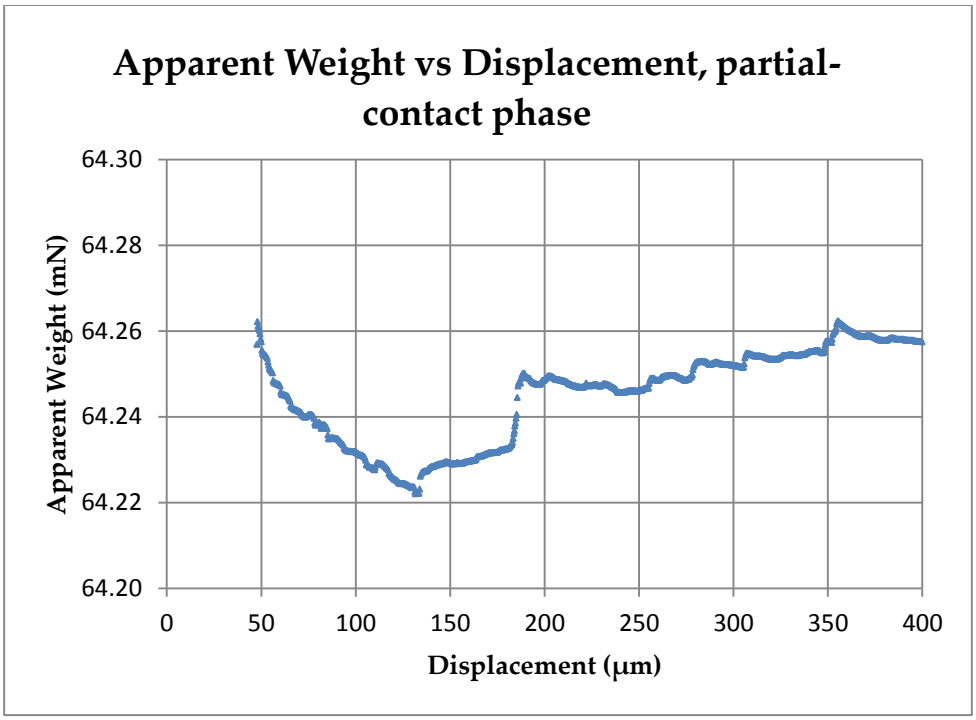

Figure 49: Partial-contact phase of apparent weight vs displacement curve, 300 ppm pH 5 solution 3 weeks.

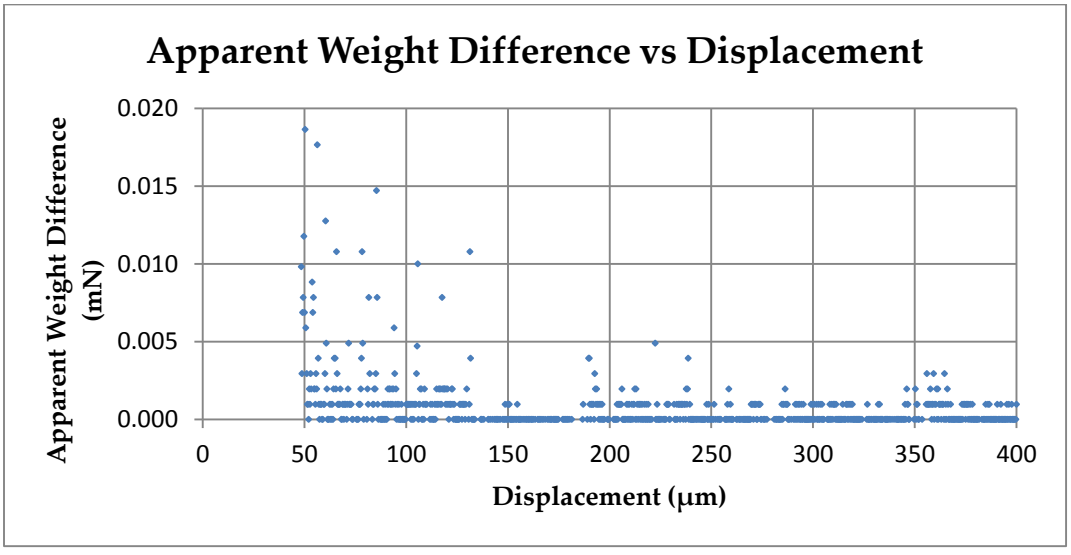

Figure 50: Difference in Apparent Weight between neighboring data points in partial-contact phase, 300 ppm pH 5 solution 3 weeks.

Table 4 shows the distribution of AW differences between neighboring data points for the experiment in 300 ppm pH 5 solution. Net tensile force was 0.6423 mN. The highest force difference between neighboring apparent weight measurements was 0.0186 mN at 50.333 μm separation.

Table 4: Distribution of AW differences for experiment in 300 ppm pH 5 solution for 3 weeks.

Range of AW difference (mN)	Number of Events
$0 < x \leq 0.0100$	332
$0.0100 < x \leq 0.0200$	9
$0.0200 < x \leq 0.0300$	0
$0.0300 < x \leq 0.0400$	0
$0.0400 < x \leq 0.0500$	0

SEM images of silica grain surfaces after the experiment ended are shown in Figure 51 and 52. Large amount of silica gen can be seen growing near silica grain stressed contact region, bonding debris caused by aging to the main body.

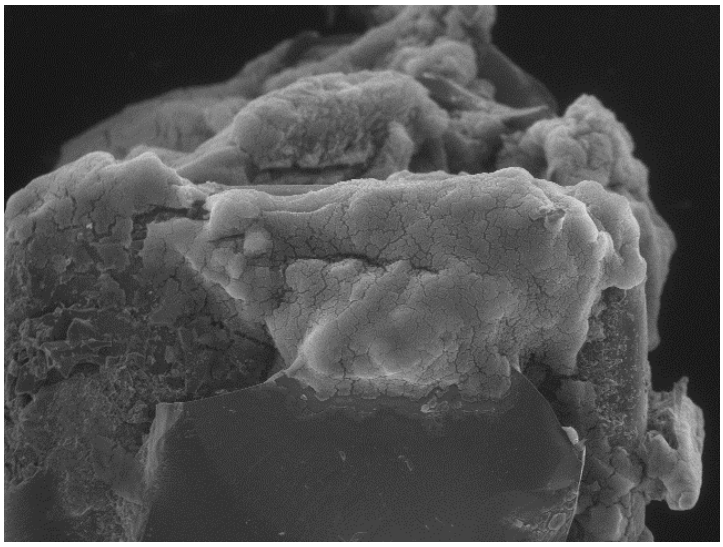

Figure 51: Silica surface near stressed contact region, after aging in 300 ppm pH 5 solution for 3 weeks.

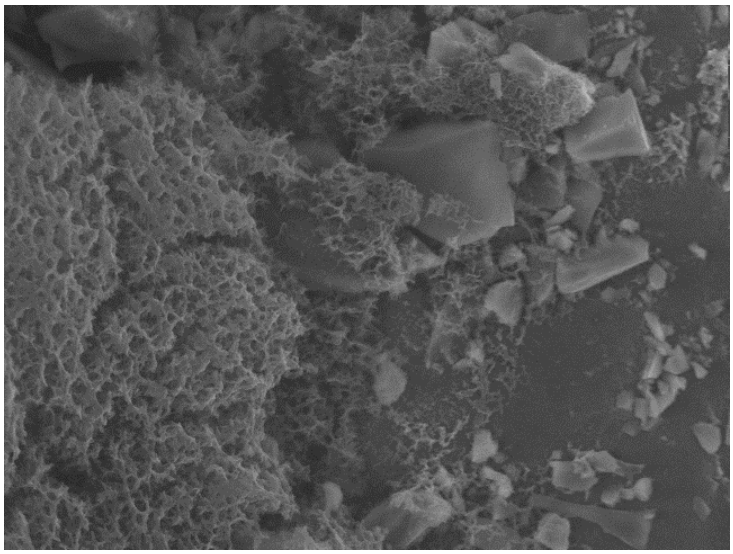

Figure 52: Local view of silica gel bonding debris together near contact region, 300 ppm pH 5 solution 3 weeks.

6.4.4 In 200 ppm solution

The same GIP experiment was repeated in 200 ppm solution for 3 weeks. The overall AW vs displacement, AW vs displacement at partial-contact phase, and AW difference vs displacement curves were shown in Figure 53 to 55 respectively.

A portion of AW data was missing between displacements 298 μm and 357 μm due to video camera power failure, but it did not affect evaluation of AW changes in the partial-contact phase.

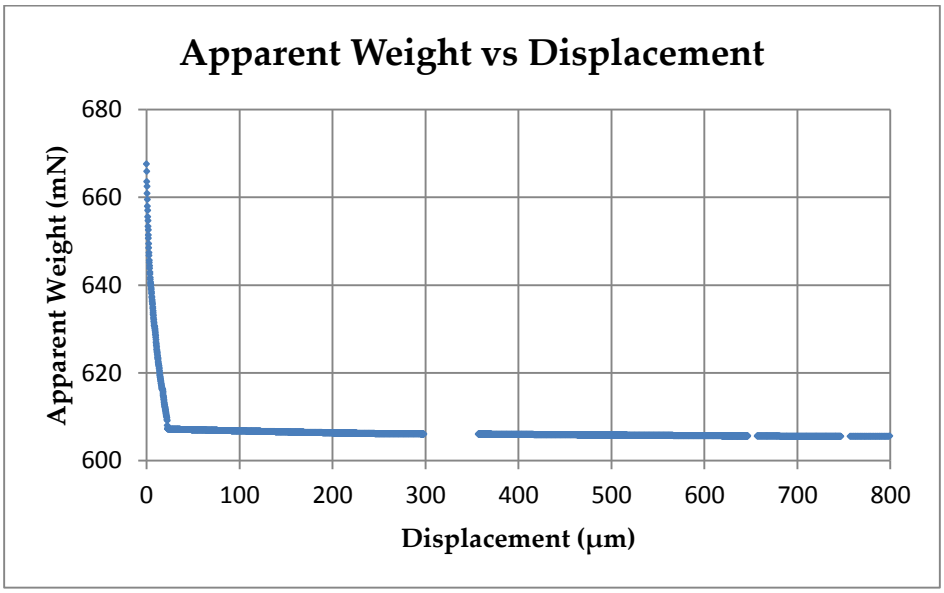

Figure 53: Plot of Apparent Weight vs Displacement for experiment in 200 ppm solution after 3 weeks aging.

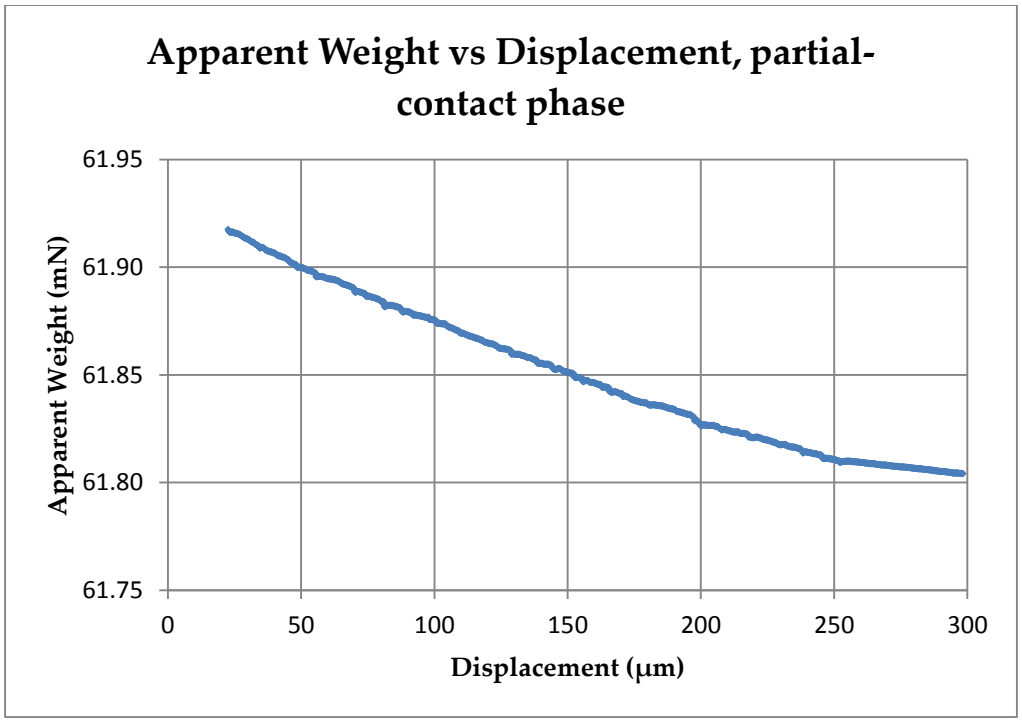

Figure 54: Partial-contact phase of apparent weight vs displacement curve, 200 ppm solution 3 weeks.

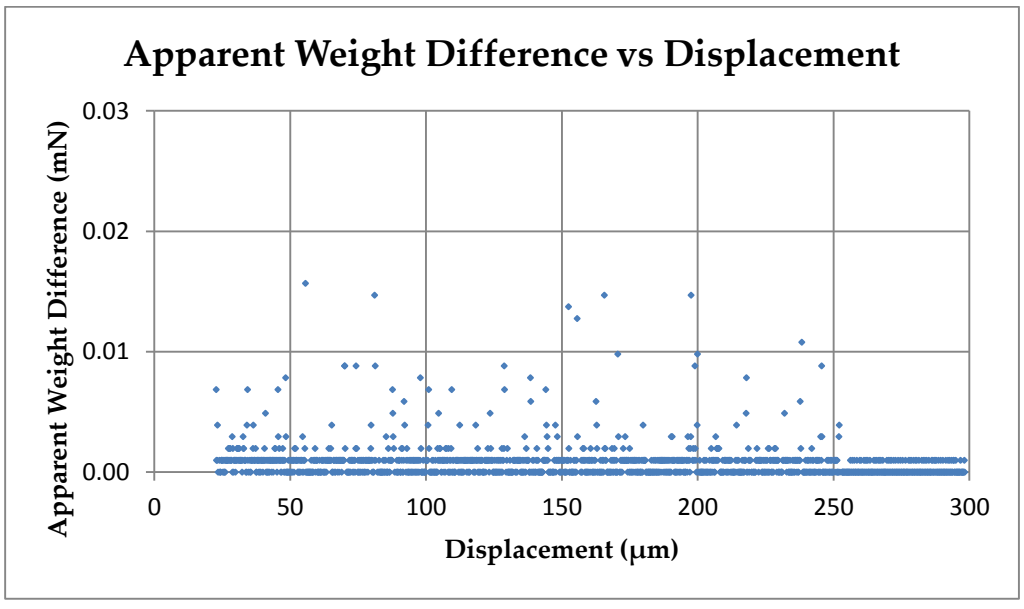

Figure 55: Difference in Apparent Weight between neighboring data points in partial-contact phase, 200 ppm solution 3 weeks.

Table 5 shows the distribution of AW differences between neighboring data points for the experiment in 200 ppm solution. Net tensile force was 0.5953 mN. The highest force difference between neighboring apparent weight measurements was 0.0157 mN at 55.667 separation.

Table 5: Distribution of AW differences for experiment in 200 ppm solution for 3 weeks.

Range of AW difference (mN)	Number of Events
$0 < x \leq 0.0100$	776
$0.0100 < x \leq 0.0200$	7
$0.0200 < x \leq 0.0300$	0
$0.0300 < x \leq 0.0400$	0
$0.0400 < x \leq 0.0500$	0

6.4.5 Control Experiments

Four different control experiments were conducted using 3 mm x 3 mm x 3 mm silica grains in GIP to assess the effect of electronic scale sensitivity, silica surface contacts, and water capillary bridge between silica grains on AW measurements. All four control experiments were conducted with an aging time of one minute to practically eliminate aging effect.

In the first control experiment, two silica grains were in contact in dry condition with no force applied to them before they were pulled apart, thus excluding the effects of stressed contact and silica solution from intergranular contact. Its AW vs Displacement plot is shown in Figure 56.

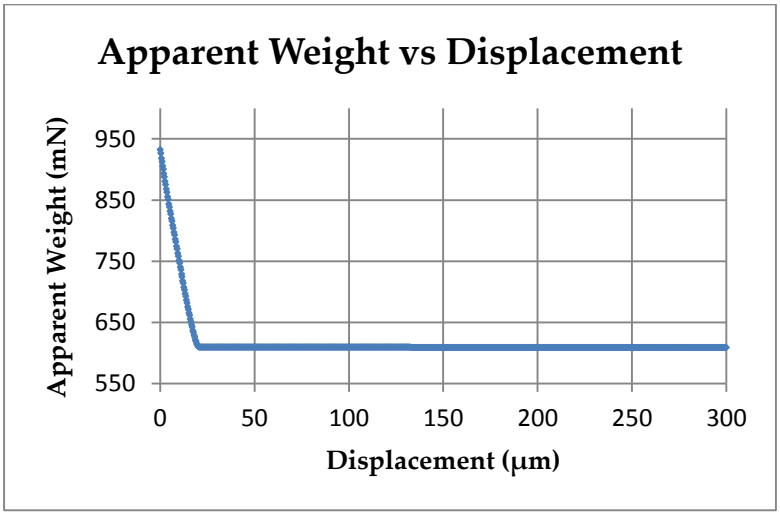

Figure 56: Plot of Apparent Weight vs Displacement for control experiment in unstressed dry conditions.

In the second control experiment, the grains were compressed in dry condition with 150 N force applied, so the intergranular contact was stressed without the presence

of silica fluid (Figure 57). As expected, a visible crack was seen developed on the upper grain where its flat surface was in contact with the edge of the lower grain.

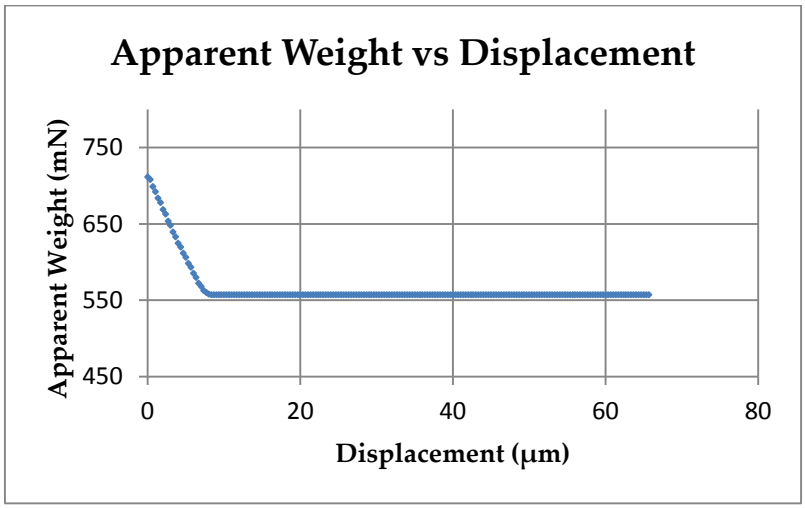

Figure 57: Plot of Apparent Weight vs Displacement for control experiment in stressed dry conditions.

In both control experiments in dry conditions, AW equilibriums were reached rapidly. No sudden change in AW was recorded.

In the third control experiment, silica grains were in contact in 500 ppm solution with no force applied to them in order to isolate the effect of silica fluid on intergranular contact. The result of subsequent pulling is shown in Figure 58 and 59. Total capillary force calculated by summing all positive AW differences was 0.3403 mN.

In the last control experiment, two silica grains were compressed in 500 ppm solution with 150 N force applied, thus replicating the standard experiment conditions without the effect of aging. The resulting AW vs displacement curve and AW difference

vs displacement curves are shown in Figure 60 and 61 respectively. Total capillary force calculated by summing all positive AW differences was 0.4590 mN.

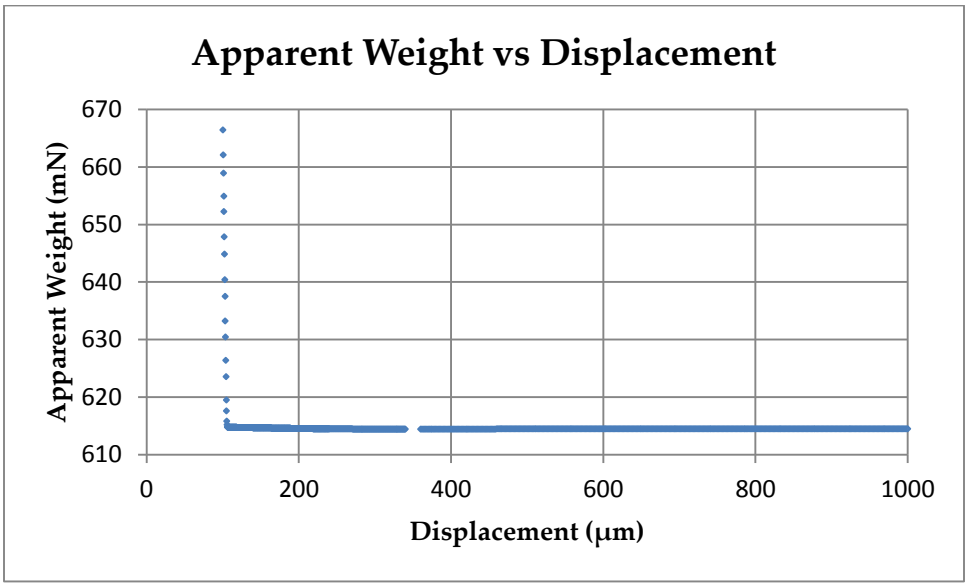

Figure 58: Plot of Apparent Weight vs Displacement for control experiment in unstressed saturated (500 ppm) conditions.

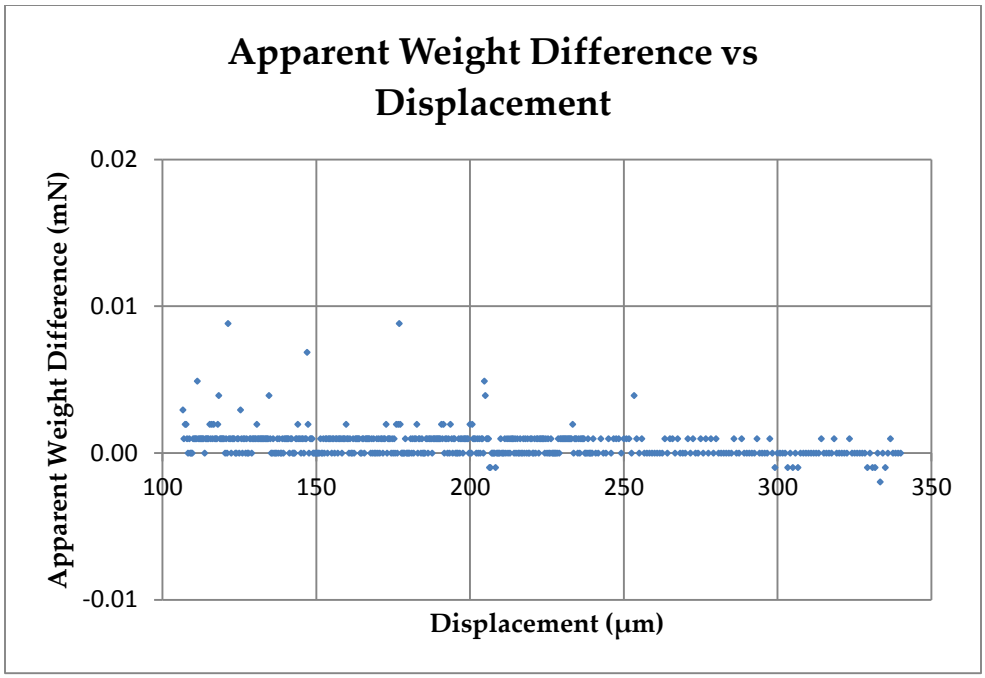

Figure 59: Difference in Apparent Weight between neighboring data points in partial-contact phase, unstressed saturated (500 ppm) conditions.

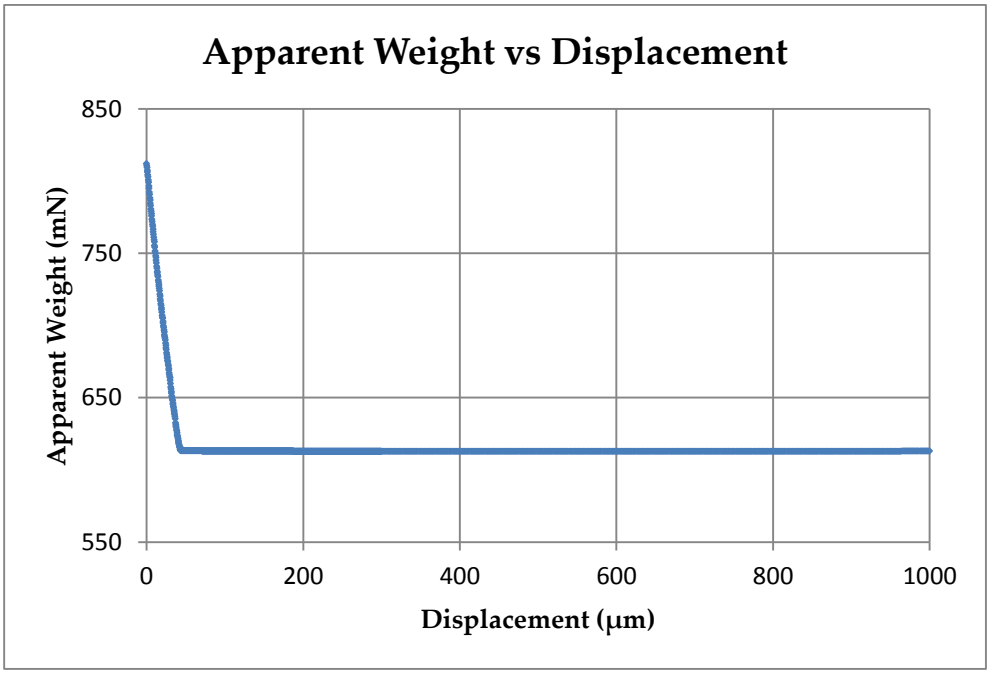

Figure 60: Plot of Apparent Weight vs Displacement for control experiment in stressed saturated (500 ppm) conditions.

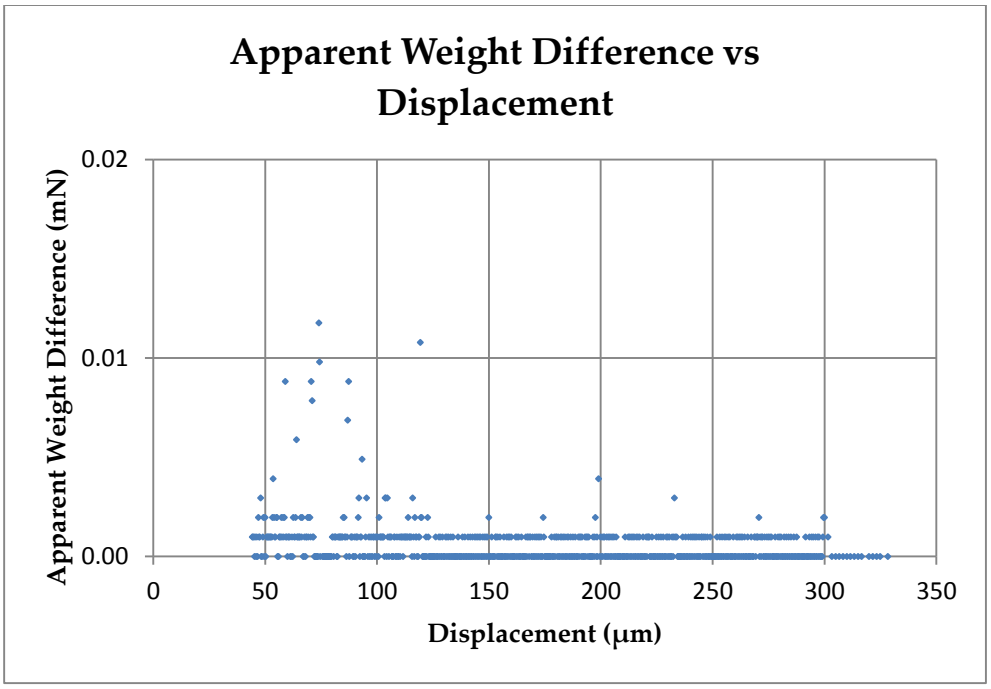

Figure 61: Difference in Apparent Weight between neighboring data points in partial-contact phase, stressed saturated (500 ppm) conditions.

6.5 Mica-induced silica gel growth

Two silica grains 1.5 mm x 1.5 mm x 1.0 mm were compressed in the Pneumatic Grain Indenter in 300 ppm Si ion concentration solution for 2 weeks with a layer of 10-micron thick muscovite mica sheet between them. Configuration is shown in Figure 62. Plenty of polymers are seen growing in the vicinity of the contact region between mica sheet and silica grain surfaces (Figure 63 and 64). Even though no visible cracks were found on either grains, the sheet of mica was penetrated near the edge of one grain, indicating stressed contact there (Figure 63). Further away from the contact region, however, no polymers were seen growing on mica sheet or silica grain surface.

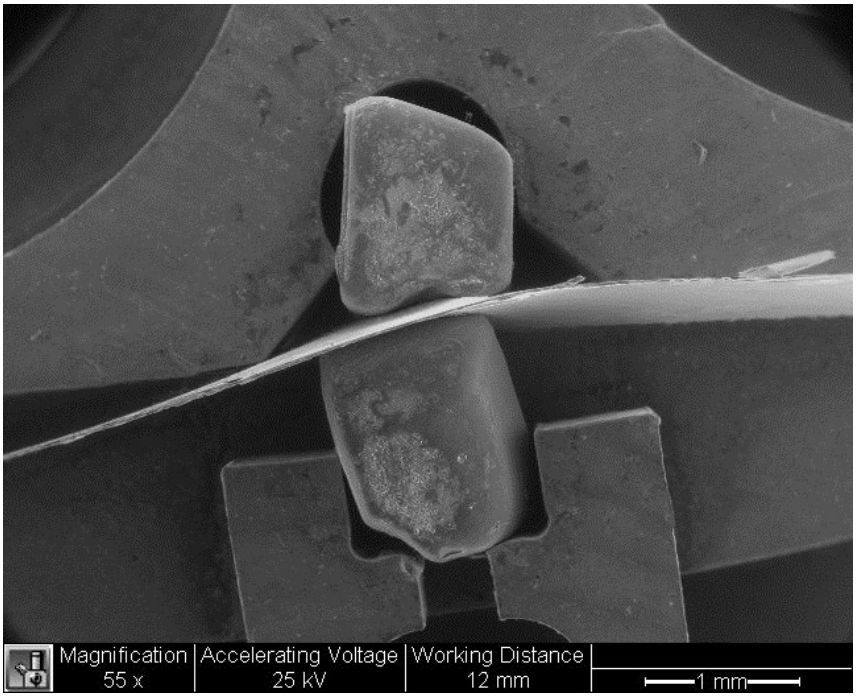

Figure 62: Two silica grains in stressed contact with a sheet of mica after 2 weeks aging in 300 ppm solution, 55x magnification.

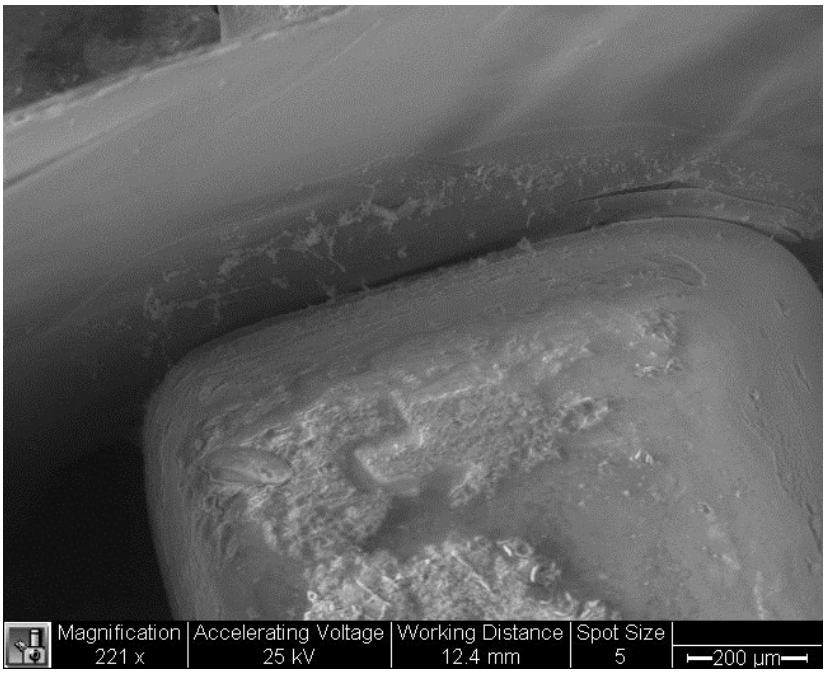

Figure 63: Stressed contact region between silica grain and mica sheet after aging in 300 ppm solution for 2 weeks, 221x magnification.

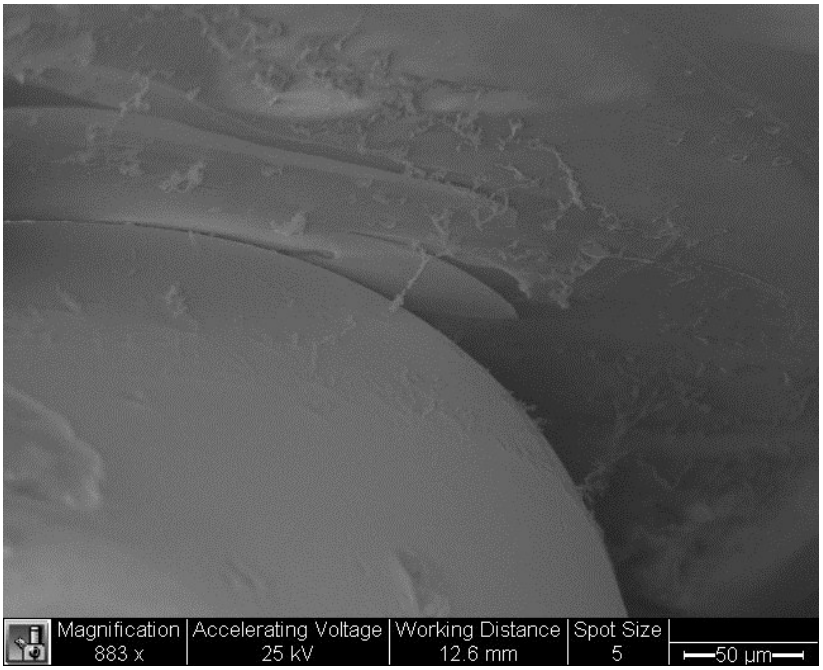

Figure 64: Silica polymer growing between silica grain and mica surface, after 2 weeks aging in 300 ppm solution, 883x magnification.

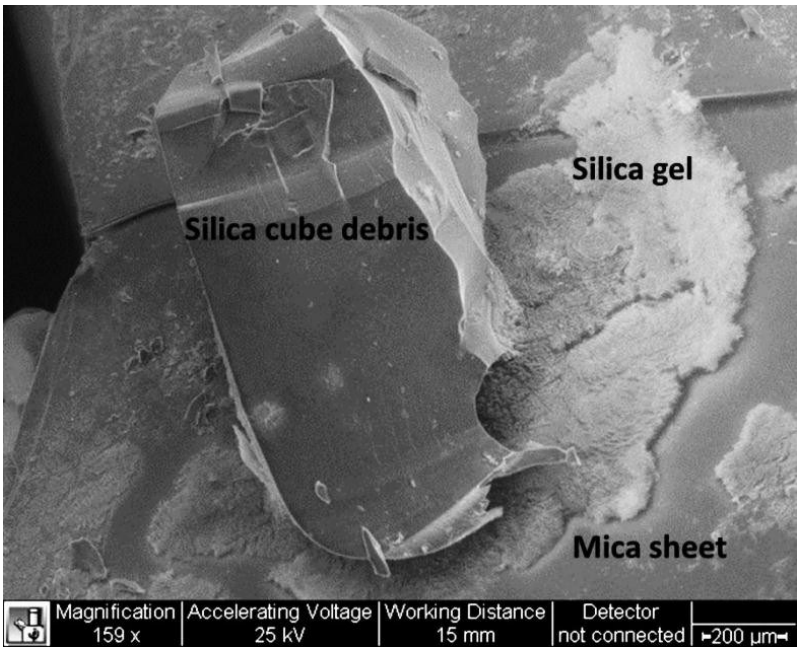

Figure 65: SEM image of silica-mica contact after 3 weeks aging in 300 ppm pH 5 solution, 159x magnification.

Two similar experiment were conducted, one in 500 ppm solution and had an aging period of 3 weeks (Figure 65 and 66), and the other was in 200 ppm solution and aged for 4 weeks (Figure 67). Figure 65 shows the configuration in 500 ppm solution, where a visible crack can be seen on mica sheet between silica grains. Figure 66 is a close-up view showing clearly silica polymers growing on silica grain surface near silica-mica contact.

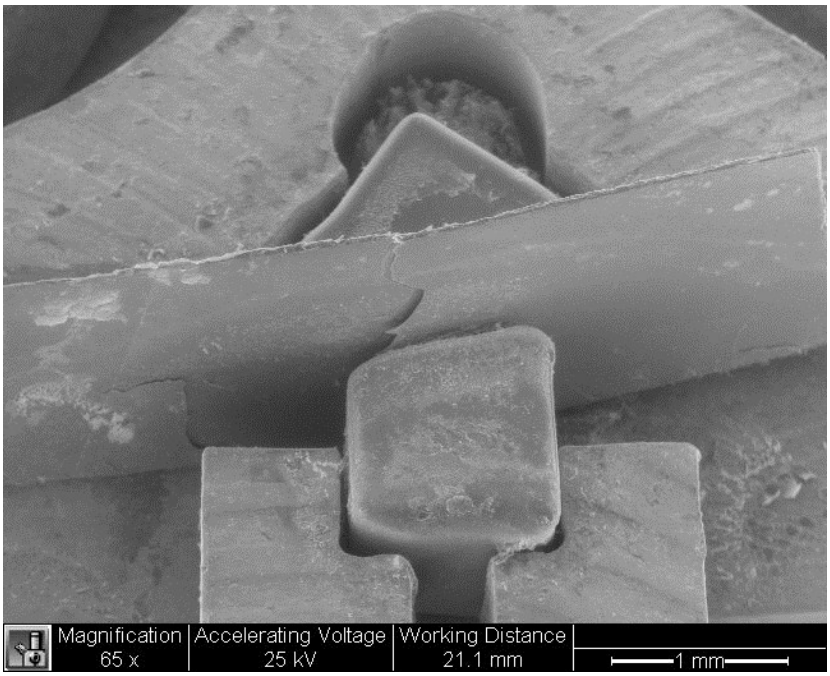

Figure 66: Configuration of silica grains in stressed contact with mica in 500 ppm solution for 3 weeks, 65x magnification.

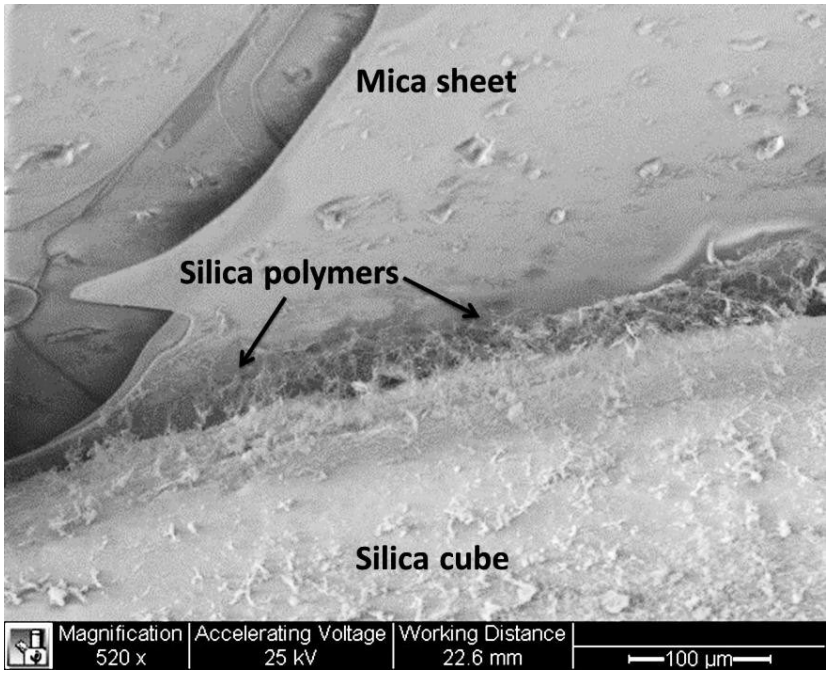

Figure 67: A close-up view of silica-mica contact showing growth of silica polymers, after aging in 500 ppm solution for 3 weeks, 520x magnification.

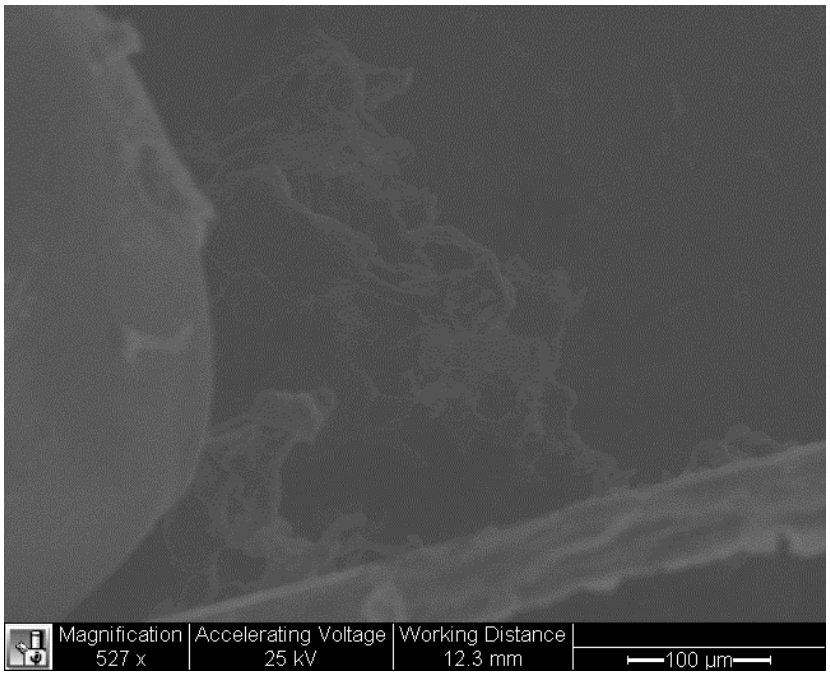

Figure 68: Silica polymer found growing on grain surface after aging in 200 ppm solution for 4 weeks, 527x magnification.

Mica powder that passes through No. 200 sieve was introduced in silica solution during aging experiments conducted using Pneumatic Grain Indenter but no visible effect was seen in SEM images. Furthermore, mica powder rested on silica surfaces and hindered microscope observation of silica surfaces.

6.6 Water capillary effect between grains

To study how much water capillary effect contributes to intergranular bonding forces between silica grains in Grain Indenter-Puller experiments, silica grains are compressed together with a drop of water (4 μl) between them and three pulling experiments were conducted. A typical capillary force vs grains separation plot is shown in Figure.

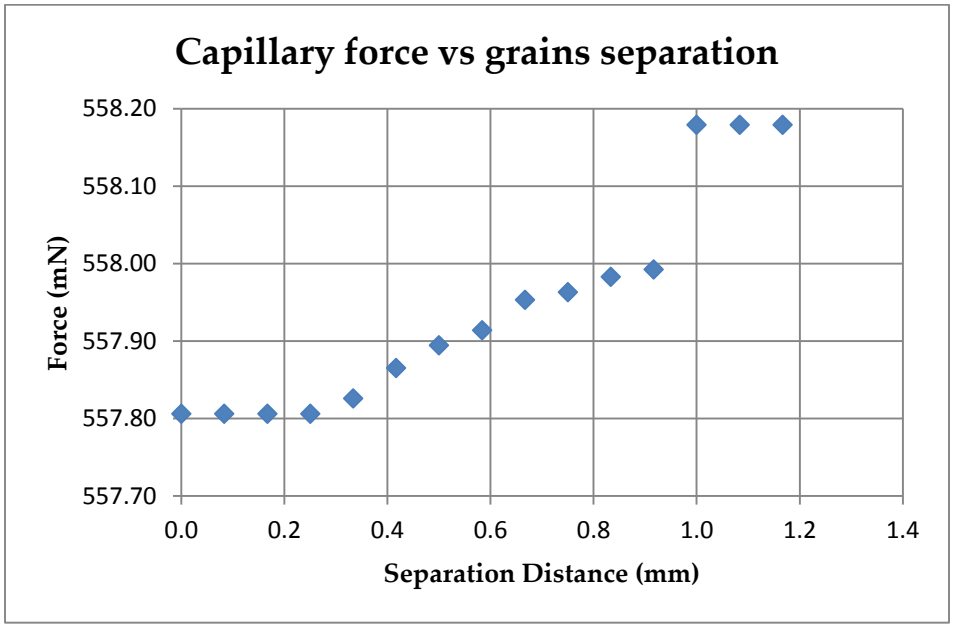

Figure 69: Plot of capillary force vs grains separation.

When the grains were pulled away at 1mm/min, the three experiments produced capillary forces of 0.373-, 0.216-, and 0.108 mN respectively.

The pulling experiments of grains with a drop of water between them were also recorded by a high-speed camera (Phantom v711 with Pixelfly) at 4 frames per second to capture the contact angle between water and silica surfaces as well as the radii of

curvatures of fluid neck and fluid main body. Figure 70 to 72 show shapes of water body at the start of the pulling experiment, just before capillary bridge collapsed, and just after capillary bridge collapsed, respectively.

Capillary force can be calculated by measuring the radii of curvature of the gorge forming between the two grains at the equator plane and the external meridian curvature using the following equations:

$$\Delta p = \gamma(\frac{1}{r_g} + \frac{1}{r_{ext}})$$

$$F_C = \Delta p \cdot \pi {r_g}^2 + 2 r_g \pi \cdot \gamma$$

where Δp is Laplace pressure, γ = 0.0496 N/m is the experimentally measured surface tension of water, r_g is the radius of curvature of the gorge at the equator plane, r_{ext} is the radius of external meridian curvature, and F_c is capillary force (Hueckel et al. 2013). Radius of curvature can be estimated by measuring the radius of the best-fit-circle on the water capillary bridge.

To assess the effect of changing capillary force on intergranular bonding force of silica polymers, capillary force at the start of the partial-separation phase is calculated. Subsequently, at the cut-off distance, corresponding capillary force is calculated again based on images similar to those shown in Figure 70 and 71. It is found that the change in capillary force, ΔF_c is 0.34 mN, which is approximately 15% smaller than the capillary force measured experimentally. The discrepancy is expected because the formulae

assumed a axisymmetric configuration whereas in this experiment, width of capillary bridge along the grains' contact edges is longer.

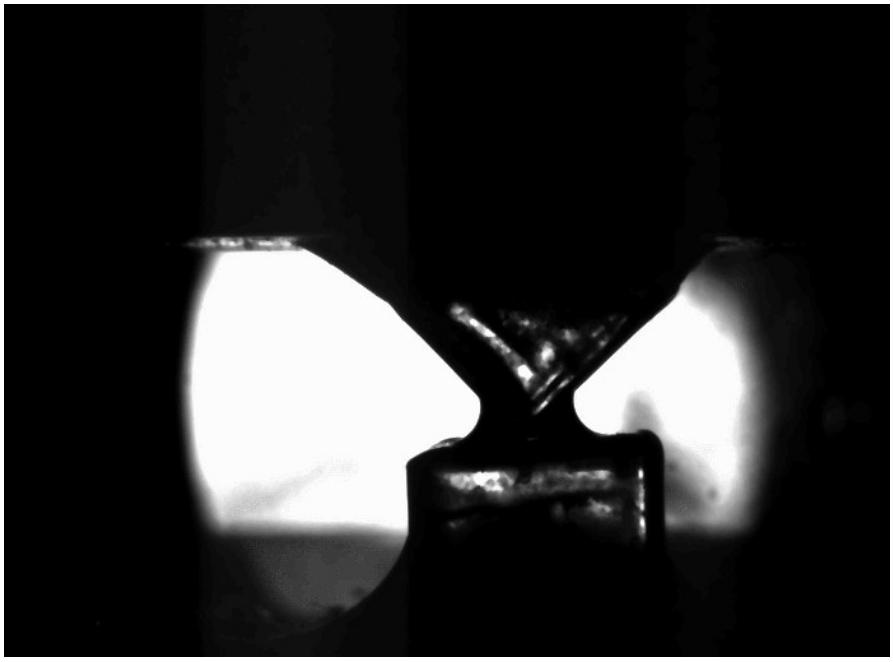

Figure 70: Shape of water body when two silica grains are almost touching each other.

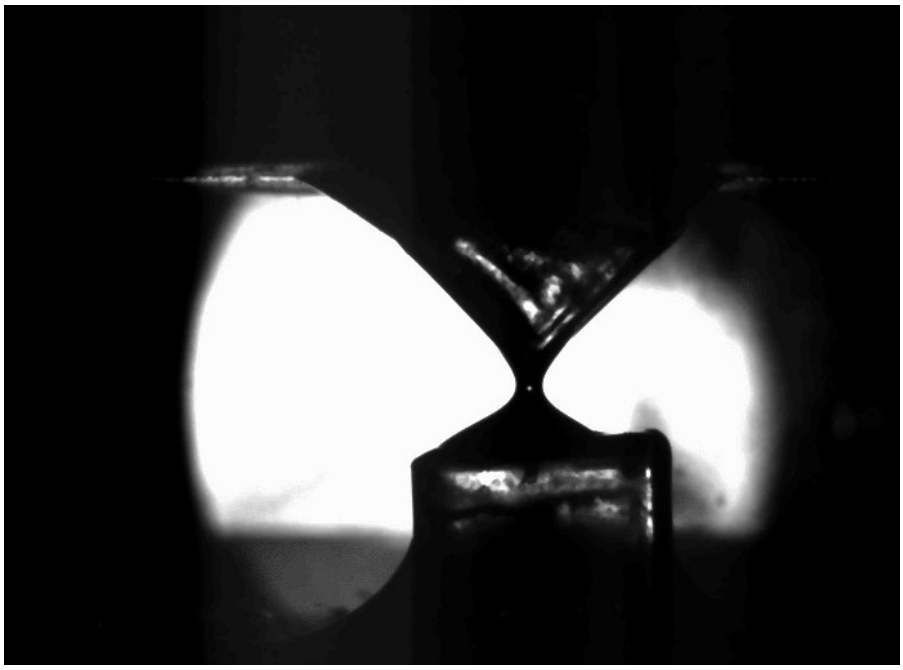

Figure 71: Shape of water body moment before capillary bridge collapsed.

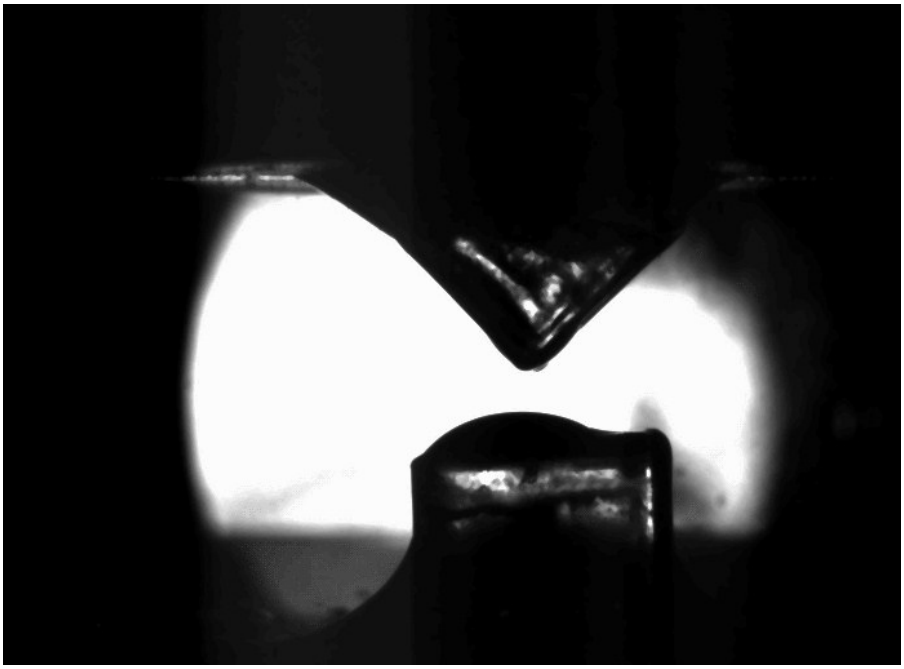

Figure 72: Shape of water body moment after capillary bridge collapsed.

7. Constitutive Model

7.1 Silica dissolution

Silica dissolution occurs in an excess of water in the following chemical reaction:

$$SiO_2(s) + 2H_2O(l) \leftrightarrow Si(OH)_4(aq)$$

A silica dissolution kinetics model between temperature 0-300 °C in simple silica-water system has been developed by Rimstidt and Barnes (1980). For amorphous silica, in neutral pH, they established that the dissolution rate constant k_+ (sec^{-1}) can be expressed as a function of temperature:

$$\log k_+ = a + bT + c/T$$

where a = -0.369, b = -7.890×10^{-4}/K, c = -3438K and the activation energy E_{act} = 60.9-64.9 $kJmol^{-1}$.

7.2 Silica precipitation

An amorphous silica precipitation kinetics model is developed by Carroll *et al.* (Carroll et al. 1998). If a solution is supersaturated with amorphous silica by a factor less than 1.3, precipitation rate has a first-order relationship with a function of the Gibbs free energy of reaction $f(\Delta G_r)$:

$$Rate_{ppt}([Si]m^{-2}s^{-1}) = k_{ppt}exp(-E_{act}/RT)(1 - exp\Delta G_r/RT)$$

where $k_{ppt} = 10^{-1.9}$ [Si] $m^{-2}s^{-1}$ is a rate constant that may depend on various conditions such as temperature, pressure, total reactive surface area, and any unidentified effect of the solution composition. E_{act} = 61 ± 1 kj mol^{-1} falls within the range of activation energy found in Rimstidt and Barnes (1980). ΔG_r can be expressed as:

$$\Delta G_r = RTln(Q/K_{eq})$$

For amorphous silica in distilled water with temperature between 18-300 °C, Q/K_{eq} = 1.7 (Rimstidt and Barnes 1980). R is the gas constant (8.318 J mol^{-1} K^{-1}). Q is the activity quotient of the system, $Q = (a_{H_4SiO_4})/(a_{SiO_2})(a_{H_2O})^2$. K_{eq} is the equilibrium constant.

If a solution is supersaturated with amorphous silica by a factor larger than 1.3, precipitation rate has a nonlinear relationship with $f(\Delta G_r)$

$$Rate_{ppt}([Si]m^{-2}s^{-1}) = 10^{-10.00\pm0.06}(exp\Delta G_r/RT)^{4.4\pm0.3}$$

Note that this equation is valid only if the concentration of silica, [Si], is above degree of saturation in water, at around 120 ppm. At [Si] < 120 ppm, $Rate_{ppt} = 0$.

7.3 Intergranular bonding strength

All the obtained data indicate that at all investigated grain-scales, strength of bonding between the aging grains increases with time in a 'logarithmic way': faster at the beginning, slower later. The data available about the structure of the polymer are insufficient at this time to attempt a structural model of polymers. However, it is still possible to advance a 1-D model of a grain-scale strength of intergranular bonding. It is hence proposed that, in a system with two grains in a stressed contact, the total intergranular bonding (tensile) strength (failure force over surface area) around contact region is a function of the mass of precipitated silica. Thus

$$F = f(A, m_{ppt})$$

where m_{ppt} is the mass of precipitated silica, A is an effective bonding area, which is the surface area around contact region at which precipitation occurs, and F denotes the total intergranular tensile failure force of the precipitated silica polymers. The critical issue for the proposed relationship is the identification of the exact meaning of the variables involved and the in which they are determined.

7.4 Identification of the variables

7.4.1 Contact surface area

Contact area can be estimated by two methods. In the first method, from the SEM image taken after 2 weeks of aging in 300 ppm solution (Figure 73), silica polymers are identified as growing around a contact region about 150 μm wide on each side of the contact. Applying this to the contact region between two grains in crushing experiments, the effective bonding area is:

$$A = 0.15mm \times 3mm \times 2 = 0.9\ mm^2$$

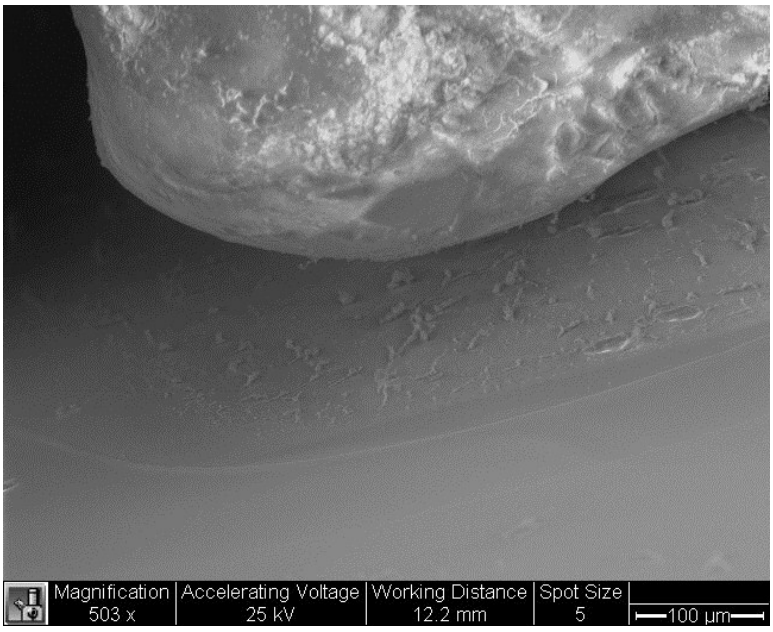

Figure 73: SEM image of silica polymer growth after 2 weeks aging in 300 ppm solution, 503x magnification.

In the second method, cut-off separation distance, L, is used as an estimate for the longest polymers that is attached to both grains. Assuming the contact angle

between cubes is 45°, the width of the effective bonding area is represented by the dark line in Figure 74.

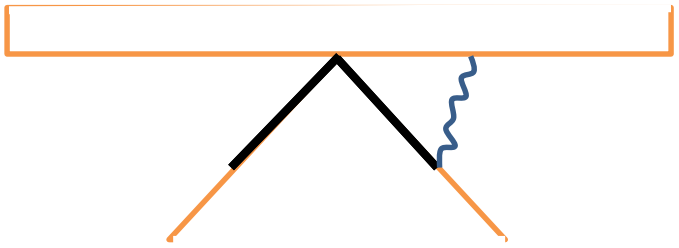

Figure 74: Simplified 2D representation of stressed silica grain contact.

Hence the effective bonding area for cubes in 500 ppm solution with an average cut-off distance L = 0.380 mm is:

$$A = 0.380\sqrt{2} \times 3 \times 2 = 3.224\ mm^2$$

The second method makes the determination of the effective bonding area sensitive to the solution concentration, as higher concentrations produce longer polymers which in turn increase effective bonding area. But in reality the further away from the actual contact, there is less of larger polymers forming and of longer polymers bonding to both surfaces. Based on the number of apparent weight difference events recorded at different concentrations, it appears that a uniform layer of silica polymer network would develop that is not much affected by the difference in silica ion concentrations in the solution. At higher concentrations, a small number of larger polymers would develop in this effective bonding area. It is logical to assume that these larger polymers grow in close proximity to stressed contact points, thus they are within the boundaries of the small but uniform polymer network. Therefore the first method of

estimation is used where the effective bonding area is assumed to be constant regardless of solution concentrations.

As shown previously in Figure 28, silica is also found to precipitate inside cracks and between asperities produced from stressed aging. Since they are not attached to both grains' contact surfaces, they do not contribute to the total intergranular tensile force measured in pulling experiments. But at this stage it is impossible to separate the mass of polymers found in cracks from the mass of polymers growing between contact surfaces. Because, based on SEM images, the amount of silica found precipitating inside cracks and between asperities is minor comparing to silica polymers growing between contact surfaces, the mass of precipitated silica inside cracks and asperities is assumed to be insignificant and thus ignored in the calculation.

7.4.2 Mass of Silica Polymers

The experimental data from aging for 3 weeks in GIP are summarized in Table 6:

Table 6: Summary of Grain Indenter-Puller experimental data.

Si Concentration in Solution (ppm)	Average Net Tensile Force at Rupture (mN)	Average Total Tensile Force at Rupture (mN)	Average Cut-off Distance (mm)
500	0.9395	1.4456	0.380
400	0.6679	1.0675	0.210
300	0.6423	1.0419	0.130
200	0.5953	0.9949	0.250

In 500 ppm solution, silica concentration in solution was:

$$[Si] = 500\ ppm = 500 \times 10^{-3} g/kg$$

At room temperature, the Gibbs free energy of reaction is:

$$\Delta G_r = RTln\left(Q/K_{eq}\right) = (8.318\ J\ mol^{-1}\ K^{-1})(298.15\ K)ln(1.7) = 1.315\ kJ\ mol^{-1}$$

Assuming amorphous silica has a solubility of 120 ppm at neutral pH and room temperature (Iler 1979), 500 ppm solution is supersaturated with amorphous silica by a factor of 4.2 which is larger than 1.3, use the following relationship:

$$Rate_{ppt}([Si]m^{-2}s^{-1}) = 10^{-10.00\pm0.06}\left(exp\frac{\Delta G_r}{RT}\right)^{4.4\pm0.3} \approx \frac{3.17 \times 10^{-10}[Si]}{m^2 s}$$

Assuming that there is enough solution so that precipitation does not affect its concentration, it follows that rate of precipitation will not change over time. For 500 ppm solution, over an area of 0.90 mm^2 in 3 weeks, the mass of polymerized silica is:

$$m = 3.17 \times 10^{-10} \times 500 \times 0.9 \times 10^{-6} \times 1.8144 \times 10^{6} = 2.588 \times 10^{-7} g$$

A summary of mass of silica polymer, effective bonding area estimated from experiments for the different concentration solutions are listed in Table 7:

Table 7: Mass of polymerized silica in aging experiments using solutions with different Si concentrations.

Si Ion Concentration (ppm)	Total Tensile Force at Rupture (mN)	Cut-off Distance (mm)	Effective Bonding Area (mm^2)	Intergranular Tensile Stress at Rupture (Pa)	Mass of Polymerized Silica (μg)
500	1.4456	0.380	0.90	1.606	0.259
400	1.0675	0.210	0.90	1.186	0.207
300	1.0419	0.130	0.90	1.158	0.155
200	0.9949	0.250	0.90	1.104	0.104

Intergranular tensile stress at rupture exhibited between grains is plotted against mass of silica polymers in Figure 75.

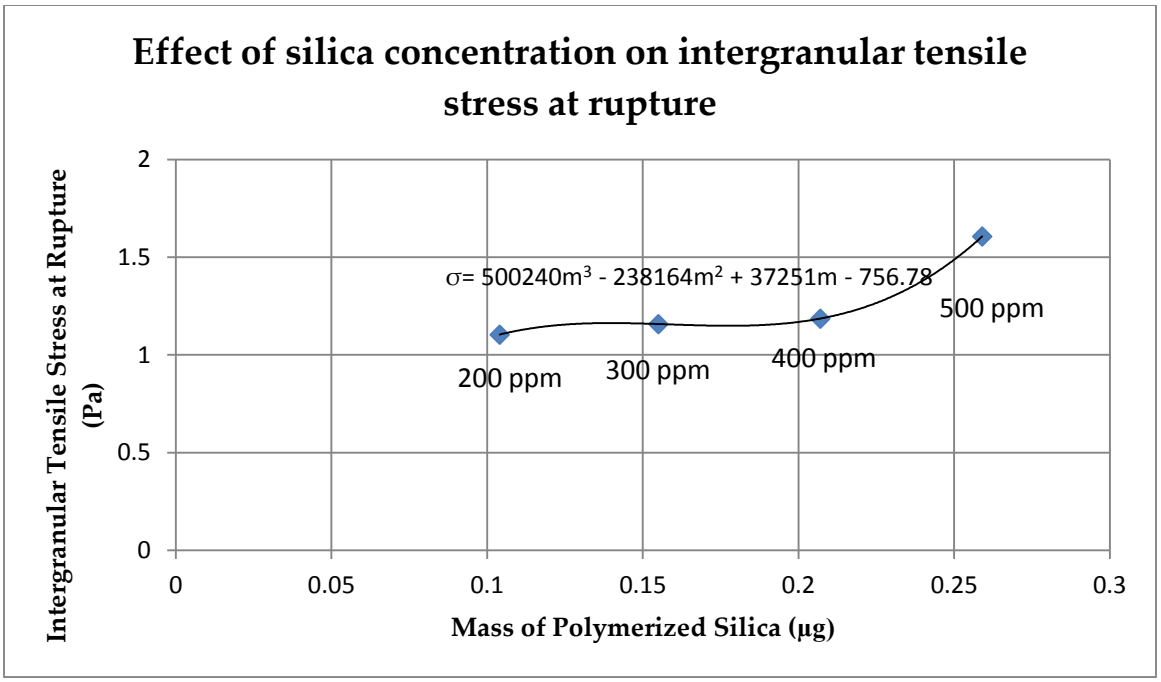

Figure 75: Plot of total intergranular tensile stress vs mass of polymerized silica.

A polynomial function is fitted to the data:

$$\sigma = \alpha m^3 + \beta m^2 + \gamma m + \kappa$$

where σ is the intergranular tensile stress, m is the mass of polymerized silica, α = 500240 $(g^2ms^2)^{-1}$, β = -238164 $(gms^2)^{-1}$, γ = 37251 $(ms^2)^{-1}$, and κ = -756.78 g/ms^2. This equation is only valid when Si ion concentration in solution is higher than 120 ppm, the degree of saturation of silica in natural water, which converts to 0.062 µg of polymerized silica. At local Si concentration lower than 120 ppm, no precipitation of silica can occur.

8. Discussion and Conclusions

Silica gel growth in undisturbed solution experiments provides a qualitative benchmark for measuring the mass of silica gel in an stressed intergranular environment. In solution with 180 ppm Si ion concentration, it takes seven days for small silica nuclei to form. In 300 ppm or 500 ppm solutions with pH value 5.0, silica gel can be observed by the naked eye 2 weeks after experiments start. These observations serve as an initial verification of our hypothesis that silica gel is able to grow in solution in the same amount of time that aging phenomenon in granular soil is observed in literature. Natural pore water has concentration of silica on the order of 120 ppm. No silica gel was observed growing on the free (unstressed) silica grain surfaces in solution with Si ion concentrations below 150 ppm. However, in subsequent experiments conducted in solutions with Si ion concentration below 150 ppm, there were clear sightings of silica polymers on silica surfaces in contact under load, which hence can be attributed to accelerated silica dissolution and polymerization by aging at stressed contact. Observations made by AFM and SEM provide an initial estimate that silica polymers are at least 10 nm thick.

In Pneumatic Grain Indenter experiments conducted with 500 ppm solution, polymers a few hundred μm in length are found near the contact region. It can be seen in Figure 21 that silica polymers in the contact region adhere to both the left and right silica grains in contact. Such a configuration, it is believed, would create adhesion

between silica grains at the microscopic level and thus enhance the granular tensile strength of granular material on the macroscopic level.

In another experiment using the same set-up except in 300 ppm solution instead, deposits of silica gel is found in grain cracks (see Figure 27). Such deposits are roughly one magnitude smaller than those found from aging experiment in 500 ppm solution.

To determine how much effect a stressed contact between grains has on precipitation and polymerization of silica, a Pneumatic Grain Indenter experiment was conducted in 300 ppm solution with some minor adjustments to test conditions. The compressive force applied to the grains in this test was small enough to be able to just bring the two grains firmly together without damaging either grain. The level of stress at silica-silica contact region was kept to a minimum. No cracks are found on either grain after 2 weeks, and no silica gel deposits are seen anywhere on grain surfaces (see Figure 29). Therefore it is shown that the rate of silica precipitation and polymerization in the stressed contact region between silica grains is higher when the stress between grains is high enough to cause local damage that generates extra surfaces and asperities which would accelerate silica dissolution and precipitation processes.

Images taken from PGI experiments conducted in 200 ppm pH 2.5 solution showed clusters of silica polymers attached to very thin polymers (Figure 31). The results indicate that once grown, silica polymers exert an adhesive force to nearby silica

surfaces. This is a further verification that silica polymers grown in stressed contact regions exert bonding forces to the grains.

In AFM pulling experiments, step-like force patterns during cantilever withdrawal (see Figures 23 to 25) suggest that clusters of polymers are present on silica grain surface. When an AFM cantilever tip picks up a polymer, the polymer is stretched, between the cantilever tip and the surface where it grows, with an increasing force until one segment breaks, at which point a sudden reduction in force is measured. As the tip was continuously raised higher from the stage, more segments of the polymer are stretched and broken, resulting in a step-like pattern. The maximum distances between peaks of the withdrawing curves and the flat approaching curve are measured and converted based on cantilever spring constant to show that the tensile strengths of silica polymers growing on free silica surfaces are in the order of 100 nN. The distances between peaks in the withdrawing force curve indicate that the lengths of those polymers are in the order of 100 nm.

Comparing the SEM images of silica grains after they are compressed and aged with, and without mica sheets show that larger quantities of silica polymers are seen growing near mica-silica contacts. It is also observed that silica polymers have a tendency to grow in the vicinity of stressed contacts (see Figures 63 to 68). Further away from mica-silica contact regions, no polymers are seen growing on mica sheet. Such phenomenon may be due to accelerated dissolution and subsequent precipitation of

silica in the local stressed mica-silica contact regions. It indicates the important role of stressed contacts in the dissolution, precipitation, and polymerization of silica.

8.1 Net intergranular tensile force

Experiments in Pneumatic Grain Indenter and AFM have confirmed that silica polymers grow between two compressed silica grains, as originally suggested by Denisov and Reltov, 1961. The silica polymer growth concentrated near contact region under compression inducing local damage after aging for a few weeks (Guo and Hueckel 2013). The Grain Indenter-Puller was thus designed to measure the intergranular tensile strength a polymer structure develops between silica grains during stressed aging. As the load frame slowly pulls the upper grain away from the bottom grain, silica polymers attached to both grains near contact region are stretched, exerting a tensile force that lifts up the lower grain sitting on an electronic scale. As a result, a sharply fluctuating apparent weight measurement is recorded on an otherwise consistently downward-trending apparent weight vs displacement curve. During the stretching of the polymer, the scale would record episodes of a higher-than-normal decrease in apparent weight, followed by a slight increase in weight as the individual polymer links are stretched too far and locally break. A positive force difference indicates the scale recorded a finite drop in apparent weight, whereas a negative force difference on the curve indicates that the scale recorded an increase in apparent weight. From measuring the magnitudes and lengths of the finite weight drops, polymer size and tensile strength can be estimated since the rate of displacement is known. Adding up the magnitudes of all the apparent weight drops occurring between 0 to 400 μm of

grain separation displacement in the experiment, the net tensile force applied by silica polymers growing between two silica grains during aging has been estimated. Capillary forces in the intergranular water are superposed on the forces induced by extension.

As the top grain was pulled away from the bottom grain, water capillary effect between grains weakens continuously (Mielniczuk *et al.* 2014). Thus the apparent weight of the bottom grain recorded by the scale would also decrease continuously during pulling experiment. Any increase in weight reading on the scale would occur only after negating the continuous decrease in weight due to diminishing capillary effect. Thus total intergranular tensile strength can be calculated by combining the change in capillary force during pulling and net tensile force in the polymer network.

Control experiments were conducted to determine machine error and water capillary effect on weight measurements during pulling. In the control experiments conducted in solution with 500 ppm silica ion concentration, but with no aging, the apparent weight vs displacement curves were very smooth. Capillary forces are attractive forces arising at the contact between the interface of air, water and solid, and are primarily dependent on the surface tension of the liquid and the curvature of air/liquid interface. Changes in capillary forces after 400 μm separations were measured for grains with unstressed contact and grains with stressed contact amounting to 0.3403- and 0.4590 mN, respectively. In the stressed control experiment, grain surfaces were severely damaged with cracks observable by the naked eye. In other experiments,

damages to grains were much more local with micro asperities and small debris generated within contact. Thus, the approximate capillary force adopted was the average of the two values obtained in control experiments, hence taken as equal to 0.4 mN. As it was seen in the experiments with pure water capillary bridges, the total intergranular force between two spherical silica grains tends to decrease with the kinematically driven extension of the separation (Lian et al. 1993, Mielniczuk et al. 2014). The force either decreases monotonically to zero, or the bridge breaks and there is a force jump to zero. The magnitude of the force does depend on the size of grain and size of the initial gap between the two grains, but for the grains of 10 mm diameters, the order of magnitude of the capillary force is about 0.5 mN, which is the order of the forces measured in this research.

Apparent weight vs displacement curves generally reach a minimum for displacements of the grains between 300 to 400 μm, indicating a complete separation of the grains at this stage. After the minimum of force is reached, the grains are completely separated and weight measurements are affected by capillary effect only. The magnitude of the capillary force decreases continuously as separation between the grains grows larger until finally capillary bridge breaks down.

In the experiments where grains were aged in 500 ppm solution for three weeks, three weeks but with a half speed during pulling, and for four weeks again at a standard pulling rate of 20 μm/min, the maximum tensile force measured were 0.9395-,

0.8669-, and 1.3318 mN respectively. The tensile rupture forces after four weeks aging was by more than 30% higher than that after three weeks. Thus, it is possible that at higher silica concentration, the polymerization process within the first three and four weeks progresses substantially with the time of the process.

It is interesting to note the test at half rate of pulling (down from 20 μm/min to 10 μm/min), produces the tensile force at failure that is about 8% smaller. It indicates that the silica polymer is a visco-elasto-plastic structure, but with a relatively weak rate sensitivity. Most notably the number of events was ten times lower as far as low amplitude events are considered, whereas the number of the events of higher amplitude is of the same order during faster and slower pulling.

High force differences occurred in the early separation phase, with magnitudes of 0.0245-, 0.0265-, and 0.0226 mN respectively, for the above identified cases. This is possibly due to polymer links that being strained most and broken in the early separation process are the most robust, possibly shortest, of the entire population. This point deserves a closer attention. SEM images of grain surfaces taken after pulling experiment showed evidence that silica polymers were indeed growing on grain surfaces and bridging between cracks (Figure 42).

In the experiment where grains were aged in 400 ppm solution under compression for 3 weeks, the total maximum intergranular tensile force recorded was 0.6679 mN, which is nearly 30% less than that at 500 ppm. Nevertheless, SEM images of

grain surfaces taken after pulling (Figure 46 and 47) show also at 400 ppm a massive gel growth on surfaces near the contact region, connecting debris with the main grain body.

In 300 ppm solution, after 3 weeks aging, the maximum tensile force was 0.6423 mN, slightly smaller than those in 400 ppm solution, but visibly smaller than in higher, i.e. 500 ppm silica ion concentration solutions. SEM images of silica grains in 300 ppm solution taken after 2 weeks aging (Figure 51 and 52) show that the boundaries of cracked patterns on silica grain surfaces matched the boundaries of thicker gel structures growing on the same surface. This suggests that the cracked patterns on silica grains are silica gel residue after drying in the SEM chamber. The images also suggest that at 300 ppm the region of bonding less intense than in 400- and 500 ppm. The tensile force reached a peak at 134 μm of separation and started decreasing after that. That type of softening of the polymer was not seen in other tests at different silica concentrations.

In the experiment where grains were aged under compression for 3 weeks in 200 ppm solution, net intergranular tensile force was 0.5953 mN, again less than that at all higher concentrations (Figure 76). Interestingly, the cut-off distance between grains when no further change in apparent weight can be observed was 250 μm, longer than those in 300- and 400 ppm solutions. Cut-off distance is defined as the separation distance between grains beyond which no further change in the apparent weight was observed on the scale. It is an indication of maximum force that the polymer may sustain. Unfortunately, the force was not measured beyond the separation of 300 μm.

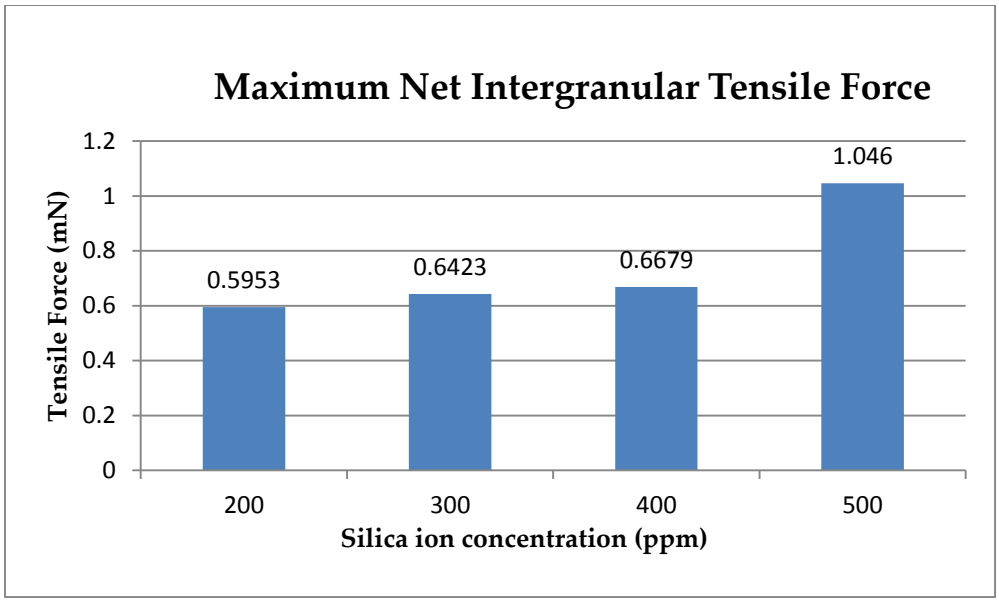

Figure 76: Maximum net intergranular tensile force measured in Grain Indenter-Puller experiments at different Si ion concentrations.

Based on the experiments, it can be concluded that as concentration of silica ions in solution increased, so did maximum intergranular tensile force in the silica gel on grains during the separation increase, as shown in Figure 76. This is most likely because less silica gel was formed at lower concentration around contact region between silica grains. It is hence established that the maximum intergranular tensile force that silica polymer network can exert in tension on grains in a solution with slightly over-saturated silica ions is in the order of 1 mN.

The maximum total intergranular tensile force expected to be generated by completely submerged polymer network, that is without capillary contribution is calculated by combining net intergranular tensile force and change in (attractive) capillary force. The results are shown in Figure 77.

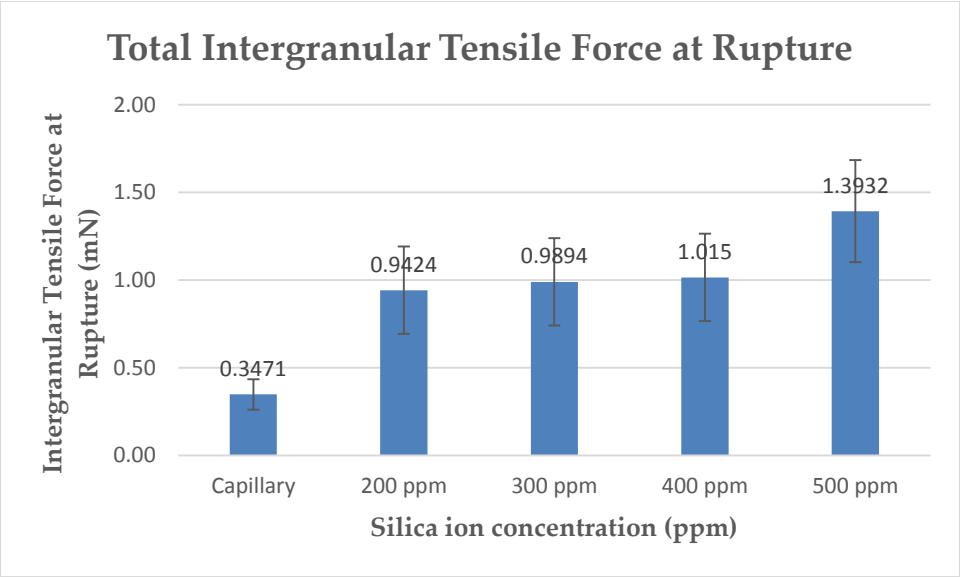

Figure 77: Total intergranular tensile force at rupture measured between grains in pulling experiments at different Si ion concentrations.

Data obtained in control experiments in wet and dry conditions are used to estimate the water capillary effect and machine errors on force measurements respectively. Specifically the control experiment in dry condition with no stress applied between grains indicates a machine error of up to 0.1253 mN. Standard deviation of the mean capillary effect was 0.0872 mN. Using data from all three experiments conducted in 500 ppm solutions, the standard deviation of net intergranular tensile force is calculated as 0.2042 mN. The error bar for total intergranular tensile force is calculated by adding the standard deviation of experiments conducted in each concentration level and the standard deviation of water capillary effect in the apparatus.

8.2 Silica gel network size

The cut-off separation, at which the total intergranular force becomes zero represents, in a sense, the maximum length to which a polymer network may be extended between the grains. As seen in the SEM images (Figure 41 and 47) collected after the network failure, the polymer is still attached to the grain surface. This confirms our hypothesis that failure of the polymer network takes place by a breakage of the individual links, rather than via detachment from the grain substrate. A summary of cut-off separation vs silica ion concentration is shown in Figure 78.

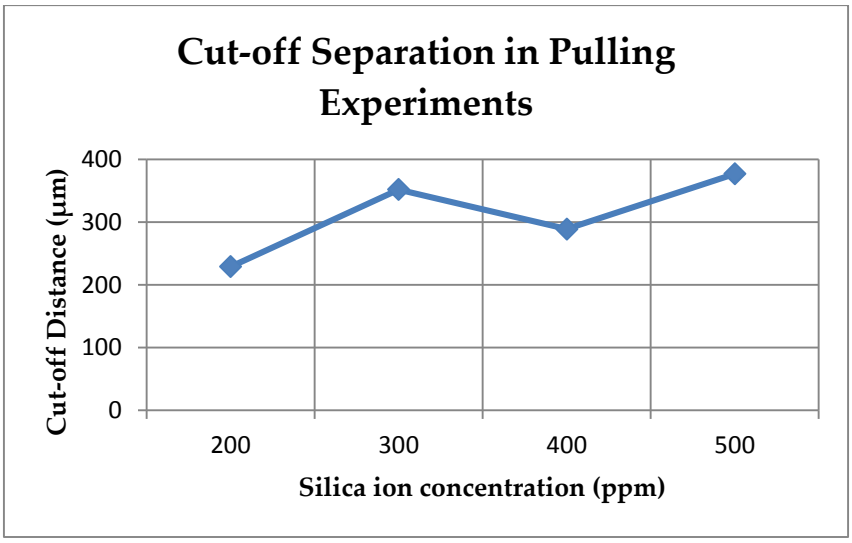

Figure 78: Cut-off separation in pulling experiments after aging in solutions containing various Si ion concentrations.

Apart from the test in 400 ppm solution, there is a consistent trend that higher silica ion concentration in solution yields the polymer networks that could be extended the more. The maximum separation to which the polymer could be extended is 0.4 mm.

An additional information about the evolution of the silica polymer during pulling experiments is obtained from the distribution of the number of force difference amounts belonging to a given range of force drops presented in a semi-log scale, shown in Figure 79. It is worth reminding that measurement points are taken every second. Each point with positive magnitude is believed to represent the strength of an individual silica polymer link that has been stretched and broken during pulling. Points with negative magnitudes meant no polymer was being stretched during the second.

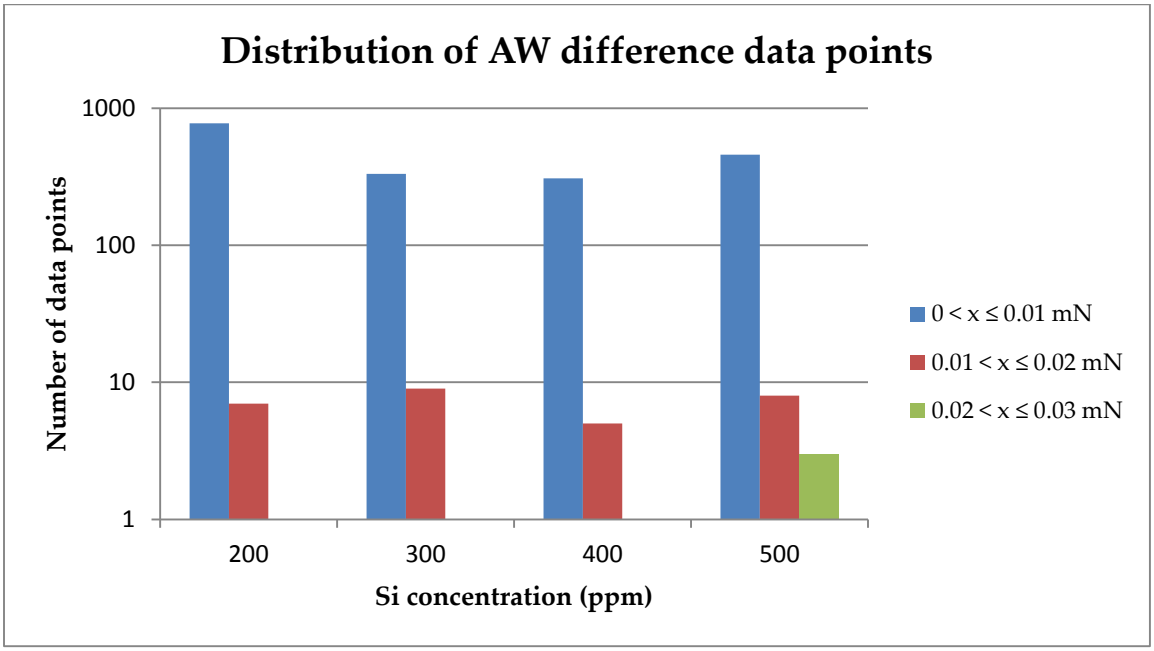

Figure 79: Distribution of force difference data points in pulling experiments after aging for 3 weeks in different Si ion concentration solutions.

At lower concentrations, all data points with positive magnitudes were less than 0.02 mN, whereas at higher concentrations a small number of points with large magnitudes have been detected. This observation suggests that a small number of robust

polymer links was growing at contact regions only in high silica ion concentration solutions. At lower concentrations, a gel network of uniformly low strength links would grow between grains. That clearly refers to polymers developed within 3 to 4 weeks.

Mica powder in solution does not seem to have any obvious effect on silica polymer growth in grain crushing experiments. We postulate that it is because suspended mica particles in solution do not create enough contact surfaces with silica comparing with compression between silica grains and mica sheets to have an impact.

8.3 Conclusion

The main and novel potential contribution of this research to the literature lies in the exploration of the mechanisms behind soil aging in stressed and submerged conditions. By simulating soil contacts on a granular scale in laboratory settings, we isolated and identified the source that generate bonding between silica grains and quantified the strength of such bonds. We had previously postulated and subsequently proved that such bonds are provided by silica polymers and gel structures on and between individual silica grains. Quantifying the strength of such bondage between grains allowed us to build a microscopic model of granular soil aging that connects the increase in the tensile strength of silica grain assembly to silica concentration in the surrounding solution. Such model allows for a more accurate prediction of in-situ soil properties based on laboratory measurements.

This research found, for the first time, the mechanical strength of a single silica polymer growing in-situ between silica grains and its effect on granular soil properties such as stiffness. New evidence was discovered that directly links growth of silica polymers in engineering timescale to the increase in the intergranular tensile strength between two amorphous silica grains under prolonged compression in the presence of water. Tensile strength and size of silica polymers growing around stressed contact regions between two grains have been quantified. The overall increase in intergranular tensile strength of silica grain system has been estimated.

Investigation into the effect of mica in the vicinity of stressed silica contact on soil aging has been used to verify a current school of thought that the difference in electrochemical potential between mica and silica is the driving force behind enhanced silica dissolution.

For the first time we have a chain of observations that confirms a long-existing hypothesis that a stressed contact with microcracks generates dissolved silica in the contact (asperity) vicinity, which eventually polymerizes, forming a structure between the grains. Such structure is sufficiently strong to represent a significant increase of tensile strength or, through a rotational deformational mode, compressive strength within a period of time that is of the order of weeks. One of the most important findings is that the failure pulling force of a single link of silica polymer is 330-450 nN. Multiple interwoven polymer links are contained in a single intergranular polymer bond.

Following the finding that silica polymers of a consistent strength growing in an intergranular space submerged in water, the strength of such inter-particle bonds are measured. Several sets of experiments were run with a different pre-test aging, which is simply an immersion in water with a prescribed concentration of silicic acid under an applied constant external load. The concentration varied between 200- and 500 ppm. 120 ppm is a concentration closest to that of amorphous silica in natural water. Higher concentrations were used in order to accelerate the process of silica dissolution and precipitation.

It appears that the tensile strength of the precipitated and polymerized silica between two amorphous silica grains reaches significant values within relatively short periods of time. These values for 200- and 500 ppm of silica reach the amount of 1 – 1.5 mN. Such values are two to three times higher than capillary forces arising in the same system. The latter observation informs us that silica polymers generated (or enhanced) in the process of an intergranular damage may play a significant role in time-dependent building of the material compressibility and/or strength. Macroscopic compressibility is known to be dependent on intergranular tensile and rotational strength (Oda and Iwashita 1999).

There is a host of new questions raised by this research. The first among them is, whether the observed intergranular silica polymer bonding spontaneously building at the intergranular damage site is sufficient to account for the time dependent strengthening of sediments observed in the literature (Hueckel et al. 2001, Hueckel et al. 2005). The current answer is yes, the measured forces are 2-3 times higher than capillary force, classically believed to be responsible for the apparent cohesion increase. It is clearly realized that in natural systems, there is more than one mechanism that may contribute to the time dependent strengthening of sediments. The others are: capillary forces (Mielniczuk et al. 2014), calcite precipitation, and porosity reduction (Hueckel et al. 1998) and precipitation of salts during drying.

9. Suggestions for Future Research

Further experiments using Grain Indenter-Puller can be conducted in solutions with different silica ion concentrations to verify the model proposed in this research. Different environmental factors, such as temperature, impurities in solution, and other ions should be investigated for any effect they might have on silica dissolution, precipitation, and polymerization in stressed contact regions.

Impact of mica on the polymerization of silica in the vicinity of stressed contact may be further evaluated to have a clearer picture of how and how much can mica-silica contact affect silica aging.

The next main focus should be on how the growth of silica microstructures on silica grain surfaces in the vicinity of stressed contact affects granular soil on a macroscopic scale. A variety of experimental methods can be utilized, such as consolidation test, and penetration test on sand to quantify the effect of aging due to the dissolution, precipitation, and polymerization of silica near stressed contacts.

Different types of sand may respond differently to aging in submerged conditions, due to grain size distribution, grain shape, and composition. It is worthy to investigate how these conditions affects and are affected by aging due to the growth of silica microstructures.

Bibliography

Alcantar, N., et al. (2003). "Forces and ionic transport between mica surfaces: implications for pressure solution." Geochimica et Cosmochimica Acta **67**(7): 1289-1304.

Alexander, G. B., et al. (1954). "The solubility of amorphous silica in water." Journal of Physical Chemistry **58**(6): 453-455.

Banagan, B. L., et al. (2010). "Microbial strengthening of loose sand." Letters in Applied Microbiology **51**(2): 138-142.

Baxter, C. D. P. and J. K. Mitchell (2004). "Experimental study on the aging of sands." Journal of Geotechnical and Geoenvironmental Engineering **130**(10): 1051-1062.

Becker, A. (1995). "Quartz pressure solution: influence of crystallographic orientation." Journal of Structural Geology **17**(10): 1395 - 1405.

Bjorkum, P. (1996). "How important is pressure in causing dissolution of quartz in sandstones?" JOURNAL OF SEDIMENTARY RESEARCH **66**({1, Part a}): 147-154.

Bowman, E. T. and K. Soga (2003). "Creep, ageing and microstructural change in dense granular materials." Soils and Foundations **43**(4): 107-117.

Carroll, S., et al. (1998). "Amorphous silica precipitation (60 to 120 degrees C): Comparison of laboratory and field rates." Geochimica et Cosmochimica Acta **62**(8): 1379-1396.

Charlie, W. A., et al. (1992). "Time-dependent cone penetration resistance due to blasting." Journal of Geotechnical Engineering **118**(8): 1200-1215.

Denisov, N. Y. and B. F. Reltov (1961). "The influence of certain processes on the strength of soils." Proceedings of the 5th International Conference of Soil Mechanics and Foundation Engineering **1**: 75-78.

Dowding, C. and R. Hryciw (1986). "A Laboratory study of blast densification of saturated sand." Journal of Geotechnical Engineering **112**(2): 187-199.

Eyring, H. (1936). "Viscosity, plasticity, and diffusion as examples of absolute reaction rates." Journal of Chemical Physics **4**(4): 283-291.

Gratier, J., et al. (2009). "A pressure solution creep law for quartz from indentation experiments." J. Geophys. Res. **114**(B3): B03403-.

Greene, G. W., et al. (2009). "Role of electrochemical reactions in pressure solution." Geochimica et Cosmochimica Acta **73**(10): 2862-2874.

Guo, R. and T. Hueckel (2013). "Growth of polymer microstructures between stressed silica grains: a chemo-mechanical coupling." Geotechnique **63**(4): 322-330.

Heald, M. T. (1955). "Stylolites in sandstones." Journal of Geology **63**(2): 101-114.

Hickman, S. and B. Evans (1995). "Kinetics of pressure solution at halite-silica interfaces and intergranular clay films." JOURNAL OF GEOPHYSICAL RESEARCH-SOLID EARTH **100**({B7}): 13113-13132.

Houseknecht, D. W., et al. (1987). "Relationships among Vitrinite Reflectance, Illite Crystallinity, and Organic Geochemistry in Carboniferous Strata, Ouachita Mountains, Oklahoma and Arkansas - Reply." Aapg Bulletin-American Association of Petroleum Geologists **71**(3): 347-347.

Hu, L. B. and T. Hueckel (2007a). "Coupled chemo-mechanics of intergranular contact: Toward a three-scale model." Computers and Geotechnics **34**(4): 306-327.

Hu, L. B. and T. Hueckel (2007b). "Creep of saturated materials as a chemically enhanced rate-dependent damage process." International Journal for Numerical and Analytical Methods in Geomechanics **31**(14): 1537-1565.

Hueckel, T., et al. (2005). "Field derived compressibility of deep sediments of the Northern Adriatic." Special Volume SISOLS2005, Millpress Rotterdam: 51-64.

Hueckel, T., et al. (2001). "Aging of oil/gas-bearing sediments, their compressibility, and subsidence." Journal of Geotechnical and Geoenvironmental Engineering **127**(11): 926-938.

Hueckel, T., et al. (1998). "Constitutive properties of thermo-elasto-plastic behavior of deep carbonatic clays." International Journal for Numerical and Analytical Methods in Geomechanics **22**(7): 549-576.

Hueckel, T., et al. (2013). Micro-scale study of rupture in desiccating granular media. Geo-Congress; Stability and Performance of Slopes and Embankments, San Diego, CA.

Icenhower, J. P. and P. M. Dove (2000). "The dissolution kinetics of amorphous silica into sodium chloride solutions: effects of temperature and ionic strength." Geochimica et Cosmochimica Acta **64**(24): 4193 - 4203.

Iler, R. K. (1955). "The Colloid Chemistry of Silica and Silicates." Soil Science **80**(1): 86.

Iler, R. K. (1979). The Chemistry of Silica: Solubility, Polymerization, Colloid and Surface Properties, and Biochemistry, John Wiley & Sons, Inc.

Israelachvili, J. N. (2011). Intermolecular and Surface Forces. Burlington, MA, Academic Press.

Joshi, R., et al. (1995). "Effect of aging on the penetration resistance of sands." Canadian Geotechnical Journal **32**({5}): 767-782.

Krauskopf, K. B. (1956). "Dissolution and precipitation of silica at low temperatures." Geochimica et Cosmochimica Acta **10**(1-2): 1 - 26.

Kristiansen, K., et al. (2011). "Pressure solution - The importance of the electrochemical surface potentials." Geochimica et Cosmochimica Acta **75**(22): 6882-6892.

Kuhn, M. R. and J. K. Mitchell (1993). "New perspectives on soil-creep." Journal of Geotechnical Engineering-ASCE **119**(3): 507-524.

Lee, K. L. (1977). "Adhesion bonds in sands at high pressures." Journal of the Geotechnical Engineering Division-Asce **103**(8): 908-913.

Lian, G. P., et al. (1993). "A theoretical study of the liquid bridge forces between two rigid spherical bodies." Journal of Colloid and Interface Science **161**(1): 138-147.

Mesri, G., et al. (1990). "Postdensification penetration resistance of clean sands." Journal of Geotechnical Engineering **116**(7): 1095-1115.

Meyer, E. E., et al. (2006). "Experimental investigation of the dissolution of quartz by a muscovite mica surface: Implications for pressure solution." JOURNAL OF GEOPHYSICAL RESEARCH-SOLID EARTH **111**(B8).

Mielniczuk, B., et al. (2014). "Rupture of a liquid bridge between two grains due to its evaporation." Acta Geotechnica **in print**.

Mitchell, J. K. (1993). Fundamentals of soil behavior, Wiley.

Mitchell, J. K. and Z. V. Solymar (1984). "Time-dependent strength gain in freshly deposited or densified sand." Journal of Geotechnical Engineering-ASCE **110**({11}): 1559-1576.

Oda, M. and K. Iwashita (1999). Mechanics of Granular Materials - an Introduction. Rotterdam, A. A. Balkema.

Oelkers, E. H., et al. (1992). The Mechanism of Porosity Reduction, Styolite Development and Quartz Cementation in North-Sea Sandstones. 7th International Symposium on Water-rock Interaction, Park City, UT.

Oelkers, E. H., et al. (2008). "An experimental study of the dissolution mechanism and rates of muscovite." Geochimica et Cosmochimica Acta **72**(20): 4948-4961.

Parry, R. H. G. (2004). Mohr circles, stress paths and geotechnics. London, Spon Press.

Paterson, M. S. and K. Kekulawala (1979). "Role of water in quartz deformation." Bulletin De Mineralogie **102**(2-3): 92-98.

Perkins, S. W., et al. (2000). "The influence of biofilm on the mechanical behavior of sand." Geotechnical Testing Journal **23**({3}): 300-312.

Renard, F., et al. (1997). "Pressure solution in sandstones: influence of clays and dependence on temperature and stress." Tectonophysics **280**(3–4): 257-266.

Rimstidt, J. and H. Barnes (1980). "The kinetics of silica-water reactions." Geochimica et Cosmochimica Acta **44**(11): 1683-1699.

Rimstidt, J. D. (1997). "Quartz solubility at low temperatures." Geochimica et Cosmochimica Acta **61**(13): 2553 - 2558.

Rubin, C. J. (2009). A Novel Apparatus for the Study of Intergranular Silica Microstructures. Durham, NC, Duke University.

Schmertmann, J. H. (1991). "The Mechanical aging of soils." Journal of Geotechnical Engineering **117**(9): 1288-1330.

Scholz, C. H. and J. T. Engelder (1976). "Role of asperity indentation and plowing in rock friction .1. Asperity creep and stick-slip." International Journal of Rock Mechanics and Mining Sciences **13**(5): 149-154.

Schott, J., et al. (2009). The Link Between Mineral Dissolution/Precipitation Kinetics and Solution Chemistry. Thermodynamics and Kinetics of Water-Rock Interaction. E. H. Oelkers and J. Schott. **70:** 207-258.

Soulie, F., et al. (2007). Effect of capillary and cement-led bonds on the strength of unsaturated sands. Experimental Unsaturated Soil Mechanics. T. Schanz. **112:** 185-193.

Tada, R., et al. (1987). "A new mechanism for pressure solution in porous quartzose sandstone." Geochimica et Cosmochimica Acta **51**(9): 2295-2301.

Vigil, G., et al. (1994). "Interactions of Silica Surfaces." Journal of Colloid and Interface Science **165**(2): 367-385.

Wang, Y. H. and K. Y. Tsui (2009). "Experimental Characterization of Dynamic Property Changes in Aged Sands." Journal of Geotechnical and Geoenvironmental Engineering **135**(2): 259-270.

Wang, Y. H., et al. (2008). "Discrete element modeling of contact creep and aging in sand." Journal of Geotechnical and Geoenvironmental Engineering **134**(9): 1407-1411.

Worden, R. H. and S. Morad (2000). Quartz cementation in oil field sandstones: a review of the key controversies. Quartz cementation in sandstones. R. H. Worden and S. Morad. Malden, MA, Blackwell Science**:** 1-20.

Biography

Rui Guo reluctantly came to your world on September 24th, 1985 in Wuhan, the provincial capital city of Hubei, China, where he remained until the age of 16, with unlimited supplies of Hot Dry Noodles and Spicy Duck Necks. Then he went to Singapore, grew 7 inches, played some basketball, performed in band and choir, and completed his high school GCSE A-Level education. He spent his next three years in the UK, where he skipped more classes than he attended and barely received his Bachelor of Engineering with Honors degree in Mechanical Engineering from University College London. He also developed a deep passion for Arsenal Football Club there. In pursuit of his eventual wife, he accepted an offer from Professor Tomasz Hueckel and enrolled in a Ph.D. program in Civil and Environmental Engineering Department at Duke University in 2009; that season, Duke won its latest NCAA Men's Basketball National Championship. He spent most of his time in Durham, North Carolina playing computer games, getting better at tennis, losing March Madness brackets, raising a dog and a cat, and marrying the love of his life. He also published a peer-reviewed paper, "Growth of polymer microstructures between stressed silica grains: a chemo-mechanical coupling", in Geotechnique, completed a Master of Science degree from Duke University, and received Engineer In Training and LEED Green Associate certificates in 2013. He is currently working as a Geotechnical Engineer in New York City.